ANNUAL REPORT 2012














Orphée
Laboratoire Léon Brillouin

Laboratoire Léon Brillouin

ANNUAL REPORT 2012

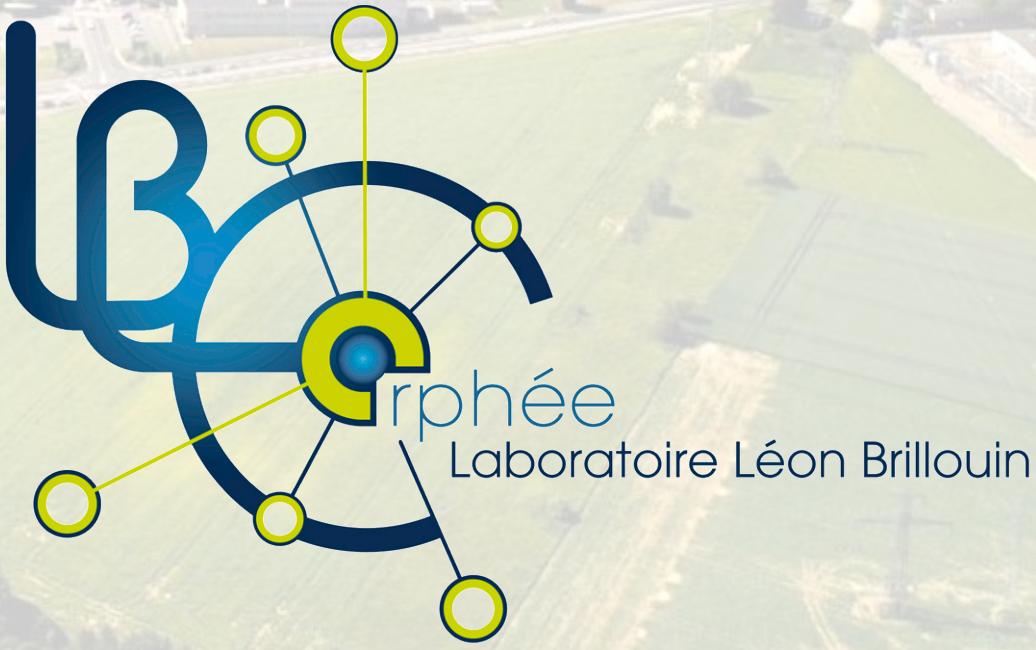

Director's word

The year 2012 has seen several milestones for the infrastructure:

An amendment to the agreement defining the procedures for the organization and operation of the Léon Brillouin Laboratory has been signed by its two supervisory bodies, CEA and CNRS.

The composition of the steering committee of LLB was profoundly renewed with the arrival of the new Director of the Department of Material Sciences (DSM) of the CEA, Gabriele Fioni (left), as well as the new director of the Institute of Physics (INP) of CNRS, jean-François Pinton (right).

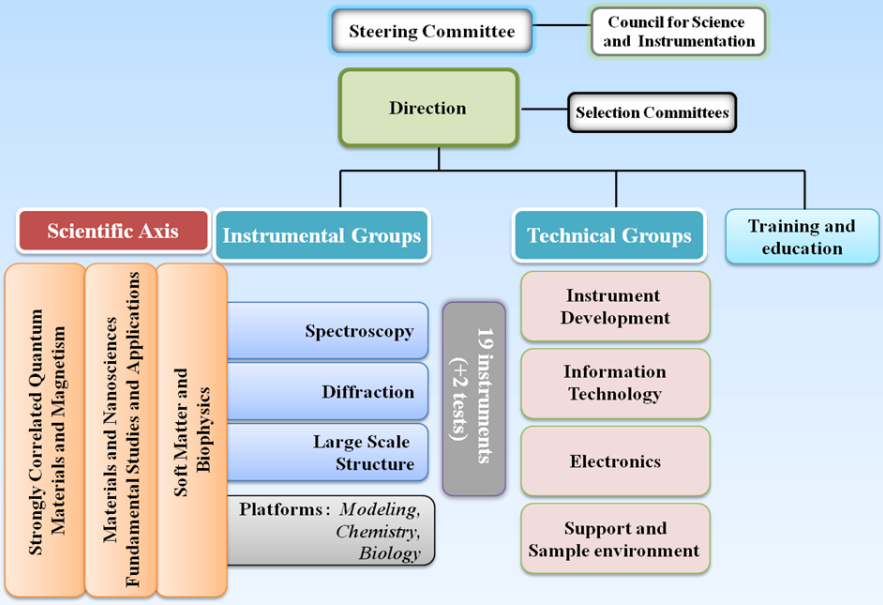

The internal organization of LLB was modified to increase the coherence and optimize the use of resources. The management of the spectrometers rests on three instrumental groups (spectroscopy, diffraction, large-scale structures) with the support of the four technical groups (Sample Environment, Instrument Development, Information Technology, Electronics) and cross-platform (modeling, chemistry, biology). In addition, scientific animation is done with the three scientific axes (strongly correlated quantum systems and magnetism - Materials and Nanosciences: Fundamental Studies and Applications - Soft Matter and Biophysics).

A new Scientific and Instrumental Council was established to support the Steering Committee of LLB. This council, under the direction of Ian Anderson, had its first meeting in October.

In 2012, the Laboratoire Léon Brillouin participates or is behind a number of initiatives at national and international level:

The year 2012 saw the restart of the NMI3 European contract for a new period of 4-years that allows finance access for European users to the facility.

In April took place the first users meeting of the LLB. During this meeting, information was given on the development of the instrumental park of the infrastructure, as well as the changing landscape of the neutron sources in Europe.

The launch of ESS European Spallation Source in Lund has brought new responsibilities to LLB which was chosen to be the entry point of the French community for proposals of contribution to studies and/or construction of instrumentation at the future ESS. In this context, a working group of French neutronicians was created, representing the national community, and had a first meeting in early October.

EUROPEAN SPALLATION SOURCE

From the standpoint of instruments and neutron source, several events are worth noting:

Two historical instruments of LLB, Mibemol and Paxe, were decommissioned and dismantled during the summer. They will soon be replaced by two new instruments that will be among the best in their class, Fa# for the time of flight and PA20 for small angle scattering.

The Orphée reactor has undergone two major maintenance operations that required the prolongation of the usual winter and summer breaks. The first break allowed replacing the two cold sources and the second changing the thimble of the channel 9F.

Finally, to help users cope with the prolonged shutdown of the ILL, it was decided to change the dates for submission of **proposals for experiments** at the LLB in 2013 to **1st of April and 1st of October**.

The technical teams LLB were also heavily solicited during the summer stop for the dismantling and movements of instruments to enable the reactor maintenance and to prepare the guide hall for the future instruments.

C. Alba-Simionesco and J.-P. Visticot

2012 EVENTS IN PICTURES

URBANISME

L'Etat s'engage pour Saclay

Objectif : rejoindre le top 10 des clusters mondiaux. Lors d'un forum organisé mardi par le groupement d'entreprises Paris-Ile-de-France Capitale économique sur le développement du site de Saclay (Essonne), le Premier ministre, Jean-Marc Ayrault, a affirmé que le gouvernement débloquerait si nécessaire un milliard d'euros en 2015 pour permettre la réalisation du métro automatique du Grand Paris Express.

Jean-Marc Ayrault a par ailleurs confirmé « la dotation exceptionnelle d'un milliard d'euros » destinée à rapprocher les deux universités, les onze grandes écoles et les six organismes de recherche du site. Elle s'ajoutera aux 850 millions d'euros alloués dans le cadre de l'opération Campus et à « une dotation supplémentaire de près d'un milliard d'euros au titre des investissements d'avenir ». ■ HÉLÈNE COLAU

ment débloquera si nécessaire un milliard d'euros en 2015.

SCIENTIFIC AND INSTRUMENTAL COUNCIL (OCTOBER)

LLB USERS MEETING (APRIL)

VISIT OF A CHINESE DELEGATION (APRIL)

RETIREMENT OF J. TEIXEIRA AND DISCOMMISSIONING OF PAXE

ORGANISATION OF PNCMI CONGRESS

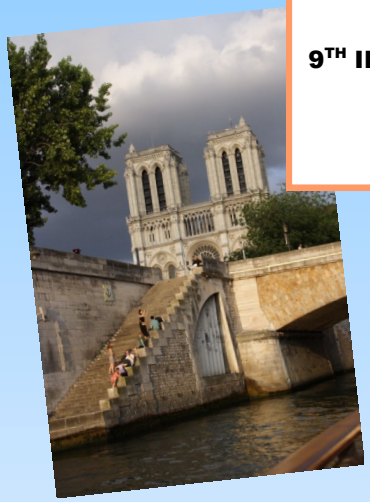

PNCMI'2012 RESEARCH CONFERENCE
9TH INTERNATIONAL WORKSHOP ON POLARISED NEUTRONS IN CONDENSED MATTER INVESTIGATIONS.

(PARIS, JULY)

CONFERENCES SPONSORED BY THE LLB

JOURNEES SURFACES ET INTERFACES

(ST AUBIN, JANUARY)

SMARTER CRYSTALLOGRAPHY

(VERSAILLES, SEPTEMBER)

AXE 1:

Strongly Correlated Quantum Materials and Magnetism.

AXE 2:

Materials & Nanosciences: Fundamental Studies and Applications.

AXE 3:

Soft Matter & Biophysics.

SCIENTIFIC HIGHLIGHTS

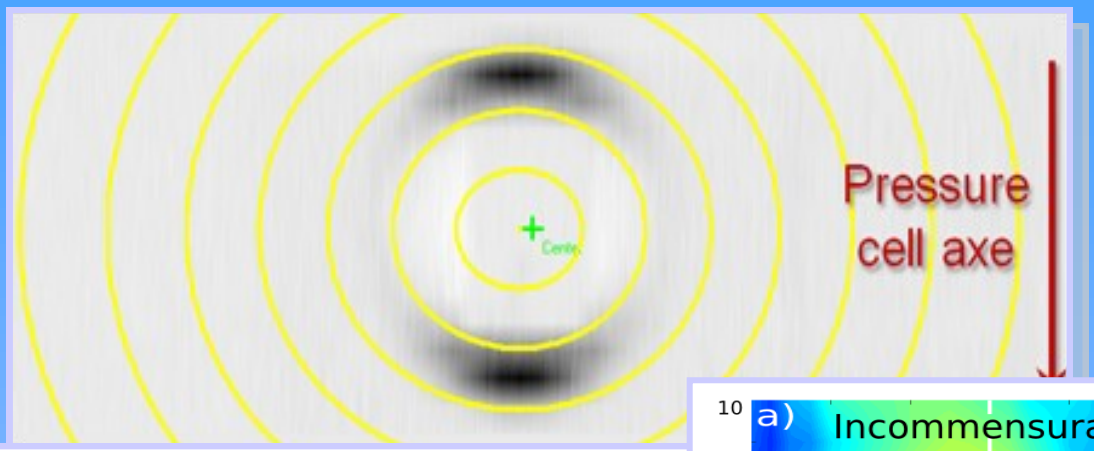
Pressure
cell axe

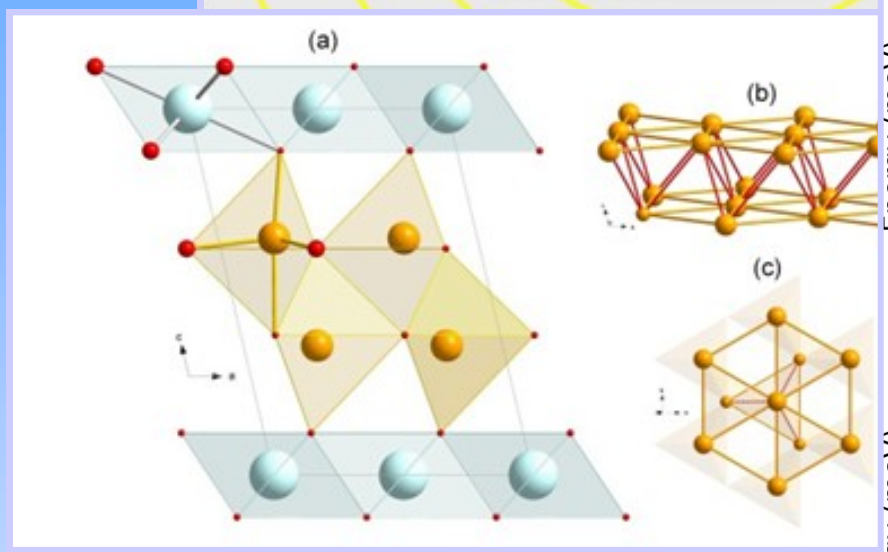
(a)
(b)
(c)

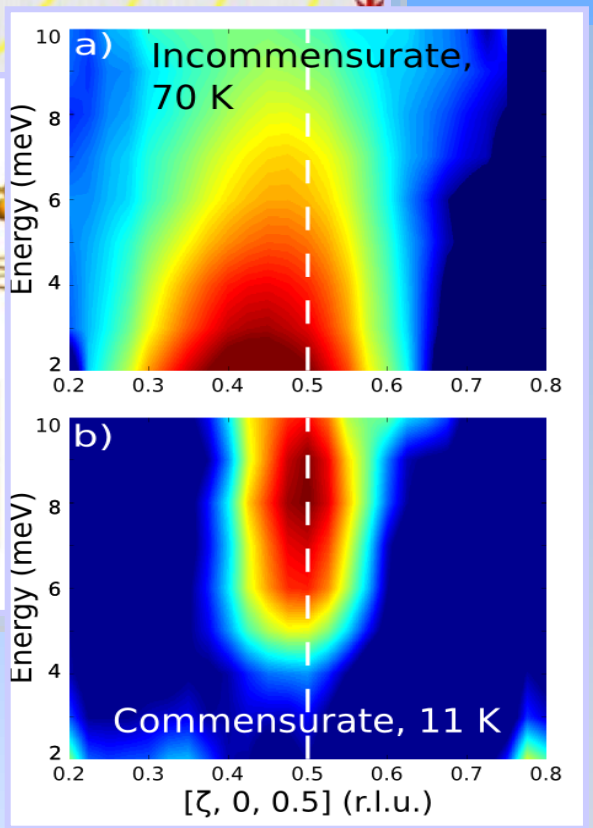
a)
Incommensurate,
70 K
b)
Commensurate, 11 K
Energy (meV)
[ζ, 0, 0.5] (r.l.u.)

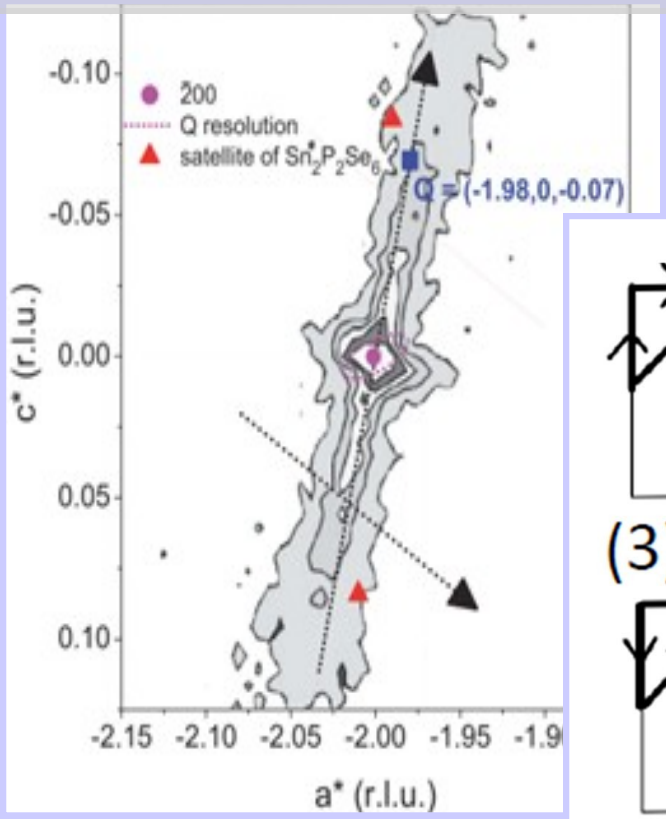
200
Q resolution
satellite of Sn2P2Se6
Q = (-1.98,0,-0.07)
c* (r.l.u.)
a* (r.l.u.)

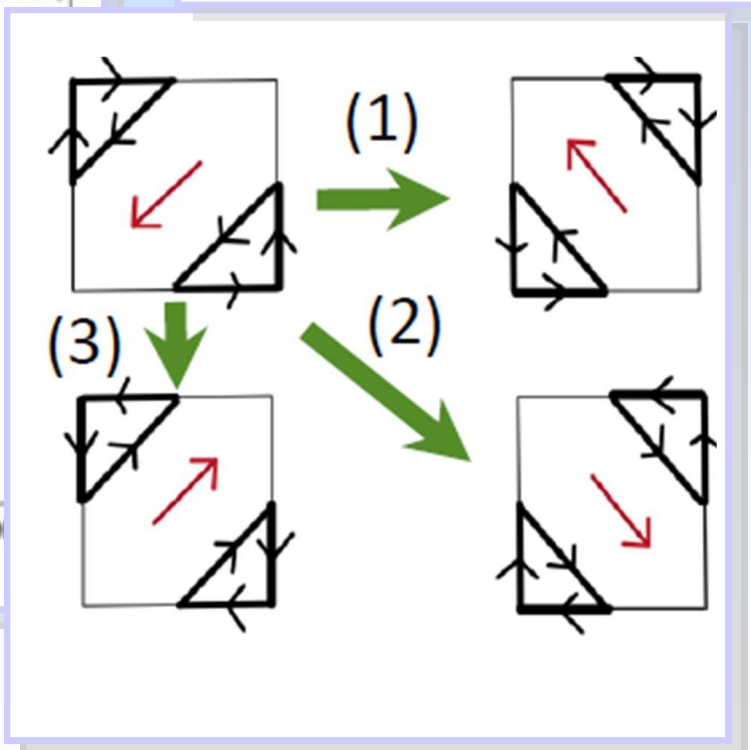
(1)
(2)
(3)

AXE 1:

Strongly Correlated Quantum Materials and Magnetism.

The "strongly correlated electron systems" denote a class of materials and physical phenomena which cannot be described in terms of the standard theory for a Fermi gas of non-interacting electrons. Such situations mainly occur in compounds containing transition-metal or rare-earth elements, because *d* and *f* orbitals have a more pronounced localized character. One common feature in many of these materials is the coexistence of several degrees of freedom associated with the electron- (charge, spin, orbital) or lattice subsystems, whose interplay is responsible for a large variety of ground states and excitation spectra. Well-known examples studied at LLB, both experimentally and theoretically, include cuprate or ferropnictide high-T_c superconductors, "giant magneto-resistance" manganites, compounds with short-range magnetic interactions subject to geometrical frustration (multiferroics, spin-ices, etc.), lanthanide-based heavy-fermion systems and "Kondo insulators", as well as a number of materials in which unconventional orders occur, such as the "magnetic blue phase" of MnSi, or the multipole-order states found in rare-earth hexaborides. Because neutrons interact with both the atom nuclei and their electron shells, neutron scattering is one of the best tools to study this type of physics involving interplay of lattice and magnetic properties. Polarized neutron beams, implemented on several spectrometers at LLB, further enhance the potential of neutron experiments for studying strong correlation phenomena in condensed matter.

- **Neutron scattering study of ferroelectric $Sn_2P_2S_6$ under pressure**
  P. Ondrejkovic, M. Kempa, Y. Vysochanskii, P. Saint-Grégoire, P. Bourges, K. Z. Rushchanskii and J. Hlinka

- **Evidence of magnetic phase separation in $LuFe_2O_4$**
  J. Bourgeois, G. André, S. Petit, J. Robert, M. Poienar, J. Rouquette, E. Elkaïm, M. Hervieu, A. Maignan, C. Martin and F. Damay

- **Neutron diffraction study of the chiral magnet MnGe**
  O. L. Makarova, M. Deutsch, F. Porcher, A. V. Tsvyashchenko and I. Mirebeau.

- **Competition between commensurate and incommensurate magnetic ordering in $Fe_{1+y}Te$**
  D. Parshall, G. Chen, L. Pintschovius, D. Lamago, Th. Wolf, L. Radzihovsky and D. Reznik

- **New step towards the search for the origin of high-transition temperature superconductivity: exploration of the phase diagram and observation of magnetic excitation modes in cuprates**
  Y. Li, G. Yu, M. K. Chan, V. Balédent, Y. Li, N. Barišić, X. Zhao, K. Hradil, R. A. Mole, Y. Sidis, P. Steffens, P. Bourges and M. Greven

Neutron scattering study of ferroelectric $Sn_2P_2S_6$ under pressure

P. ONDREJKOVIC[A], M. KEMPA[A], Y. VYSOCHANSKII[B], P. SAINT-GRÉGOIRE[C], P. BOURGES[D], K. Z. RUSHCHANSKII[E], J. HLINKA[A]

a Institute of Physics, Academy of Sciences of the Czech Rep., Prague, Czech Republic

b Institute for Solid State Physics and Chemistry, Uzhgorod University, Ukraine

c Laboratory MIPA, Dept. of Sciences and Arts, University of Nimes, France

d Laboratoire Léon Brillouin, CEA Saclay, France

e Peter Grünberg Institut, FZ Jülich, Germany

ondrejkovic@fzu.cz

Ferroelectric phase transition in the semiconductor $Sn_2P_2S_6$ single crystal has been studied by neutron scattering in the pressure-temperature range near the anticipated tricritical Lifshitz point (P ≈ 0.18 GPa, T ≈ 296 K). The observations reveal a direct ferroelectric-paraelectric phase transition in the whole investigated pressure range (0.18–0.6 GPa). These results are in a clear disagreement with phase diagrams assumed in numerous earlier works, according to which a hypothetical intermediate incommensurate phase extends over several or even tens of degrees in the 0.5 GPa pressure range. Still, the results are in favour of a uniaxial ferroelectric transition at the tricritical Lifshitz point.

Phase transformations in solids can be often well described by the Landau theory in which different possible phases of a crystal are associated by qualitative changes of a specific physical quantity, so-called « order parameter ». In case of ferroelectrics, the order parameter is usually polarization. Our study focuses on a chalcogenide crystal $Sn_2P_2S_6$ where the theory has predicted an exotic and exciting phenomenon: three phase transformation lines should merge at a singular point of the temperature-pressure phase diagram. In the vicinity of this so-called Lifshitz point (LP), very different phases and transition behaviors would meet, involving a paraelectric phase with no polarization at all, a ferroelectric phase with non-zero polarization and an incommensurate phase with a frozen polarization wave. The search for the characteristic signature of this latter structure is the object of our work[1].

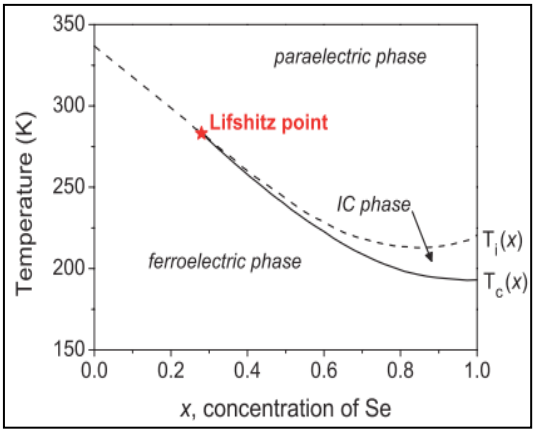

Figure 1 : Schematic temperature-composition phase diagram for the system $Sn_2P_2(Se_xS_{1-x})_6$ [2]. Dashed line: second -order phase transition, solid line: first-order phase transition..

Uniaxial ferroelectric chalcogenides represent one of the best known families of ferroelectric semiconductors. In particular, solid solutions of $Sn_2P_2S_6$ and $Sn_2P_2Se_6$ have been recognized as extremely interesting model systems[2]. All of them have an identical parent paraelectric structure at high temperatures ($P2_1/n$) and the same ferroelectric phase at low temperatures (Pn). At ambient pressure, crystals with low Se/S concentration ratio show a direct ferroelectric-paraelectric phase transition, while those of high Se/S concentration exhibit an intermediate incommensurate (IC) phase (see Fig. 1). Later, it was predicted that a similar LP could also occur in the temperature-pressure (T-P) phase diagram of pure $Sn_2P_2S_6$, which was reported by several experiments to be at P = 0.18 GPa, T = 296 K. However, diffraction investigations of the intermediate phase of $Sn_2P_2S_6$ were not reported so far and there was no direct evidence of its IC nature.

Our neutron scattering experiment was performed at LLB on the thermal 2T1 and cold 4F2 three-axis spectrometers, with the sample placed in a special helium pressure cell designed for neutron scattering experiments in the temperature range of 20–305 K and under hydrostatic pressures up to about 0.6 GPa. The investigation was performed in Brillouin zones and directions favourable for occurring satellite reflections, according to theoretical predictions and experiments on $Sn_2P_2Se_6$.

Monitoring of the (-200) reflection allowed us to probe quite accurately the ferroelectric order parameter, and thus the phase transition temperature (see Fig. 2(b)). In the vicinity of the phase transition line we have searched for possible indications of a satellite reflection. However, no obvious satellite peaks have been seen. At the same time, our observations disclosed traces of weak and broad diffuse scattering ridges, extending over the “soft” direction, roughly perpendicular to the direction along which the spontaneous polarization is formed. Fig. 3(a) shows an example of a scan

taken along this diffuse scattering ridge at several temperatures. Examples of transverse scans are shown in Fig. 3 (b). Trajectories of these scans are schematically shown in Fig. 4, along with the contour plots of the ambient-pressure diffuse scattering topography taken from Ref. 3.

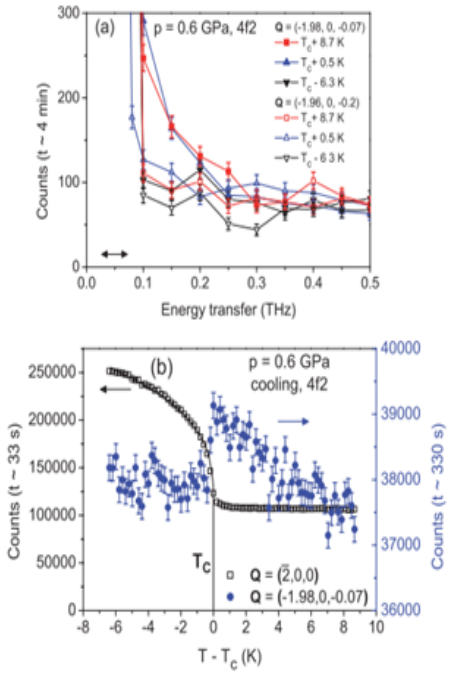

Figure 2: Temperature dependence of (a) quasielastic and (b) elastic scattering at 0.6 GPa

The diffuse scattering ridge corresponds to the smaller peak in Fig. 3(b), while the larger intensity peak is a spurious leakage of the (-200) Bragg reflection scattering due to the strongly anisotropic tails of the instrumental resolution function. The constant-Q spectra taken at selected positions in the high-temperature phase (Fig. 2(a)) suggest that this diffuse scattering is quasielastic in its nature, with FWHM of the order of 0.2 THz.

In conclusion, our results do not indicate any evidence of an intermediate incommensurate phase in the $Sn_2P_2S_6$ crystal under moderate pressure. While we cannot fully exclude the existence of an extremely long-wavelength modulation below the phase transition temperature, the most simple explanation of our observations is that at least up to 0.6 GPa, there is only a simple paraelectric-ferroelectric phase transition in $Sn_2P_2S_6$.

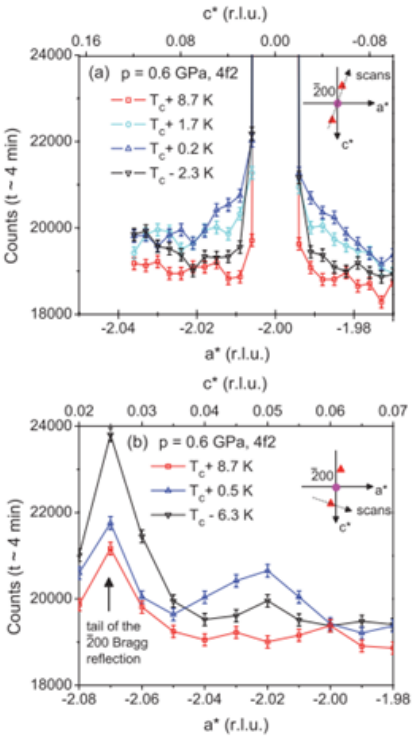

Figure 3: Elastic scans in the (-200) Brillouin zone in the vicinity of the ferroelectric phase transition ($P = 0.6$ GPa $T_C = 205.3$ K): (a) along and (b) across the diffuse streak.

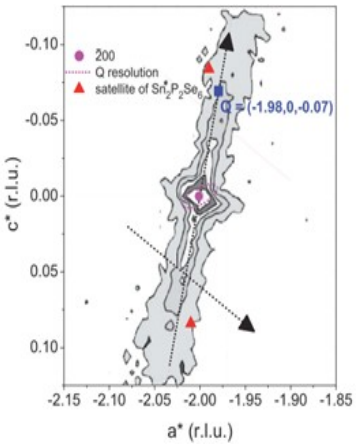

Figure 4: Schema of reciprocal-space trajectories of scans shown in Fig. 3, superposed with contour plots of the critical diffuse scattering known from ambient pressure X-ray diffraction measurements of Ref. 3.

References

1. P. Ondrejkovic, M. Kempa, Y. Vysochanskii, P. Saint-Grégoire, P. Bourges, K. Z. Rushchanskii & J. Hlinka, *Phys. Rev.* B 86, 224106 (2012).
2. Yu. M. Vysochanskii, T. Janssen, R. Currat, R. Folk, J. Banys,J. Grigas, & V. Samulionis, *Phase Transitions in Ferroelectric Phosphorous Chalcogenide Crystals* (Vilnius University, Vilnius, 2006).
3. J. Hlinka, R. Currat, M. de Boissieu, F. Livet, & Yu. M. Vysochanskii, *Phys. Rev.* B 71, 052102 (2005).

Evidence of magnetic phase separation in $LuFe_2O_4$

J. BOURGEOIS[A,B], G. ANDRÉ[A], S. PETIT[A], J. ROBERT[A], M. POIENAR[C], J. ROUQUIETTE[C], E. ELKAÏM[D], M. HERVIEU[B], A. MAIGNAN[B], C. MARTIN[B], F. DAMAY[A]

a Laboratoire Léon Brillouin, CEA Saclay, France

b Laboratoire CRISMAT, Caen, France

c Institut Charles Gerhardt, Montpellier, France

d Synchrotron Soleil, Saint-Aubin, France

francoise.damay@cea.fr

The magnetic properties of a polycrystalline sample of $LuFe_2O_4$ have been investigated by means of neutron scattering, between 1.5 and 300K. Inside a $[Fe_2O_4]_\infty$ bilayer, the magnetic arrangement on a triangular plane follows the expected ↑↓↓ pattern ; the stacking of the $[Fe_2O_4]_\infty$ bilayers is, however, degenerate, and can either be ferromagnetic or antiferromagnetic. Modeling of the diffraction data shows in addition the existence of an additional level of magnetic near-degeneracy, at the level of the bilayer itself. It results in the coexistence of magnetic phases with opposite signs of the intra-bilayer interaction, and with two distinct ordering temperatures : "ferromagnetic" bilayers order around 250K, and "antiferromagnetic" bilayers at ~ 200K. The near-degeneracy of the intra- and inter-bilayer couplings in $LuFe_2O_4$ might be a result of the geometrical frustration of spins with strong axial anisotropy.

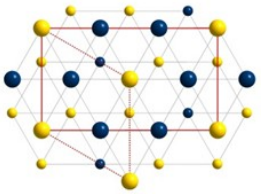

Recently, a new class of ferroelectrics, in which electronic polarization is driven by a process of charge ordering[1], has been under focus. Among them is $LuFe_2O_4$, which belongs to the family of layered rare-earth ferrites RFe_2O_4 (R = Ho to Lu, and Y). Its crystal structure can be described as a stacking along **c** of $[Fe_2O_4]_\infty$ bilayers, each consisting of two triangular $[FeO]_\infty$ planes, separated by non magnetic close-compact $[LuO_2]\infty$ layers (Fig. 1).

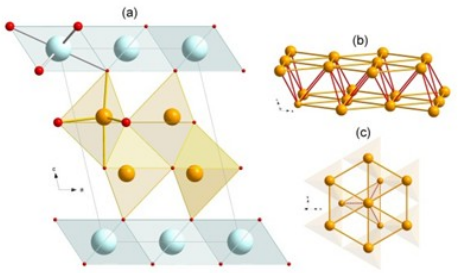

Figure 1 : (a) Monoclinic cell of $LuFe_2O_4$. (b) Perspective view of the $[Fe_2O_4]_\infty$ bilayer. (c) Projection onto the triangular plane of the $[Fe_2O_4]_\infty$ bilayer.

Clues to a coupling between electronic and magnetic degrees of freedom have been investigated[2], and theoretical models have also been proposed[3], but a clear understanding of the origin of multiferroicity in $LuFe_2O_4$ is impaired by the fact that the magnetic structure of this compound is still a matter of speculations. In this context, neutron diffraction experiments were carried out on the G4.1 diffractometer. At room temperature, a diffuse magnetic signal is observed in $LuFe_2O_4$, which becomes significant around 260 K and condenses into antiferromagnetic Bragg peaks below T_N = 240K. These magnetic peaks can be indexed with two propagation vectors, $\mathbf{k}_1 = (0\ 2/3\ 0)_m$ and $\mathbf{k}_2 = (0\ 2/3\ ½)_m$. This type of propagation vector is characteristic of a triangular lattice with an antiferromagnetic first-neighbor interaction, and corresponds to a collinear (1 ½ ½) amplitude modulated up-down-down spin arrangement.

Symmetry analysis based on a random distribution of Fe^{2+} and Fe^{3+} ions in the structure shows that the configuration within the bilayer can either be "ferromagnetic" (↑↓↓ ↑↓↓), or "antiferromagnetic" (↑↓↓ ↓↑↑). The bilayers are then stacked ferromagnetically ($\mathbf{k}_1$) or antiferromagnetically ($\mathbf{k}_2$). Based on this simple analysis, four different magnetic phases can be considered for $LuFe_2O_4$, **$\mathbf{k}_1$-F**, **$\mathbf{k}_1$-AF**, **$\mathbf{k}_2$-F**, and **$\mathbf{k}_2$-AF**, **F** and **AF** referring to, respectively, a ferromagnetic and an anti-ferromagnetic configuration of the bilayer (Inset of Fig. 2).

Refinements of the neutron diffraction data using a combination of the k_1 and k_2 magnetic phases, and involving either ferromagnetic or antiferromagnetic $[Fe_2O_4]_\infty$ bilayers, are illustrated on Fig. 2. The only refined parameters are the scale factors of the different phases, the corresponding cell parameters, and the magnetic peak width, to keep the modeling as basic as possible. Both models prove unsatisfactory to describe appropriately the magnetic intensities observed, and the magnetic ground state of $LuFe_2O_4$ is more appropriately described by a mixture of both models (Fig. 3a), suggesting that the sign of the intra-bilayer interaction can actually vary in the sample. The evolution with temperature of the intensities of the

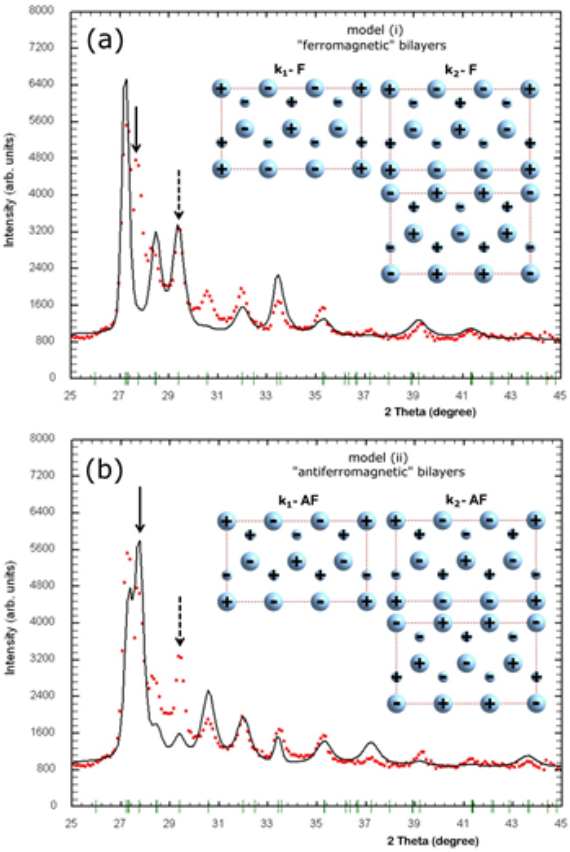

Figure 2 : Modeling of the magnetic structures at 2 K, in the case of ferromagnetic bilayers (a) and antiferromagnetic bilayers (b), and corresponding calculated diffraction patterns (experimental data : open circles, calculated profile : continuous line). The full and dotted arrows indicate the (1 -1 0) $+k_1$ and the (-1 -1 1)$+k_1$ magnetic reflections, respectively. The hkl gradual broadening of the Bragg profile is characteristic of magnetic stacking defects perpendicularly to the ab plane.

main magnetic Bragg peaks (Fig. 3b), further supports this idea. Two transition temperatures can be seen, at 250K and 200K. The first transition corresponds to an increase of the magnetic intensities on the peaks which are primarily contributed to in the ferromagnetic bilayer model. Around 200K, intensity increases on magnetic peaks which are predominant in the antiferromagnetic bilayer model.

This modeling of the magnetic scattering of $LuFe_2O_4$ thus evidences the existence of a new type of degeneracy, linked with the sign of the magnetic coupling within a $[Fe_2O_4]_\infty$ bilayer. In contrast to the bilayer stacking type, the sign of the intra-bilayer coupling actually affects the magnetic ordering temperature. The results of this study[4] also show that it is possible to get a realistic description of the magnetic ground state of $LuFe_2O_4$ without assuming an underlying charge-order model ; the next step will be therefore to clarify the possible relationships between spin and charge ordering in this compound.

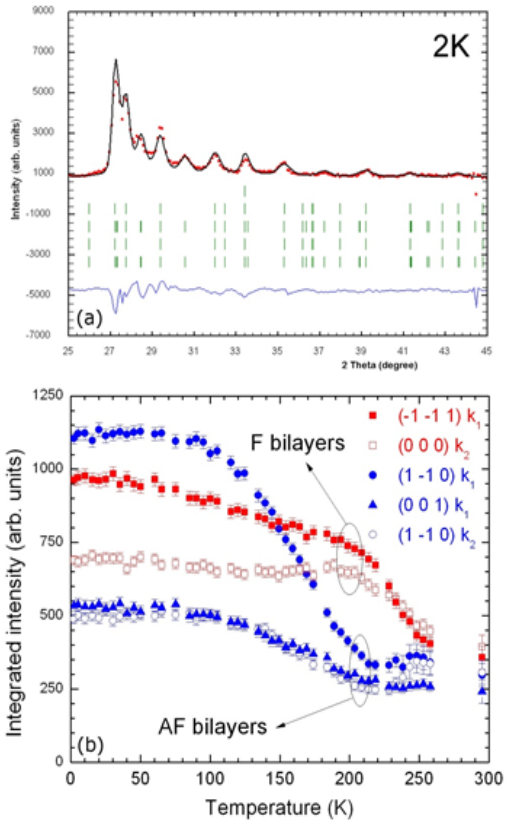

Figure 3 : (a) Modeling of the 2K magnetic ground state of $LuFe_2O_4$ using the k_1-F, k_2-F, k_1-AF and k_2-AF magnetic structures. (b) Temperature evolution of the integrated intensity of selected Bragg magnetic peaks. Red and blue symbols differentiate feature reflections of the ferromagnetic and antiferromagnetic bilayers models, respectively.

References

1. S. W. Cheong and M. Mostovoy, *Nature Materials* 6, 13 (2007)
2. M. Angst *et al.*, *Physical Review Letters* 101, 227601 (2008)
3. A. Nagano *et al.*, *Physical Review Letters* 99, 217202 (2007)
4. J. Bourgeois *et al.*, *Physical Review* B 86, 024413 (2012)

Neutron diffraction study of the chiral magnet MnGe

O. L. MAKAROVA [A,B], M. DEUTSCH[B], F. PORCHER[B], A. V. TSVYASHCHENKO[C] , I. MIREBEAU[B]

a Kurchatov Institute, Moscow, Russia

b Laboratoire Léon Brillouin, CEA Saclay, France

c Inst. For High Pressure Physics, Troitsk, Russia

isabelle.mirebeau@cea.fr

Electronic and magnetic properties of chiral magnets of B20 structure (Fig.1) are strongly coupled, which now attracts considerable interest. Due to the non centrosymmetric space group, the relativistic spin orbit coupling also called Dzyaloshinskii-Moryia (DM) interaction does not cancel. The competition between ferromagnetic exchange and DM anisotropy results in a small twist of the spin order. Long period helixes are stabilized, up to 180 Å in MnSi and 900 Å in FeGe. Moreover, in the B20 family the band structure strongly varies, from an itinerant metal (MnSi, FeGe) to a Kondo insulator (FeSi), and is influenced by pressure and chemical substitution. MnSi and FeGe magnetism shows many exotic features, such as pressure induced quantum transition[1], swiss-roll helical structure, magnetic blue phase[2] or "skyrmions" multi-helical textures under magnetic field. Coupling magnetic and electric degrees of freedom yields even more interesting effects: a motion of the skyrmion lattice is induced under electric field, and a Topological Hall Effect (THE) is observed in the skyrmionic phase, with potential applications for the next generation of spintronic devices.

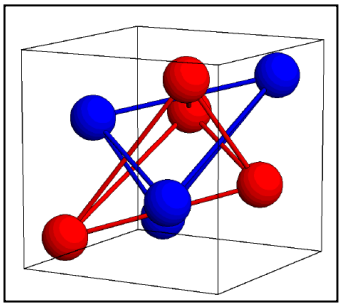

Figure 1: the B20 structure

MnGe has been much less studied, since its synthesis at 8 GPa pressure and 1600 C is difficult and the sample only exists in powder form. Surprisingly, MnGe shows the shortest helical wavelength (Fig. 2) and the largest THE response among the B20 Chiral magnets[3]. We investigated the crystal structure of MnGe by high resolution powder diffraction on 3T2. We also studied the magnetic structure versus temperature with great accuracy on G6.1 and G4.1, using cold neutrons to observe the satellite of the Q=0 reflection, unobserved before. We show that the crystal and magnetic structure are intrinsically connected, so that the spiral order is concomitant with a small lattice distortion[4]. We also started the first neutron study of MnGe under pressure.

At low temperature the helical magnetic order is clearly evidenced by an intense zero satellite, whose position evolves with temperature (Fig. 3a). Satellites of the nuclear Bragg peaks with much weaker intensity are also observed. All reflections are indexed with a propagation vector **K**=(00x), which increases upon cooling and saturates at a 0.167(4) r.l.i. below 30K, close to the commensurate value of 1/6. Magnetic refinements yield a regular helix whose wavelength decreases from about 60 Å just below T_N to about 38 Å below 30K. Nuclear Bragg peaks show a small broadening at T_N, suggesting that the transition is accompanied by a small lattice distortion (Fig. 3b). Considering that the 111 peak does not split, we assume that this symmetry lowering stabilizes an orthorhombic structure.

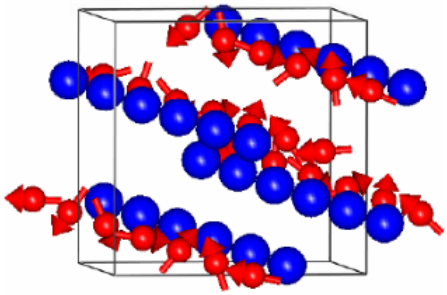

Figure 2: helical magnetic structure of MnGe.

The most intriguing features of the MnGe magnetic structure, which contrast with that of MnSi are: 1) a much higher magnetic transition (T_N= 170K) and ordered magnetic moment (M_0= 2.3μB) instead of T_N=29.5K and M_0=0.4μB in MnSi. 2) a much smaller helical wavelength (50 Å instead of 180 Å). 3) a strong temperature dependence of the helical wavelength 4) a lattice distortion at T_N and 5) a lock-in transition at 30K. The high T_N value combined with the small helical wavelength suggests that the spin orbit coupling is considerably enhanced. To get an

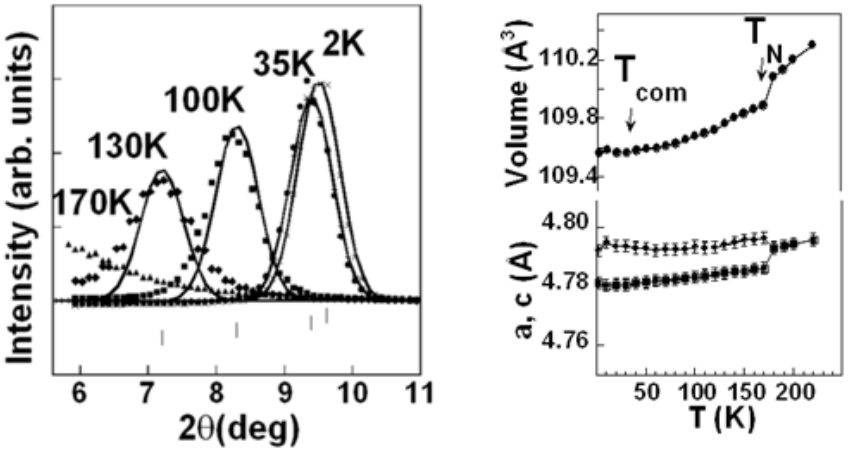

Figure 3: (a) the zero satellite measured on G6.1 and (b) the orthorhombic splitting measured on 3T2.

insight on these interactions, mean field calculations and spin waves measurements are on the way.

High pressure diffraction measurements are being performed on G6.1-MICRO, using the focusing devices and the newly installed bi-dimensional detector (Fig. 4a). In contrast with MnSi, where a small pressure of 1.4 GPa "kills" the helical order, the helixes of MnGe persist up to the highest pressure of 3.5 GPa. Here, the high intensity and neutron wavelength of the new G6.1 are crucial. Thanks to the 2D character of the detector, we have also observed that the helixes reorient along the axis of the pressure cell (Fig. 4b). This magnetic texture, similar to that induced by a magnetic field[5], suggests a pressure-induced structural transition, whose fingerprints are also seen on the nuclear Bragg peaks. A hypothesis to check in future.

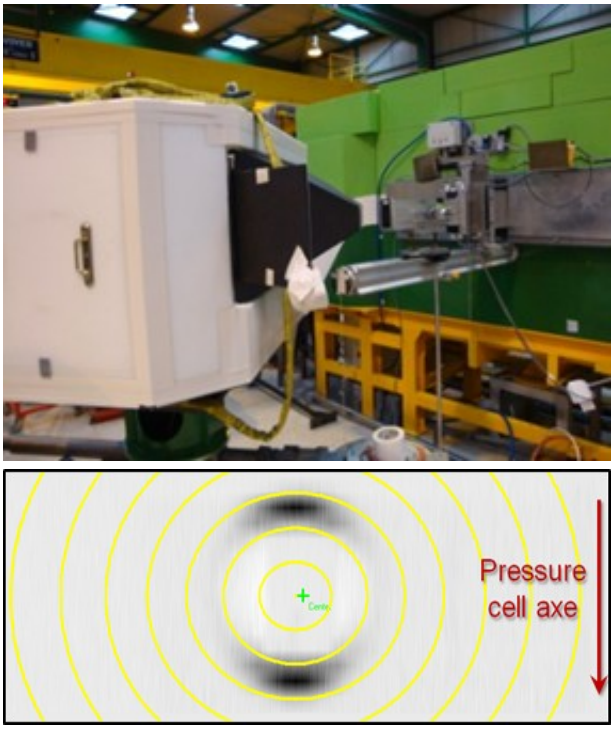

Figure 4: (a) the 2D detector and focusing devices on G6.1 in high pressure version. (b) The pressure induced magnetic texture is clearly visible on the zero satellite using the 2D detector, by an enhancement of the intensity along the axis of the pressure cell.

References

1. S. Mulhbauer *et al., Science* 323 915, (2009).
2. A. Hamann *et al., Phys. Rev. Lett*. 107, 037207, (2011).
3. N. Kanazawa *et al., Phys. Rev. Lett*. 106, 156603, (2011).
4. O. L. Makarova *et al., Phys. Rev*. B 85, 205205 (2012).
5. N. Kanazawa *et al., Phys. Rev*. B 86, 134425, (2012).

Competition between commensurate and incommensurate magnetic ordering in $Fe_{1+y}Te$

D. PARSHALL[A] , G. CHEN[A] , L. PINTSCHOVIUS[A] , D. LAMAGO[B,C] , TH. WOLF[B] , L. RADZIHOVSKY[A] , D. REZNIK[A]

a University of Colorado, Department of Physics, Boulder, Colorado 80309, USA

b Karlsruhe Institut für Technologie, Institut für Festkörperphysik, P.O. Box 3640, D-76021 Karlsruhe, Germany

c Laboratoire Léon Brillouin, CEA Saclay, France

dan.parshall@colorado.edu

$Fe_{1+y}Te$ is a parent compound in the family of iron-based high-temperature superconductors and develops long range antiferromagnetic order at low temperatures. The ordering wave vector depends on y, the occupation of interstitial sites with excess iron: it is commensurate for low y and becomes incommensurate for high y. The origin of this behavior is controversial. Using inelastic neutron scattering on $Fe_{1.08}Te$, we find incommensurate magnetic fluctuations above the Néel temperature, even though the ordered state is commensurate. This behavior can be understood in terms of a competition between commensurate and incommensurate order, which we explain as a lock-in transition caused by the magnetic anisotropy.

$Fe_{1+y}Te_{1-x}Se_x$ belongs to the recently discovered iron-based superconductors (FeSCs)[1] with quite high transition temperatures. These compounds contain a simple square lattice of iron atoms, coordinated with pnictogen or chalcogen atoms forming planes of tetrahedra. Their high-T_c superconductivity may be related to the magnetic order[2], which seems to be the result of Fermi-surface nesting[3]. There is also intrinsic interest in magnetism in these materials, but it has not been as extensively explored.

The magnetic order in the $x = 0$ endpoint of the $Fe_{1+y}Te_{1-x}$ Se_x series is a highly unusual "bicollinear" magnetic structure[4] with a wave vector along

$\mathbf{q}_{AFM}$ = [1/2, 0, 1/2]. The ordering wave vector is commensurate for small y and becomes incommensurate near the critical value $y = 0.12$.

We made a detailed inelastic neutron scattering (INS) investigation of a sample with intermediate $y = 0.08$ on the 1T1 triple-axis spectrometer at the Laboratoire Léon Brillouin[5]. We found strong evidence for competition between commensurate and incommensurate ordering in the form of spin excitations which abruptly shift from the incommensurate $\mathbf{q}_{inc} \approx [0.45, 0, 0.5]$ to the commensurate wave vector $\mathbf{q}_{AFM}$ = [1/2, 0, 1/2] when passing below the Néel temperature T_N (see Fig. 1). Fig. 2 shows $S(q,\omega)$, and summarizes the energy and wave-vector dependence of the magnetic inelastic scattering above and below T_N. Above T_N it is incommensurate, broad, and ungapped. Below T_N it is commensurate, narrow, and gapped. Both have nearly vertical dispersion within the experimental uncertainty.

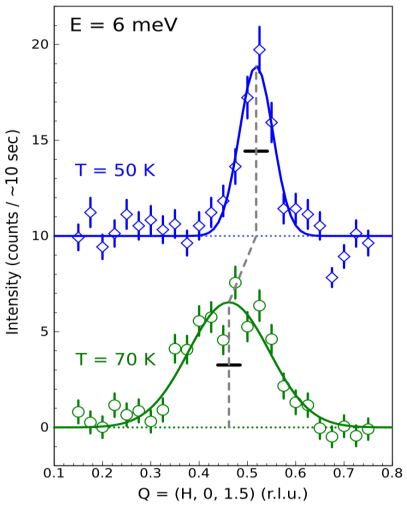

Figure 1 Scans through [H,0, 12] with E = 6 meV, taken above and below $T_N = 67.5$ K. The black horizontal bar shows the estimated resolution width. The shift of the spin fluctuations from the commensurate to incommensurate position (when warming from the ordered to paramagnetic state) is also shown. Data are background-substracted, and offset for clarity.

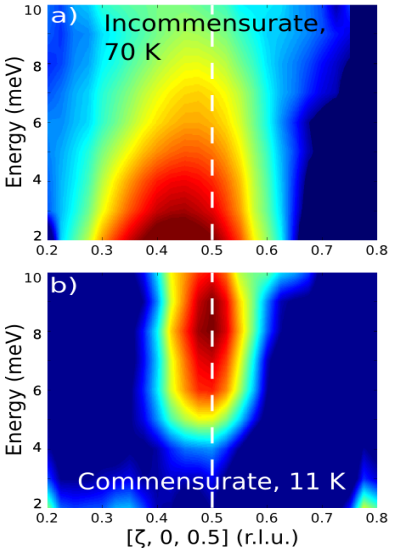

Figure 2 : Energy dependance of the spin excitations. $S(q,\omega)$ at $T = 70$ K (a) and 11 K (b). The data have been smoothed and background-substracted. Intensity is plotted on a logarithmic scale (arb. units).

Upon approaching the Néel transition from above, the height of the incommensurate peak becomes greater. This can largely be accounted for by enhanced correlations along the c-axis, preserving the overall intensity (data not shown). This behavior is reminiscent of a second-order transition, in which critical fluctuations build up eventually condensing into a new Bragg peak. However, close to T_N, the intensity of the incommensurate

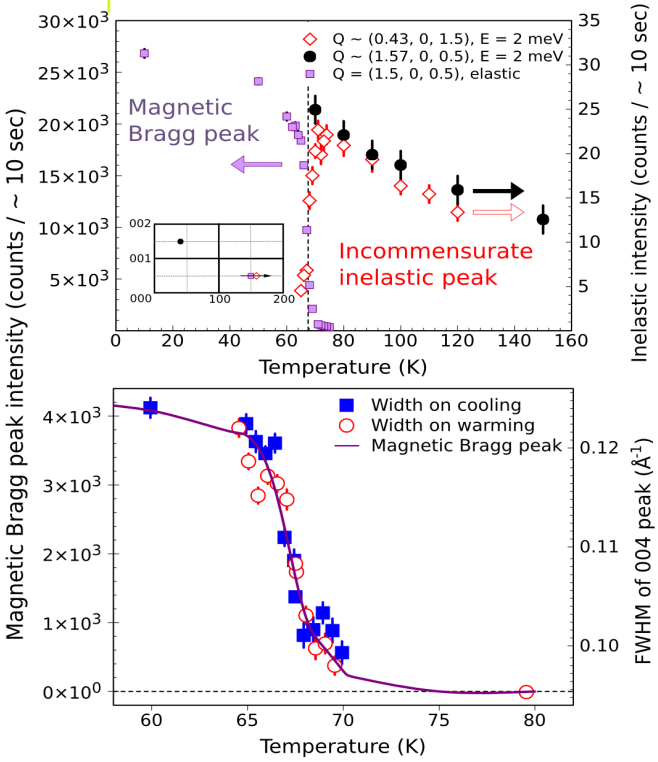

Figure 3 : Temperature dependance of the magnetic and structural behavior. (a) Peak intensities of the incommensurate magnetic excitation and the [1.5, 0, 0.5] magnetic Bragg peak as a function of temperature. Inset: Map of reciprocal space, showing the locations of the scans. (b) Width of the [0,0,4] nuclear Bragg peak (an indicator of monoclinic splitting) as a function of temperature, showing the structural transition at 67.5 K. This is plotted together with the intensity of the [2.5,0,0.5] magnetic Bragg peak, demonstrating the close coincidence between the structural and magnetic scattering.

fluctuations drops rapidly to zero. At the same time, a magnetic Bragg peak appears at the commensurate wavevector, with a rapid rise of the intensity characteristic of a first-order transition. This magnetic transition is concurrent with a change in structure from tetragonal to monoclinic (Fig. 3).

Our results may be captured by a simple model, in which the spin rotation symmetry is explicitely broken by the single-ion anisotropy. The low T monoclinic phase features both an orthorhombic distortion with shortening along the *b* axis, as well as a monoclinic shearing of Te planes along the *a* axis. Thus the crystal field environment becomes anisotropic, and the degeneracy between the d_{xz} and d_{yz} orbitals is lifted. This anisotropy creates an energy gap, which „locks-in" the spins along the *b* axis, even though the exchange energy would prefer an incommensurate value. At higher doping, the incommensurabilty is greater, and eventually the penalty from the exchange energy to form a commensurate wavevector outweighs the benefit of the anisotropy gap. At this doping, the ordering becomes incommensurate.

To conclude, we have observed clear signatures of a competition between commensurate and incommensurate magnetism in a well-characterized sample of $Fe_{1.08}Te$. We find incommensurate fluctuations above T_N, which give way to commensurate order below T_N with a gap in the excitation spectrum. This behavior can be understood in terms of a lock-in transition induced by the spin anisotropy gap which is present in the monoclinic bicollinear phase and absent in the tetragonal phase.

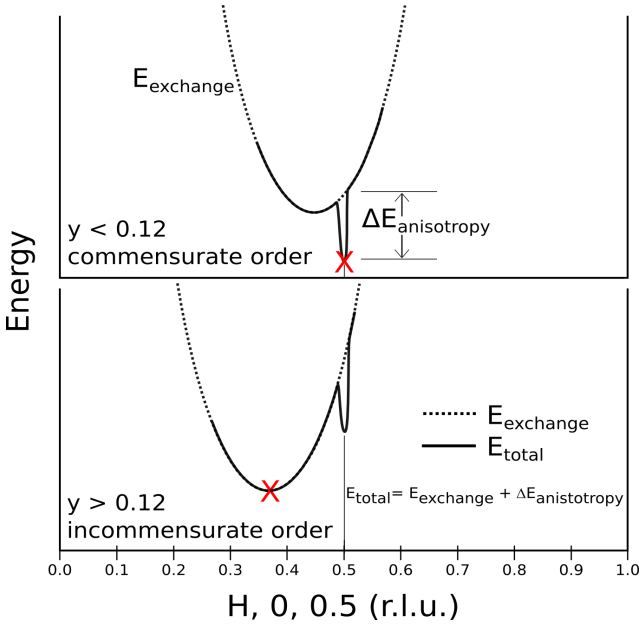

Figure 4 : Schematic of the magnetic energy in Fe_{1+y} at zero temperature, for two values of the excess iron concentration.

References

1. Y. Kamihara, T. Watanabe, M. Hirano, & H. Hosono, *J. Am. Chem. Soc.* **130**, 3296 (2008).
2. I. I. Mazin, D. J. Singh, M. D. Johannes, & M. H. Du, *Phys. Rev. Lett.* **101**, 057003 (2008).
3. D. J. Singh & M.-H. Du, *Phys. Rev. Lett.* **100**, 237003 (2008).
4. W. Bao *et al.*, *Phys. Rev.Lett.* **102**, 247001 (2009).
5. D. Parshall, G. Chen, L. Pintschovius, D. Lamago, Th. Wolf, L. Radzihovsky, & D. Reznik, *Phys. Rev.* B **85**, 140515 ® (2012).

New step towards the search for the origin of high-transition temperature superconductivity: exploration of the phase diagram and observation of magnetic excitation modes in cuprates

YUAN LI[A,B] G. YU[C], M. K. CHAN[C], V. BALÉDENT[D], YANGMU LI[C], N. BARIŠIĆ[C,F], X. ZHAO[C,F], K. HRADIL[G], R. A. MOLE[H], Y. SIDIS[D], P. STEFFENS[I], P. BOURGES[D], M. GREVEN[C]

a Department of Physics, Stanford University, Stanford, California 94305, USA,

b Max Planck Institute for Solid State Research, 70569 Stuttgart, Germany,

c School of Physics and Astronomy, University of Minnesota, Minneapolis, Minnesota 55455, USA,

d Laboratoire Léon Brillouin, CEA Saclay, France

e Physikalisches Institut, Universität Stuttgart, 70550 Stuttgart, Germany

f State Key Lab of Inorganic Synthesis and Preparative Chemistry, College of Chemistry, Jilin University, Changchun 130012, China.

g Institut für Physikalische Chemie, Universität Göttingen, 37077 Göttingen, Germany,

h Forschungsneutronenquelle Heinz Maier-Leibnitz, 85747 Garching, Germany,

i Institut Laue Langevin, 38042 Grenoble CEDEX 9, France.

yvan.sidis@cea.fr

Understanding the origin of new supraconductivities is a major challenge and essential for the development of these materials and their current and future applications. Prior to the recently discovered pnictides, cuprates still hold the record temperature for superconductivity. For this class of material, magnetism plays a central role in the phase diagram that it is therefore necessary to explore, in close connection with the properties of superconductivity.

A collaboration of researchers (German, Chinese and French of LLB) investigated by neutron scattering the spin-polarized magnetic phase diagram of these compounds as well as different modes of magnetic excitations associated. All of the available modes predicted by the original loop currents theory of C. M. Varma, assigning a magnetic cause to the origin of superconductivity in these compounds, have been observed.

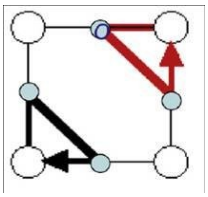

In the phase diagram of cuprate superconductors, a phase of "pseudo-gap" appears as a precursor of the superconducting state. Without defining a perfect superconducting gap, the electronic structure of this phase shows a very low density of states around the Fermi level, and condensed matter physicists regard it as the "Rosetta Stone" to help to discover the fundamental physical principles at the origin of the exotic properties of these materials.

Since 2006, measurements of elastic scattering of spin polarized neutron give new information on this phase. These measurements in fact reveal the presence of long-range magnetic order[1,2]. The magnetic state, observed similarly in 4 families of cuprate superconductors, is consistent with the existence of a *state of orbital currents charges loops*, as proposed in the theory of pseudo-gap of C. M. Varma[3]. In this model, the current loops appear spontaneously in every unit cell between copper and neighboring oxygen when the material enters the pseudogap phase and scattering measurements of polarized neutrons carry the signature of the induced orbital magnetic moment.

Associated with the magnetic ordering of the system, an order parameter can be defined that has a degeneracy of four basic states defined by the rotation direction of the current loops (see Fig. 1). This degeneracy enables the emergence of collective electronic excitations in the system, which are also characteristics of the established order. Collective fluctuations in the condensed system in one of the four basic states, allow the system to be excited in any of the other 3 (Fig. 1)[4].

In 2010, measurements of inelastic neutron scattering have revealed the existence of a first *magnetic excitation specific to the pseudogap phase* in the monolayer compound[5] $HgBa_2CuO_{4+d}$. This almost non-dispersive excitation is compatible with a simple reversal of the current loops. Following this initial observation, the theoretical predictions were refined[6]. In a simple system (such as com-

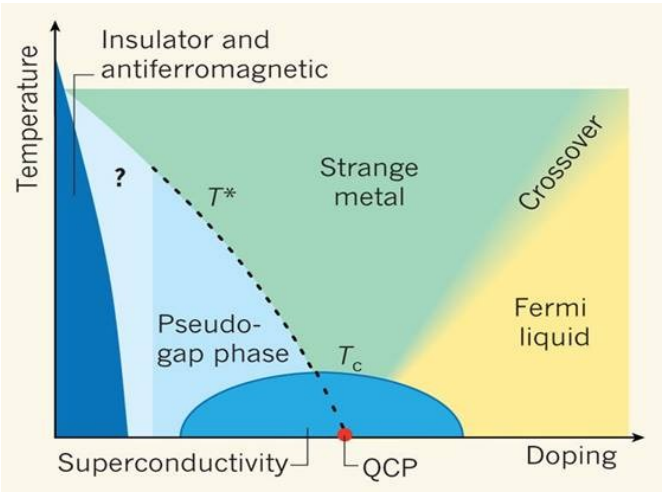

Figure 1: Generic phase diagram temperature-oxygen concentration in cuprates. QCP is the "Quantum Critical Point", the critical point at zero temperature.

pound $HgBa_2CuO_{4+x}$), the theory predicts the existence of three collective excitations (Fig. 2): two possibly observable by inelastic neutron scattering (ω_1, ω_2) and a third observable by inelastic scattering of rays X or Raman spectroscopy (ω_3). Recent measurements of inelastic neutron scattering on two samples of $HgBa_2CuO_{4+d}$ just confirmed the existence of the second magnetic excitation mode observable by neutron scattering in the pseudogap phase[7].

The observation of a magnetic order in the pseudogap state and of a single excitation spectrum, brings credit to the theory of loop currents of C. M. Varma. The work carried out in synergy between experiment and theory opens new perspectives for understanding the electronic properties of exotic superconducting cuprates. It remains to prove that the magnetic coupling from current loops is at the origin of the unconventional superconductivity in these materials.

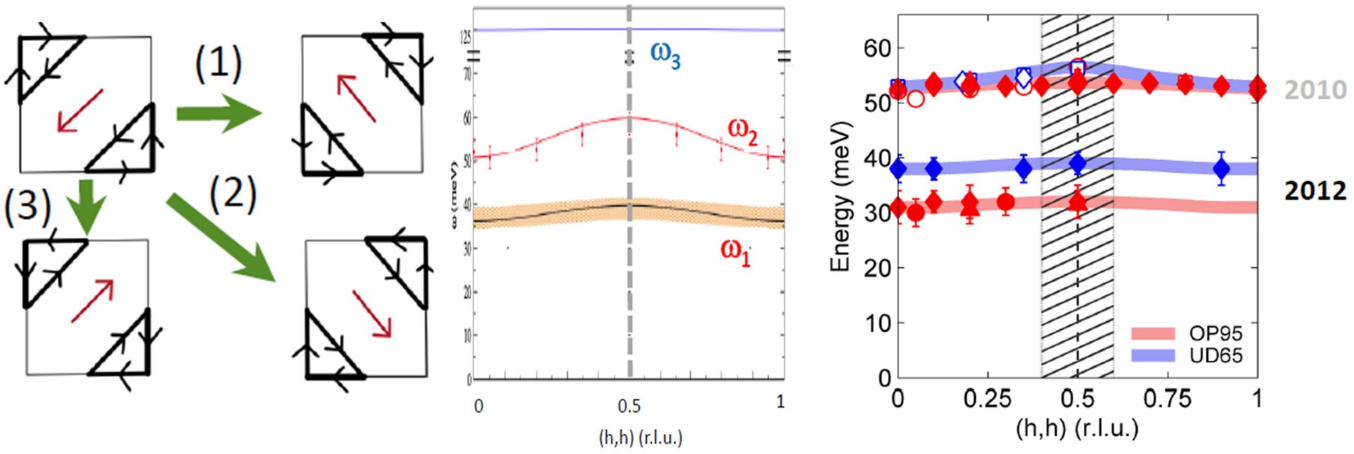

Figure 2.: A) 4 states of current loops . B) Collective excitations (ω_1, ω_2, ω_3) theoretically predicted . C) Observation of two excitations active in neutron spectroscopy in two separate samples (OP95 red and UD65 blue) of $HgBa_2CuO_{4+d}$

References

1. B. Fauqué, Y. Sidis, V. Hinkov, S. Pailhès, C. T. Lin, X. Chaud, and P. Bourges, *Phys. Rev. Lett.*, **96**, 197001 (2006).

2. Y. Li, V. Balédent, N. Barii, Y. Cho, B. Fauqué, Y. Sidis, G. Yu, X. Zhao, P. Bourges & M. Greven, *Nature*, **455**, 372 (2008).

3. C.M. Varma, *Phys. Rev.* B**, 73**, 155113 (2006).

4. C.M. Varma, News and Views, *Nature* **468** (2010) 184.

5. Yuan Li, V. Balédent, G. Yu, N. Barišić, K. Hradil, R.A. Mole, Y. Sidis, P. Steffens, X. Zhao, P. Bourges, M. Greven, *Nature*. 468 (2010) 283.

6. Yan He and C. M. Varma, *Phys. Rev. Lett*. 106 (2011) 147001.

7. Yuan Li, G. Yu, M. K. Chan, V. Balédent, Yangmu Li, N. Bariši′c, X. Zhao, K. Hradil, R. A. Mole, Y. Sidis, P. Steffens, P. Bourges and M. Greven, *Nature Physics* **8** (2012) 404.

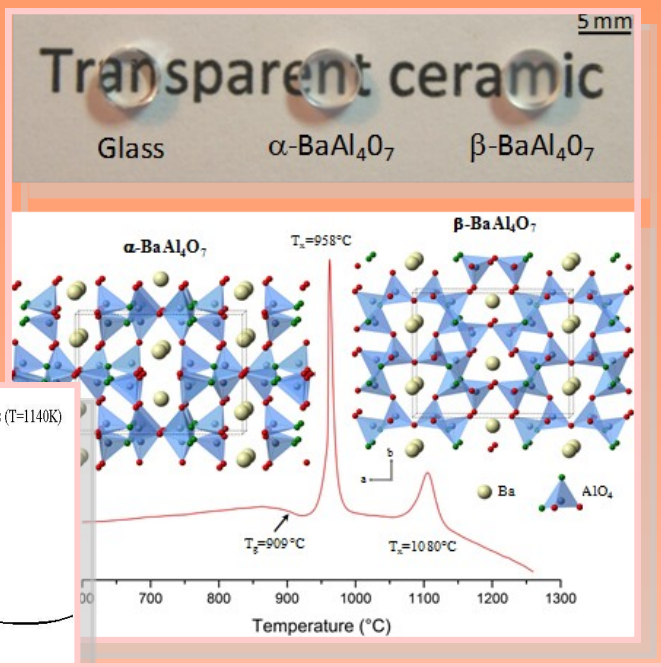
5 mm
Transparent ceramic
Glass
α-BaAl4O7
β-BaAl4O7
α-BaAl4O7
β-BaAl4O7
Tx=958°C
Tg=909°C
Tx=1080°C
Ba
AlO4
Temperature (°C)

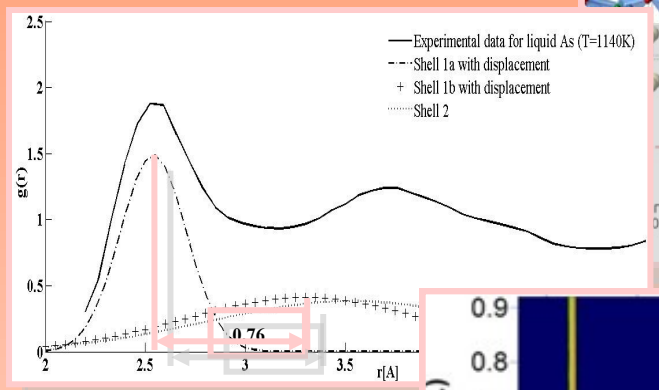
Experimental data for liquid As (T=1140K)
Shell 1a with displacement
Shell 1b with displacement
Shell 2
g(r)
r[A]
0.76

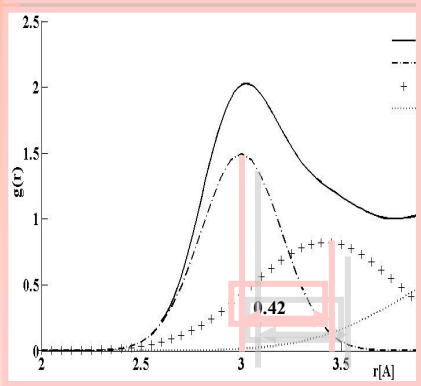
g(r)
r[A]
0.42

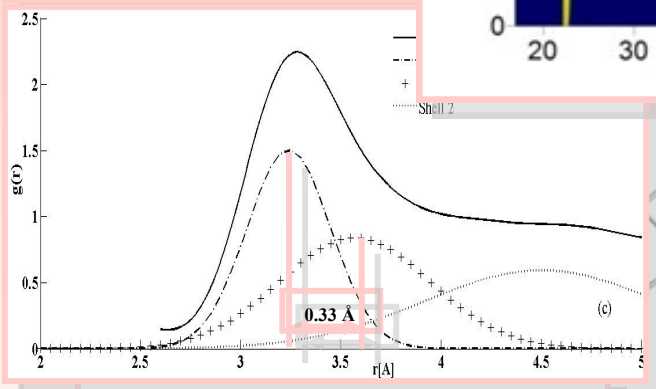
Shell 2
g(r)
r[A]
0.33 Å
(c)

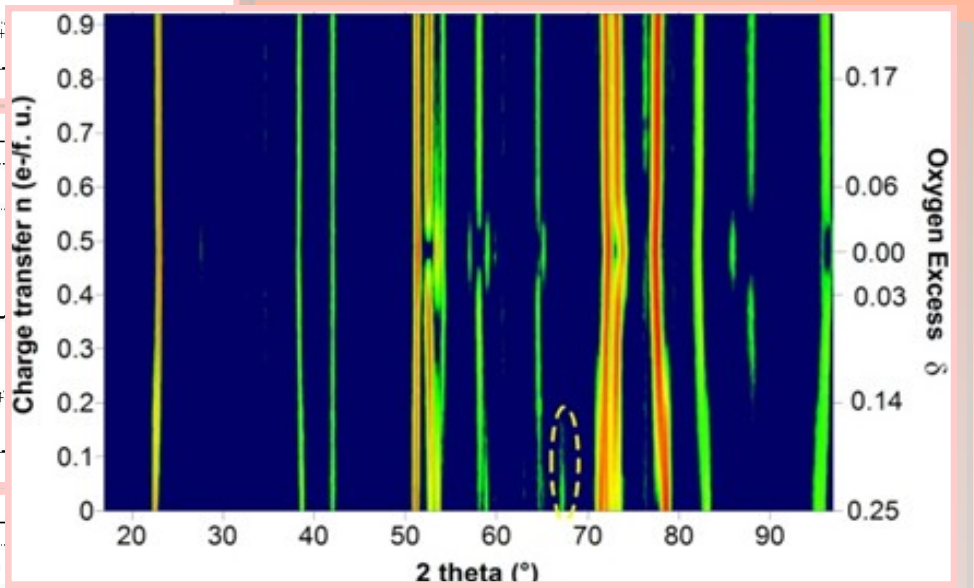
Charge transfer n (e-/f. u.)
Oxygen Excess δ
2 theta (°)

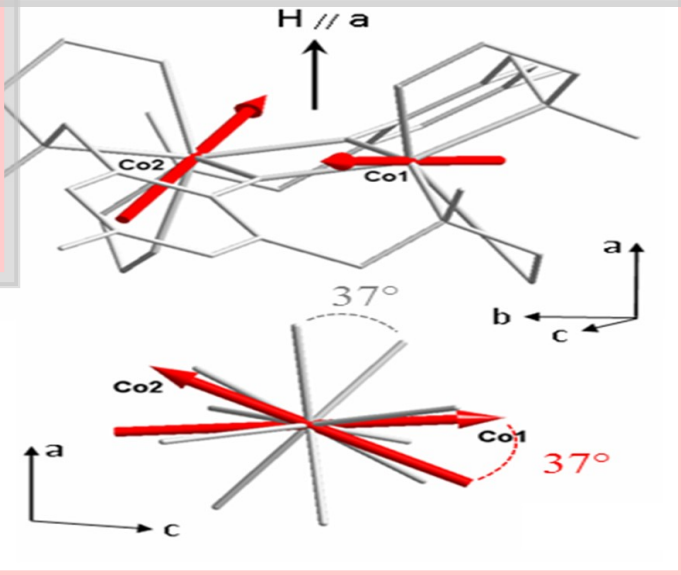
H // a
Co2
Co1
a
b
c
37°
Co2
Co1
37°
a
c

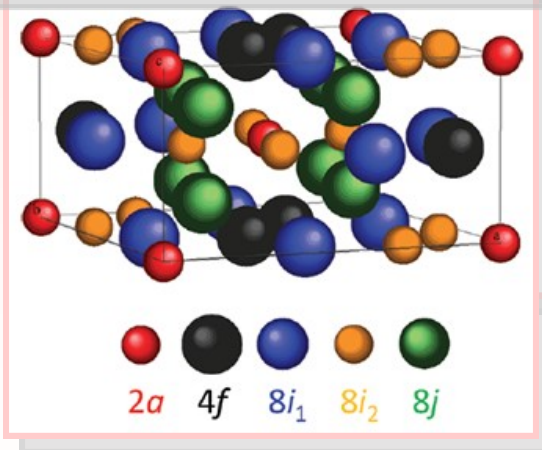
2a
4f
8i1
8i2
8j

AXE 2:

Materials and Nanosciences : Fundamental Studies and Applications.

The second axis, "Materials and Nanosciences: Fundamental Studies and Applications", covers the activities related to the research in materials sciences and more generally in hetero-systems (interfaces, alloys, composites materials, confined systems). The studies cover detailed structures of nano-objects, interactions between nano-objects, and the role of nanostructures in composite materials. The length-scales which characterize the properties of the systems range between 1-100 nm. More specifically, the following areas are addressed at the LLB: *Magnetic nanostructures* (metallic layers, oxide epitaxial layers, nanoparticles) studied by diffraction, SANS and reflectometry; *Composite materials* (polymer reinforcement by nano-particles, metallurgical composites) whose properties are studied by SANS; *Metallurgy* (both fundamental and industrial) where Textures and Strain heterogeneities are studied by diffraction in various alloys or nuclear materials; *Confined systems (*microporous materials and organized guest-hosts systems, mesoporous materials and organized guest-hosts systems) in which the dynamics of the confined elements can be studied by inelastic scattering techniques; *Amorphous materials* (disordered systems – glasses) where the local atomic order is also investigated by diffraction.

- **Short range order in anomalous liquid metals**
  Y. Shor, E.Yahel, E.N. Caspi,Y. Greenberg, B. Beuneu and G. Makov

- **Novel highly transparent barium aluminate ceramic synthesized by full crystallization from glass**
  M. Allix, S. Alahrache, F. Fayon, M. Suchomel, F. Porcher, T. Cardinal and G. Matzen

- **Structural evolution of $Nd_2NiO_{4+\delta}$ and $Pr_2NiO_{4+\delta}$ studied during electrochemical oxygen intercalation by *in situ* neutron powder diffraction**
  M. Ceretti, O.Wahyudi, A.Villesuzanne, J.M. Bassat, G. André, F. Porcher, J. Stern and W. Paulus

- **Molecular magnetism: probing the local anisotropy with polarized neutrons**
  A. Borta, B. Gillon, A. Gukasov, A. Cousson, D. Luneau, E. Jeanneau, I. Ciumacov, H. Sakiyama, K. Tone and M. Mikuriya

- **Comparison of the site occupancies determined by combined Rietveld refinement and by DFT calculations: the example of the ternary Mo-Ni-Re σ phase**
  K.Yaqoob, J.-C. Crivello, J.-M. Joubert and F. Porcher

Short range order in anomalous liquid metals[1]

Y. SHOR[A], E. YAHEL[B] , E.N. CASPI[B], Y. GREENBERG[B], B. BEUNEU[C], G. MAKOV[A]

a Materials Engineering Department, Ben Gurion University of the Negev, P.O. Box 653, Be'er Sheva, Israel 84105

b Physics Department, NRCN, P.O.Box 9001, Be'er Sheva, Israel

c Laboratoire Léon Brillouin, CEA Saclay, France

makovg@bgu.ac.il

We present an analysis of the short range order in liquids using a modified quasi-crystalline model of liquid structure. This model is shown to fit the experimental radial distribution function (RDF) very well. We apply this model to measurements of the structure factors of the pnictides taken at the 7C2 diffractometer. We find that the short range order in the liquid pnictides is dominated by an A7-like structure with two types of bonds, in close agreement with the underlying solid phase. The existence of two bond lengths is necessary, within this model, to explain the asymmetry in the first peak as well as the change in coordination number along the pnictide series.

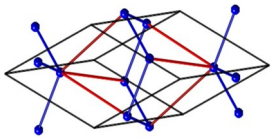

The structure of the metallic pnictides (below P) was measured by neutron diffraction at the 7C2 diffractometer at LLB by several groups[2,3,4]. It is found that the RDF exhibits an asymmetric shape of the first hard sphere (HS) peak and a sub-structure between the first and second HS peaks, which manifests itself in an additional intermediate peak in As, as a hump in Sb and as a shoulder in Bi (Fig. 1). The distorted structure observed in l-As, diminishes along the metallic pnictide series. In agreement, the number of nearest neighbors increases along the series from a coordination number of 3 for As to 6 for Sb or As at high pressure[1,2]. In Bi the coordination number increases further to 8 implying a possible transition to a bcc-like structure.

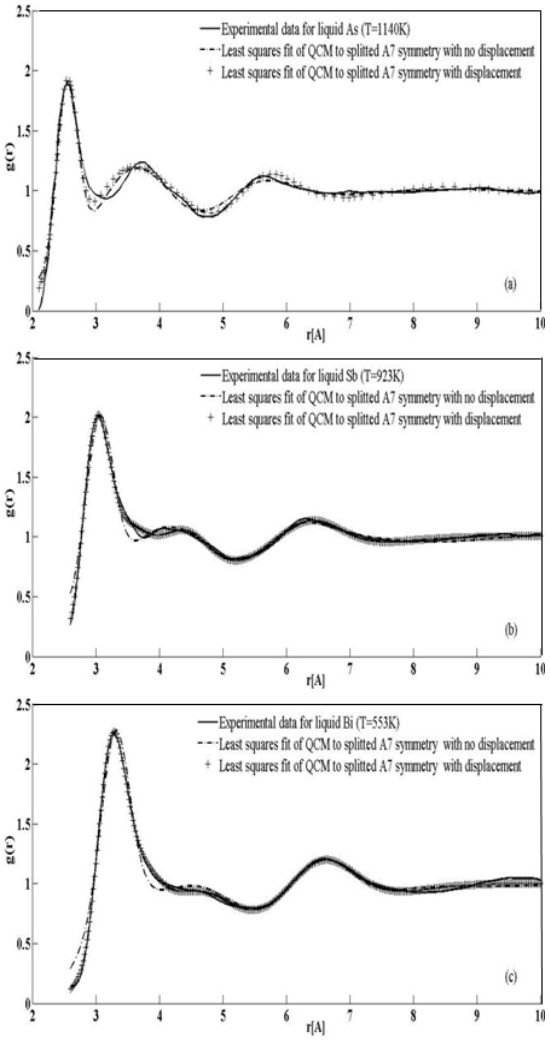

Figure 1: Radial distribution functions of the metallic pnictides and the least squares fit to a split A7 symmetry with and without displacement.

The quasi-crystalline model (QCM) analyses the short range order (SRO) of the liquid in terms of an underlying crystal lattice structure. In this model, the liquid structure is characterized by: (i) a lattice symmetry; (ii) lattice parameters; (iii) thermal broadening and (iv) a persistence length scale of SRO in the liquid. These parameters are determined by fitting the experimental RDF to the model, providing both a definition of SRO of the liquid and its symmetry and is therefore well suited to the analysis of extensive experimental data. The QCM has been shown to reproduce the RDF of simple elemental liquids and has been applied to interpret the structure of more complex liquids such as He, Hg and Ga.

The radial distribution function, g(r), of a solid crystal, may be modeled by summing the contributions of spherical shells of atoms at distances r_i from a reference atom located at the origin. At

zero temperature and in an ideal crystal, each such contribution has the form of a δ function.

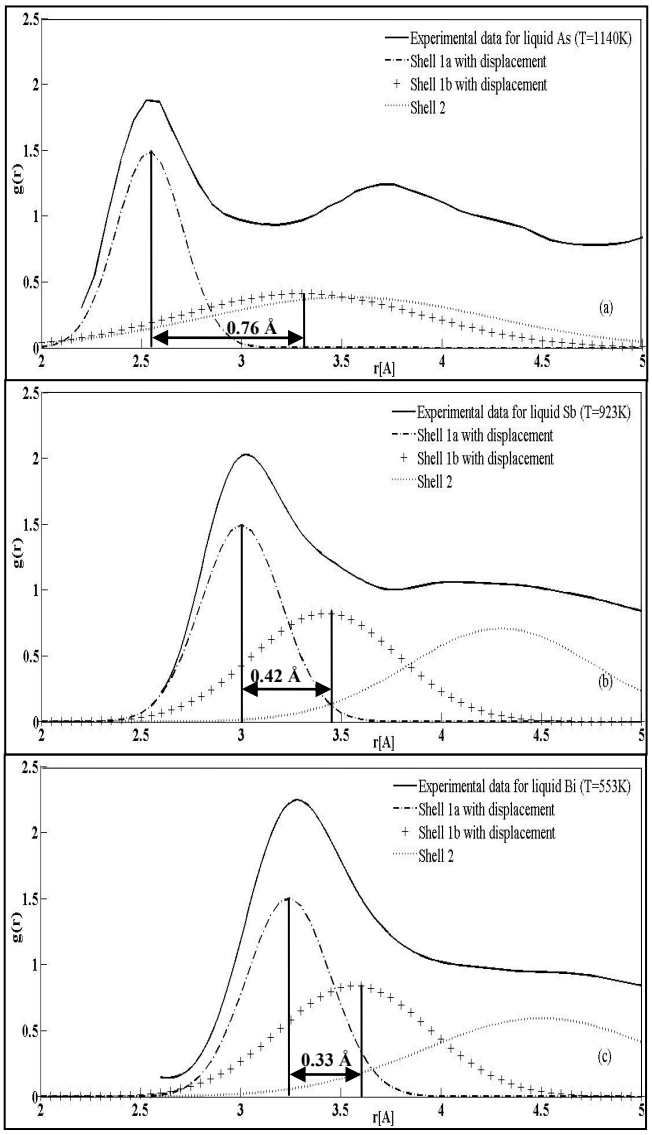

Figure 2: Detailed blow-up of the short range order in the QCM showing the displacement of the two subshells of the first nearest neighbours and their contribution to the total RDF.

At finite temperatures, each such contribution is smeared out in a Gaussian form:

$$g(r) = \sum_{i=1}^{\infty} \frac{n_i}{4\pi r_i^2} \cdot \frac{1}{\sqrt{2\pi\sigma_i^2}} \cdot e^{-\frac{(r-r_i)^2}{2\sigma_i^2}}$$

where n_i is the number of atoms on the i^{th} shell of atoms, located at radius r_i about the origin.

In a solid crystal, the variance σ_i, originates from thermal excitations, is independent of the shell number i and is determined entirely by the temperature and the elastic restoring force. The QCM of liquid structure assumes that the RDF of the liquid may be obtained in terms of an underlying crystalline lattice, by allowing the Gaussian distribution width to increase with increasing distance from the reference atom at the origin. Thus, at long distances, the structure is smeared out, namely uncorrelated and there remains no indication of the underlying crystalline order.

In the present work we found that simple linear models of the variance are insufficient to represent the experimentally determined RDF of liquids from group V. We allowed the variances of each shell to vary independently up to a certain shell and from then onwards to represent them by a linear model. This model we shall term as "the independent variances model".

A successful fit to the RDFs of the liquid pnictides was only achieved for the A7-like structure and furthermore this fit was improved if the first nearest neighbours were divided into two sub-groups displaced from each other by a short distance (Fig. 2). This short range order is in excellent agreement with the crystal structure of these elements in their solid state and in particular in the distances of the first nearest neighbours.

References

1. Y. Shor, E. Yahel and G. Makov, *J. Non-Crys. Sol.*, 358, 2687 (2012).
2. Y. Greenberg, E. Yahel, E. N. Caspi, C. J. Benmore, B. Beuneu, G. Makov, M. P. Dariel, *Europhys. Lett*.86 36004 (2009).
3. Y. Greenberg, E. Yahel, E. N. Caspi, B. Beuneu, M. P. Dariel, G. Makov, *J. Chem. Phys.*133, 094506 (2010).
4. C. Bergman, A.,Pellegatti, R.,Bellissent, A.,Menelle, R.,Ceolin, J-P.,Gaspard, *Physica* B157, 158 (1989).

Novel highly transparent $BaAl_4O_7$ ceramic obtained by full crystallization from glass

M. ALLIX[A], S. ALAHRACHE[A], F. FAYON[A], M. SUCHOMEL[B], F. PORCHER[C], T. CARDINAL[D], G. MATZEN[A]

a CEMHTI, Orléans, France

b APS, Argonne, USA

c Laboratoire Léon Brillouin, CEA Saclay, France

d ICMCB, Bordeaux, France

mathieu.allix@cnrs-orleans.fr

Transparent polycrystalline ceramics are an emerging class of photonic quality materials competing with single crystal technology for a diverse range of optical applications. A limited number of either cubic or nano-crystalline transparent polycrystalline ceramics are known, but require complex and time-consuming synthetic approaches. Here we show for the first time that fully dense transparent polycrystalline ceramics can be simply obtained by direct and complete crystallization from glass.

This is demonstrated for the previously unreported composition, $BaAl_4O_7$, which exhibits two orthorhombic polymorphs with micron grain size, both optically transparent in the visible range. This innovative synthetic route to transparent polycrystalline ceramics should facilitate the discovery of new cost-effective chemistries for transparent ceramic applications.

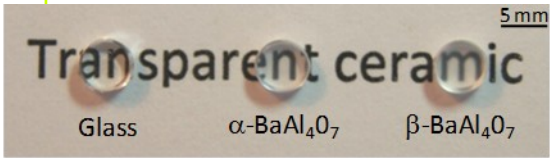

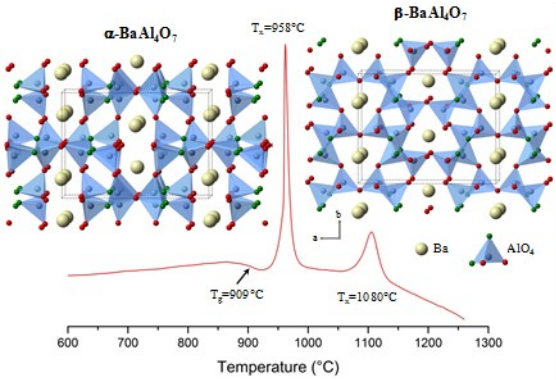

Synthesis of the barium aluminate glass precursor employed an aerodynamic levitator system equipped with two CO_2 lasers allowing for the high temperature melt (2100°C) and rapid quenching of a $33.3BaO\text{-}66.7Al_2O_3$ molar nominal composition under contactless conditions. Differential scanning calorimetry (DSC) data collected as a function of temperature clearly show the glass transition, a strong exothermic peak corresponding to crystallization of the α phase and a broader second exothermic peak corresponding to the α- to β-$BaAl_4O_7$ transition. TEM studies of the resulting materials reveal pore free, fully dense polycrystalline microstructures with extremely thin grain boundaries (Fig. 1). Large micron scale grains are observed; with a slight increase in domain size on transition from the α (0.5-2 µm) to β polymorphs (1-5µm).

Structural details of both $BaAl_4O_7$ polymorphs were elucidated by a combination of transmission electron microscopy and powder diffraction data from high-resolution synchrotron and neutron instruments. Reciprocal space reconstruction using electron diffraction data finds orthorhombic symmetry for both polymorphs with no systematic extinctions, implying primitive (P) lattices and hk0: k=2n and hk0: h+k=2n special existence conditions, suggesting $Pm2_1b$ and $Pm2_1n$ space groups for the α and β $BaAl_4O_7$ polymorphs, respectively. Electron diffraction also affirms that both crystalline $BaAl_4O_7$ phases are free from superstructure (extra reflections) and residual non-crystalline phases (diffuse streaks). Bragg peaks in the synchrotron powder diffraction data were successfully indexed using an orthorhombic cell with unit cell parameters: a=12.8821(4)Å, b=10.2357(3)Å and c=4.9075(2)Å for α-$BaAl_4O_7$, and a=12.7735(4)Å, b=9.1930(3)Å and c=5.5485(2)Å for β-$BaAl_4O_7$. For each possible space group *ab initio* structure determination was performed against the synchrotron powder diffraction data using the Superflip program implemented in the Jana software package. This approach assisted in the identification of all cation and most oxygen positions for the two phases. Rietveld method refinements of the proposed structures against neutron powder diffraction data aided in the ascertainment of final oxygen positions by an inspection of Fourier maps, and provided more reliable atomic thermal parameters for the clarified models.

The best structural models, validated by their statically match with the diffraction data, were

obtained with $Pm2_1b$ and $Pm2_1n$ space groups, for α and β phases respectively.

The structures of the two $BaAl_4O_7$ polymorphs are presented in the top figure. Both polymorphs exhibit full site occupancy on two *2a* Ba sites, four *4b* Al sites and eight (six *4b* and two *2a*) O sites. Seven of the oxygen atoms form large polyhedra surrounding Ba cations, which in turn fill channels created by corner sharing AlO_4 tetrahedra. The remaining oxygen anions are effectively shared by three AlO_4 tetrahedra in an unusual tri-coordinated environment previously observed for select calcium and strontium aluminates. Interestingly, the fraction of tri-coordinated oxygen anions in $BaAl_4O_7$ is higher in the β polymorph (28.6% of all anions) than in the α (21.4%).

The exceptional transparency displayed by both crystalline $BaAl_4O_7$ polymorphs is even more remarkably given their large micron-scale grain size and anisotropic crystal structures. Experimental measured average refractive index values (n) for the polished $BaAl_4O_7$ glass and polycrystalline samples are nearly constant (n=1.66 at l = 514.5 nm). This equates to an 88% maximum theoretical transmittance value for the three materials. These theoretical values were compared with experimental measured transmission spectra using a commercial spectrophotometer. Transparency in the glass sample is found to match the theoretical value all over the entire visible and the near IR range proving the absence of scattering centers within the quenched sample. For the sintered polycrystalline ceramics, the α-$BaAl_4O_7$ polymorph displays outstanding transparency over a wide range of wavelengths from the IR well into the visible range, with a measured transmission value of 59.2% at 633 nm. The β-$BaAl_4O_7$ polymorph shows a respectable 39.5% transmission value at 633 nm.

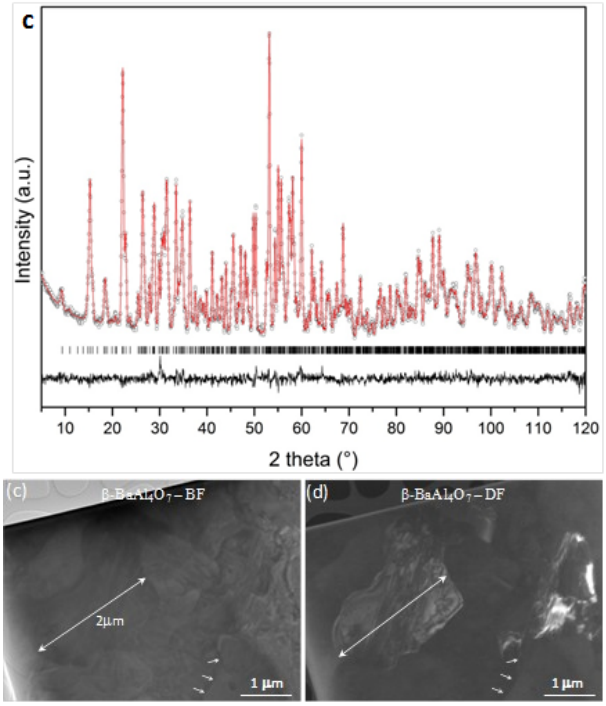

Figure 1: (top) Rietveld refinement plot of ambient temperature powder neutron diffraction data. (down) Bright field and dark field transmission electron microscopy images for the β-$BaAl_4O_7$ polymorph showing high density, narrow grain boundaries (small arrows) and fine microstructures (~ 1-5µm grain size).

All previous reports of transparency in anisotropic (non-cubic) polycrystalline ceramics have required specific synthesis approaches to achieve nanometer-size domains. To better understand the surprisingly high transparency shown by these new anisotropic $BaAl_4O_7$ polymorphs with micron scale microstructure, we have performed density functional theory (DFT) calculations of the dielectric function ε(ω) from the periodic structures of the two polymorphs. The refractive indexes were then deduced. The as-calculated average refractive indexes at λ = 514.5 nm are in good agreement with the measured values but the main interest here lies in the birefringence determination. The refractive index spectra of the two polymorphs calculated for the (100), (010) and (001) polarizations are very close over a wide wavelength range, leading to a weak calculated birefringence (from 0.014 to 0.010 for the α-phase and 0.009 for the β-phase). High transparency is thus a consequence of the rather small birefringence between different polarizations direction. We speculate that the grain size variation observed by microscopy in α- and β-phases is the origin of the transparency difference between polymorphs. These birefringence results for the polycrystalline $BaAl_4O_7$ ceramics suggests that, contrary to previous assumptions, structural and optical isotropy is not a prerequisite to achieve macroscopic transparency in micron scale grain ceramics. Therefore, the combination of weak birefringence, high density (absence of pores) and very thin grain boundaries allows the achievement of transparent ceramic with micron grain scale.

References

1. M.Allix, S.Alahrache, F.Fayon, M.Suchomel, F.Porcher, T.Cardinal, G.Matzen, *Advanced Mater.*, 24 5570-5575 (2012).

Structural evolution of $RE_2NiO_{4+\delta}$ (RE=Nd, Pr) studied during electrochemical oxygen intercalation by in situ neutron powder diffraction

M. CERETTI[A], O. WAHYUDI[B,C], A. VILLESUZANNE[C], J.M. BASSAT[C], G. ANDRÉ[D], F. PORCHER[D], W. PAULUS[A]

a Institut Charles Gerhardt, UMR Univ. Montpellier 2 CNRS 5253, Montpellier, France

b Université de Rennes 1, Rennes, France

c ICMCB, PESSAC, France.

d Laboratoire Léon Brillouin, CEA Saclay, France

monica.ceretti@univ-montp2.fr

Oxygen ion conductors at low temperatures are materials of major interest for a series of applications in the area of solid state ionics (fuel cells, battery electrodes, sensors, catalysts etc.). Nevertheless, solid oxygen ion conductors work reasonably only at fairly high operating temperatures, which make their application, especially for fuel cells, rather limited. Various compounds with K_2NiF_4 type structure have however shown topotactic oxygen uptake by electrochemical reaction at ambient temperature and thus are key systems to better understand the low temperature oxygen diffusion mechanism.

In this study we investigated for the first time the oxygen mobility by in situ neutron powder diffraction during electrochemical oxygen intercalation in $Nd_2NiO_{4+\delta}$ and $Pr_2NiO_{4+\delta}$. This allowed real time observation of the structural/phase change as a function of the charge transfer, and thus of the oxygen stoichiometry.

$RE_2NiO_{4+\delta}$ (RE=Nd, Pr) are today the most promising candidates as oxygen membranes or electrolytes in Solid Oxide Fuel Cells (SOFCs), as they show high oxygen ion mobility at already room temperature. These compound crystallize in the K_2NiF_4 structure type and can accommodate extra oxygen atoms on interstitial sites, the non-stoichiometric region being $0 < \delta < 0.25$. As fairly high oxygen ion conduction is already observed even at ambient temperature for $Nd_2NiO_{4+\delta}$ and $Pr_2NiO_{4+\delta}$, δ can be easily varied by electrochemical techniques in a reversible topotactic reaction in an aqueous alkaline electrolyte.

Stoichiometric $RE_2NiO_{4.00}$ shows at ambient temperature the LTO structure type (space group *Bmab*), with 3D ordered tilting of the NiO_6 octahedra[1]. Intercalating additional oxygen atoms generally results for $\delta < 0.2$ into a structural disordered state, all superstructure reflections are lost and the space group changes to *Fmmm*. Additional oxygen uptake beyond $\delta > 0.2$ is surprisingly accompanied by a complex disorder-order transition, which is supposed to concern predominantly the extra and apical oxygen atoms. Previous tests on single crystal and powder diffraction lead us to conclude on the formation of a complex incommensurate superstructure. This gives evidence to the formation of a highly ordered oxygen sublattice for about $\delta > 0.2$. The structural description of these ordered phases is of general importance for the understanding of the underlying low T oxygen mobility mechanisms in these phases.

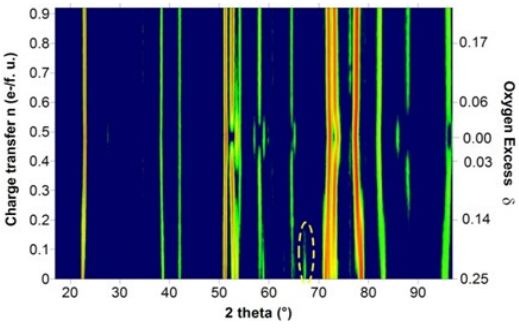

Figure 1: Evolution of the NPD patterns obtained in situ during the electrochemical reduction-oxidation of $Nd_2NiO_{4+\delta}$ (G41, λ = 2.422(2)Å). The dotted ellipsoid shows the incommensurate superstructure reflections of the starting compound (fully oxidized).

For this reason we have investigated the phase diagram of $Nd_2NiO_{4+\delta}$ and $Pr_2NiO_{4+\delta}$ at ambient temperature as a function of δ, by following the oxygen intercalation reaction by *in situ* neutron powder diffraction. The reaction kinetics is controlled electrochemically as well as the oxygen stoichiometry by the following formula:

$$RE_2NiO_{4.00} + \delta O^{2-} \leftrightarrow RE_2NiO_{4+\delta} + 2\delta e^{-} \quad (1)$$

This reaction has been carried out in a specially designed electrochemical cell equipped with working, counter and reference electrodes[3]. The basic aim is to follow the structural and magnetic evolution of the stoichiometric $RE_2NiO_{4.00}$ up to a maximum electron transfer of about 0.5 e-/formula units, corresponding to $RE_2NiO_{4.25}$.

In situ neutron powder diffraction (NPD) studies were performed on the G4.1 (with λ = 2.422(2) Å) two-axis diffractometer of the LLB in Saclay (Orphée reactor).

All the electrochemical reduction/oxidation reactions were carried out in galvanostatic mode, applying a constant current allowing direct correlation of the structural and magnetic evolutions with the charge transfer (eq. 1).

Time-resolved NPD diagrams measured *in situ* during the electrochemical reduction-oxidation of $Nd_2NiO_{4+\delta}$ are shown in Fig. 1, as a function of the charge transfer. According to the pattern evolution, a rich phase sequence becomes evident during the reaction. The reduction of $Nd_2NiO_{4.25}$ to $\delta = 0$, is associated with a charge transfer (n) of n=0.5 electron/formula unit (e-

/ f.u.). The starting material was thus proven to be $Nd_2NiO_{4.245}$, lattice parameters were refined in the *Fmmm* space group (a =5.3688(5)Å, b =5.4431(6) Å, c = 12.351(2) Å). Sufficiently strong incommensurate peaks could have been observed in the highly oxidized phase. Upon reduction a two phase region is found between n = 0.04 e^- / f.u. and n = 0.28 e^- / f.u, where orthorhombic *Fmmm* and tetragonal $P4_2/ncm$ phases co-exist ($0.23 > \delta > 0.11$). Incommensurate peaks disappear with the transformation to the tetragonal symmetry. The pure tetragonal $P4_2/ncm$ phase exists for $0.28 < n < 0.39$ e^- / f.u. ($0.11 > \delta > 0.055$). Approaching the stoichiometric $Nd_2NiO_{4.0}$ phase, tetragonal $P4_2/ncm$ and orthorhombic *Bmab* phases coexist for $0 < \delta < 0.02$. On further reduction, the single phase *Bmab* region is reached. A weak (101) peak intensity indicates AF magnetic ordering for stoichiometric $Nd_2NiO_{4.0}$ at ambient T, showing a propagation vector k = [1 0 0] and a magnetic moment of 0.686μB. The refined lattice parameters of stoichiometric $Nd_2NiO_{4.0}$ are a = 5.3759 (5) Å, b = 5.5759 (5) Å, c = 12.104 (1) Å.

Upon oxidation the reaction was shown to be not fully reversible but stops at a stoichiometry of $Nd_2NiO_{4.10}$; structural investigation of this phase on 3T2 (λ= 1.225 (3) Å) revealed a $P4_2/ncm$ structure (a=b=5.4549(5) Å, c =12.2004(1) Å). Fig. 2 shows both observed and calculated NPD, illustrating clearly the presence of a P-type (104) superstructure reflection

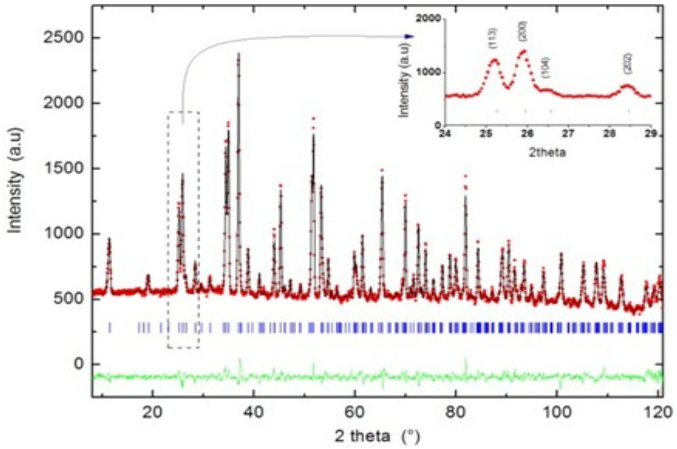

Figure 2: Neutron powder diffraction pattern of the $Nd_2NiO_{4.10}$ intermediate phase showing observed (black scattered points), calculated (red solid line) and the difference (blue solid line) diffraction profiles. Inset shows a zoom of the region 23°-32° in 2ϑ

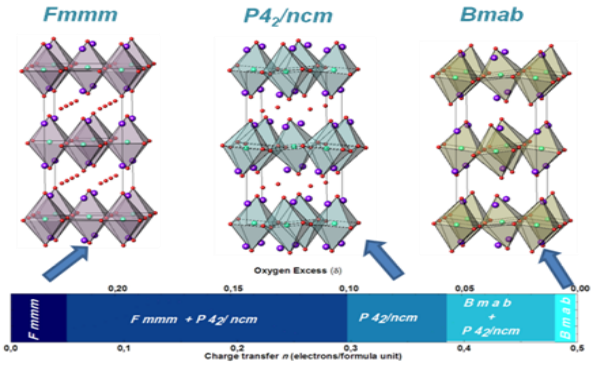

Figure 3: Phase diagram for $Nd_2NiO_{4+\delta}$ as a function of the oxygen stoichiometry δ and associated structures.

In Fig. 3 we report the phase diagram as a function of the oxygen stoichiometry as well the corresponding structure. The reduction pathway of $Pr_2NiO_{4+\delta}$ follows the same series of phases found during the reduction of the Nd homologue, ranging from an incommensurate *Fmmm* starting compound passing via an ordered intermediate tetragonal $P4_2/ncm$ single phase for $0.12 < \delta < 0.13$, to the AF ordered stoichiometric *Bmab* $Pr_2NiO_{4.00}$. Surprisingly $Pr_2NiO_{4.00}$ indicate a different intercalation mechanism upon oxidation. While electrochemically reduced $Nd_2NiO_{4.0}$ can be re-oxidized up to $Nd_2NiO_{4.10}$ only, the homologous Pr-phase re-intercalates oxygen up to a stoichiometry of δ=0.23. This is an important difference which we interpret to be related to the slightly higher ionic radius of Pr^{3+} compared to Nd^{3+}. Comparing the structure of $Nd_2NiO_{4+\delta}$ to that of $Pr_2NiO_{4+\delta}$, the slightly reduced c lattice parameter may be responsible that the oxygen intercalation is no longer reversible, probably related to lattice strain. The short c (c = 12.20 Å for $Nd_2NiO_{4+\delta}$ and c = 12.28 Å for $Pr_2NiO_{4+\delta}$) parameter results in a short inter-octahedral distance. Strong anisotropic and disk shaped apical oxygen atoms suggest a similar associated modified lattice dynamics as recently evidenced by us[4] for $La_2CuO_{4.07}$.

$Nd_2NiO_{4+\delta}$ and $Pr_2NiO_{4+\delta}$ phases are promising to access a better understanding the underlying mechanisms explaining low temperature oxygen mobility in K_2NiF_4 type structures.

References

1. Y. Toyosumi *et al.*, *J. Alloys and Compounds* 408-412 (2006) 1200-1204.
2. W. Paulus, *et al.*, *JACS* (2008)
3. R. Le Toquin, *et al.*, *J. Am. Chem. Soc.* 128 (2006) 13161-13174
4. A Villesuzanne *et al.*, *J. Solid State Electrochem.* 15, 2 (2012), 357
5. O. Wayudi, *PhD Thesis, University Rennes 1*, Dec. 2011

Molecular magnetism: probing the local anisotropy with polarized neutrons

A. BORTA[A], B. GILLON[B], A. GUKASOV[B], A. COUSSON[B], D. LUNEAU[A], E. JEANNEAU[A], I. CIUMACOV[A], H. SAKIYAMA[C], K. TONE[C], M. MIKURIYA[D]

a Univ. C. Bernard Lyon 1, Lab. Multimatériaux et Interfaces (UMR 5615), 69622 Villeurbanne, France.

b Laboratoire Léon Brillouin, CEA Saclay, France.

c Faculty of Science, Yamagata University, 1-4-12 Kojirakawa, Yamagata, 990-8560, Japan.

d School of Science and Technology, Kwansei Gakuin University, 2-1 Gakuen, Sanda 669-1337, Japan.

beatrice.gillon@cea.fr

A current challenge in molecular engineering is the storage of information at the molecular level. A key point in this area is the control of the parameters that govern the molecular magnetic anisotropy. Among other things, it is essential to understand magneto-structural relationships that play a role in this anisotropy.

The macroscopic measurements of magnetic susceptibility and magnetization providing only global behavior of the material. It is therefore necessary to have a method of investigation at the microscopic level. We showed that the polarized neutron diffraction provides a powerful tool for the study of the magnetic anisotropy in the field of molecular magnetism. The approach using local magnetic susceptibility tensors allows to visualize the magnetic moments on each atomic site of the molecule.

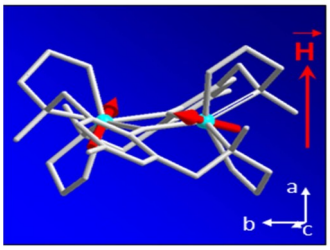

Molecular magnetism gets increasing interest since the discovery of the first single-molecule magnet [Mn_{12}], which behaves like a magnet at the molecular level below a certain temperature called blocking temperature[1]. One of the conditions for the future application of these nano-objects in the storage of information is the existence of a high energy barrier between the two spin states ±S, which requires a strong axial anisotropy. It is therefore very important to control the factors favoring this type of anisotropy, in particular the influence of molecular geometry on the magnetic anisotropy.

The magnetization of each atomic site of an anisotropic compound is not collinear with the magnetic field applied. In addition, it varies greatly depending on the direction of the applied field, as shown in the figure for a molecular complex of Co^{2+}. In this case, macroscopic magnetic measurements are inadequate because they only give information on the resulting magnetic moment induced in a fixed direction and therefore can not characterize the magnetic anisotropy at the microscopic level.

Neutrons, carrying a spin, are sensitive to magnetism by dipolar interaction with electronic magnetic moments that are responsible for the magnetism in the material. Spin polarized neutron diffraction enables to probe the real distribution of the magnetic moments in magnitude and direction in the crystalline lattice, in particular for highly anisotropic paramagnetic compounds.

The recent development in the Laboratoire Léon Brillouin (LLB) of a methodology for analyzing these data[2] based on the local magnetic susceptibility tensor, allows to visualize the moments acting on different atomic sites. This approach used so far only for inorganic compounds has been successfully applied for the first time to the study of magneto-structural relationships in a molecular compound, $[Co_2(sym\text{-}hmp)_2](BPh_4)_2]$ where hmp = hydroxymethylpyridine [3].

This molecule is composed of two Co^{2+} ions connected by two bridging oxygens in the heart of the organometallic complex $[Co_2(sym\text{-}hmp)_2]^{2+}$. Each

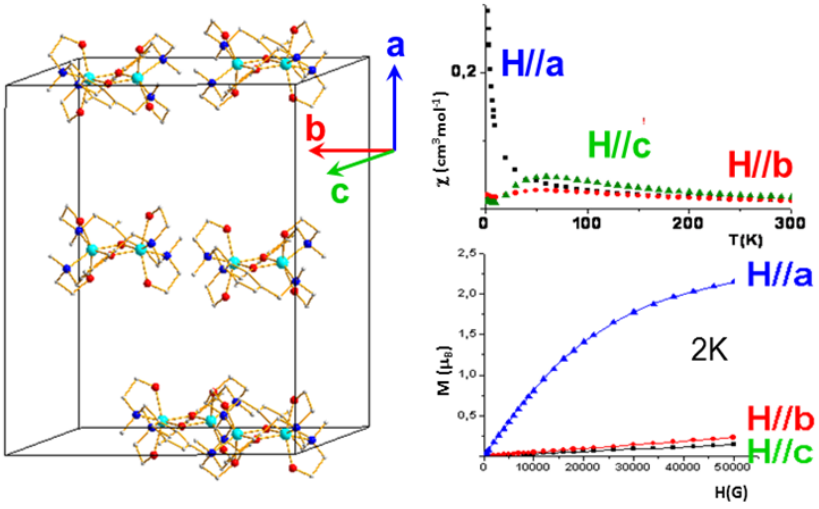

Figure 1: Left: Contents of crystallographic lattice for the compound $[Co_2(sym\text{-}hmp)_2](BPh_4)_2]$ (● Co, ● N, ● O). BPh_4 molecules are omitted for clarity . Right: Magnetic susceptibility $\chi(T)$ as a function of the temperature and magnetization M(H) as a function of the magnetic field at T = 2K for different directions of the applied field relative to the main crystallographic axes.

Co^{2+} ion is in the center of a distorted octahedron formed by two nitrogen atoms and four oxygen atoms. The first magnetic measurements on single crystal clearly show highly anisotropic behavior that can be reproduced within an usual model effective antiferromagnetically coupled spin ½, whereby the angle[3] between the local moments is 39°, in good agreement with experiment. However, this model is purely phenomenological because it does not give the true values and orientations of the moments of Co^{2+} ions, which have a 3/2 spin.

The experiment of polarized neutron diffraction on a single crystal of this compound was carried out on the 5C1 diffractometer of the Laboratoire Léon Brillouin at low temperature under a strong magnetic field applied along the **a** main axis. Data analysis by the method of local susceptibility tensor provides access to the actual value of the magnetic moments of the Co^{2+} ions (3 μB, as expected for a spin S = 3/2) and their orientation with respect to the molecular geometry : the obtained magnetic moments are symmetric with respect to the main symmetry axis (**b** axis, C2) and in the direction perpendicular to the axis of axial distortion of the octahedron centered on each Co^{2+} ion. Their directions thus are in an angle of 37 (± 1) degrees.

Figure 3: Polarized neutron diffractometer 5C1-VIP equipped with a PSD detector (Position Sensitive Detector)

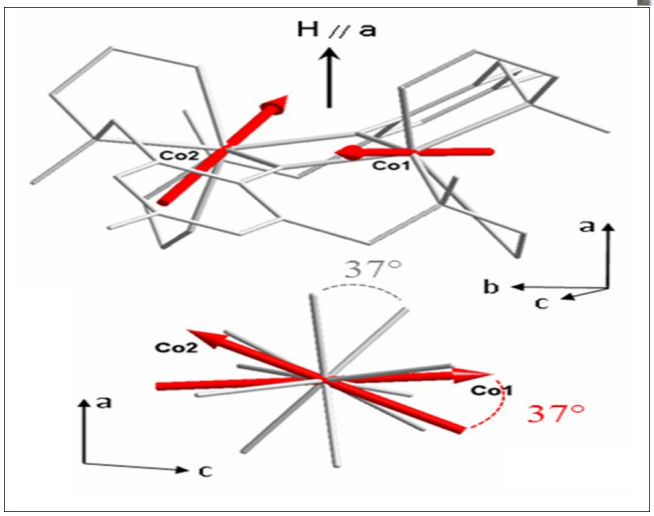

*Figure 2: Top: induced magnetic moments of the cobalt atoms by a 7-Tesla magnetic field **H**, applied along the **a** axis. Bottom: View projected along the **b** axis (only first neighbors are shown for clarity). The same 37°angle is observed between the directions of the moments and between the local distortion axes.*

In conclusion, polarized neutron diffraction shows that the molecular magnetic anisotropy in the Co^{2+} diatomic complex is governed by the local anisotropy of each Co^{2+} ion (single-ion anisotropy). The complex behaves as a system of two ions of spin 3/2 antiferromagnetically coupled, the directions of the local magnetic moments being imposed by the local geometry.

References

1. R. Sessoli, D. Gatteschi, A. Caneschi, M. A. Novak, *Nature* **365** (1993) 1413.

2. A. Gukasov & J. Brown, *J. Phys. Cond. Mat*. **14** (2002) 8831.

3. A. Borta, B. Gillon, A. Gukasov, A. Cousson, D. Luneau, E. Jeanneau, I. Ciumacov, H. Sakiyama, K. Tone, and M. Mikuriya, *Phys. Rev*. B **83** (2011) 184429.

Comparison of the site occupancies determined by combined Rietveld refinement and by DFT calculations: the example of the ternary Mo-Ni-Re σ phase

K. YAQOOB[A], J-C. CRIVELLO[A], J-M. JOUBERT[A], F. PORCHER[B]

a CMTR-ICMPE, CNRS, UMR7182, Thiais, France

b Laboratoire Léon Brillouin, CEA Saclay, France

jean-marc.joubert@icmpe.cnrs.fr

The site occupancies of Mo-Ni-Re σ-phase have been studied as a function of the composition in the ternary homogeneity domain by both experimental measurements and calculations. Because of the possible simultaneous occupancy of three elements on the five sites of the crystal structure, the experimental determination of the site occupancies was achieved by using combined Rietveld refinement of X-ray and neutron diffraction data whereas the calculation of the site occupancies was carried out by using DFT results of every ordered (i.e. 35 = 243) configuration appearing in the ternary system. The comparison of experimental and calculations results showed exceptionally good agreement

The determination of site occupancy data for binary compounds by Rietveld refinement is a rather well established procedure. However, obtaining the same type of data for sites in which three elements may be present simultaneously is a more challenging task. To solve this problem, one should use combined Rietveld refinement of diffraction of different types *i.e.* in which the diffraction contrast between the elements is different, for example, X-ray and neutron data when the relative scattering in the two techniques is also adequate. On the other hand DFT calculations combined in the frame of the Bragg-Williams approximation may yield calculated site occupancies but are sometimes limited by the large number of configurations one has to calculate.

The σ-phase (structure type FeCr, space group $P4_2/mnm$, 30 atoms per unit cell, 5 inequivalent sites: 2*a*, 4*f*, 8i_1, 8i_2, 8*j*) is a hard brittle intermetallic compound and deleterious effect on the mechanical properties of many technologically important systems. The main feature of σ-phase include its non stoichiometry which is accommodated by substitutions on different sites of the crystal structure, and its ability to accept wide homogeneity ranges. Qualitatively in σ, larger atoms show preference for the sites with high coordination number (CN 15 and CN 14) whereas smaller atoms occupy the sites with low coordination number (CN 12). The present study was the first work on ternary s-phase combining experimental and theoretical investigations.

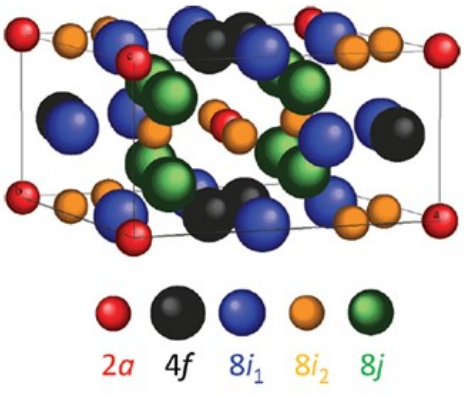

Figure 1 : Crystal structure of the s-phase ($P4_2/mnm$).

The site occupancies were determined by both experimental and theoretical methods. As the substitutional disorder in the ternary σ-phase involves three elements, thus the accurate experimental determination of site occupancies required at least two data sets with different atomic contrast. Therefore, the experimental determination of site occupancies was accomplished by combined Rietveld analysis of X-ray and neutron diffraction data. The theoretical approach for the determination of site occupancies was based on the estimation of enthalpies of formation by first principles calculations. Finite temperature properties, such as the site occupancies, were determined using the Bragg-Williams (BW) approximation, which ignores the short-range order within the defined sublattices.

The neutron diffraction measurements were performed at Laboratoire Léon Brillouin (LLB, CEA-CNRS), Saclay, France using 3T2 instrument. The sample in form of a fine powder (7.5 grams, <63 microns) was introduced in a sample holder consisting of vanadium cylinder (diameter 6 mm) supported on a cadmium pro-

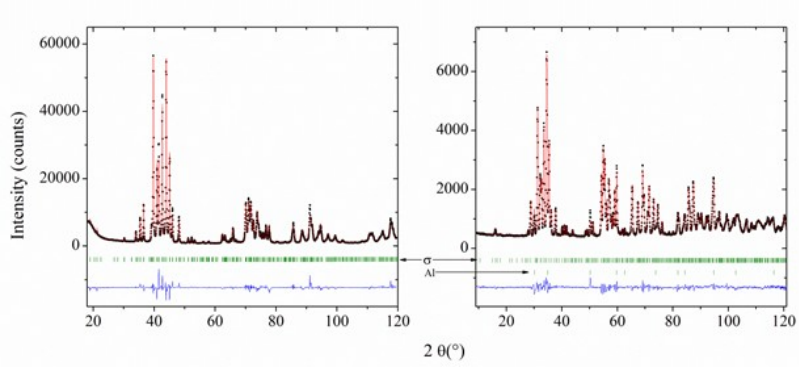

Figure 2 : Combined Rietveld refinement of the X-ray (left) and neutron diffraction (right) patterns of the composition $Mo_{0.259}Ni_{0.201}Re_{0.540}$

tected aluminum cylinder. The measurement was performed at room temperature with the Debye-Scherrer geometry (λ= 1.2253 Å).

The elements constituting the studied system gives large scattering contrast in both X-ray and neutron diffraction techniques as indicated by their atomic numbers (Z_{Mo}=42, Z_{Ni}=28, Z_{Re}=75) and Fermi lengths (b_{Mo}=6.7, b_{Ni}=10.3, b_{Re}= 9.2 fm). On the other hand, they also present different scattering contrast in two considered diffraction techniques *i.e.* Ni is the weakest scattering element in the X-ray diffraction experiment and strongest in the neutron diffraction experiment. Site occupancies were obtained by the Rietveld method allowing the three elements on each site with the only constraint of refined composition equal to that alloy.

The site occupancies determined along the line Mo_2Re to $ReNi_2$ as a function of Ni content are presented in Fig. 3. As shown in the plot, the Mo and Ni site fractions in Mo-Ni-Re σ phase along the line show similar variations (either increase or decrease). Ni whose atomic size is significantly smaller than Mo and Re substitutes them mainly on the sites with low coordination numbers *i.e. 2a* and *8i2* (CN 12). On the other hand Mo atoms being larger in size tend to occupy high coordination sites *i.e. 4f*, *8i1* and *8j* (CN15, 14, 14) where they find more space. Contrary to the behavior of Mo and Ni, the Re atom being intermediate in size {r_{Ni} (~135 pm) < r_{Re} (~137 pm) < r_{Mo} (~139pm)} shows dual preference depending on the composition proportion of the other two elements. The agreement between experiment and calculation is excellent.

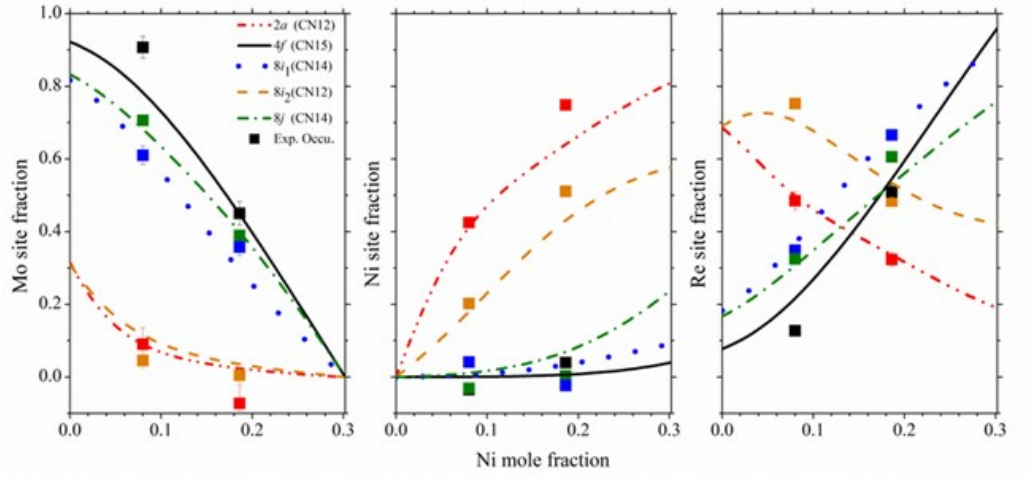

Figure 3 : Experimental and calculated site occupancies of Mo-Ni-Re σ- phase at 1873 K along the line from the ideal stoichiometry Mo_2Re to $ReNi_2$

References

1. Joubert, *Prog. Mater. Sci.,53, (2008) 528-583*
2. Yaqoob, Crivello, Joubert, *Inor. Chem.,51, (2011) 3071-3078*

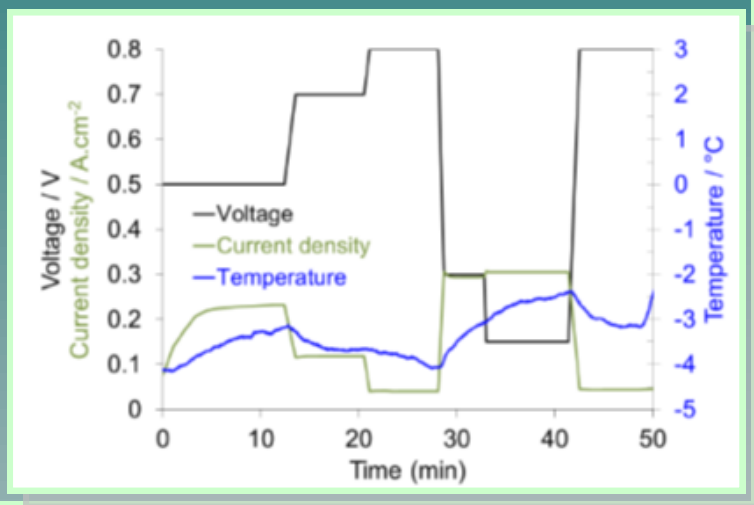
Voltage / V
Current density / A.cm-2
Temperature / °C
Time (min)
Voltage
Current density
Temperature

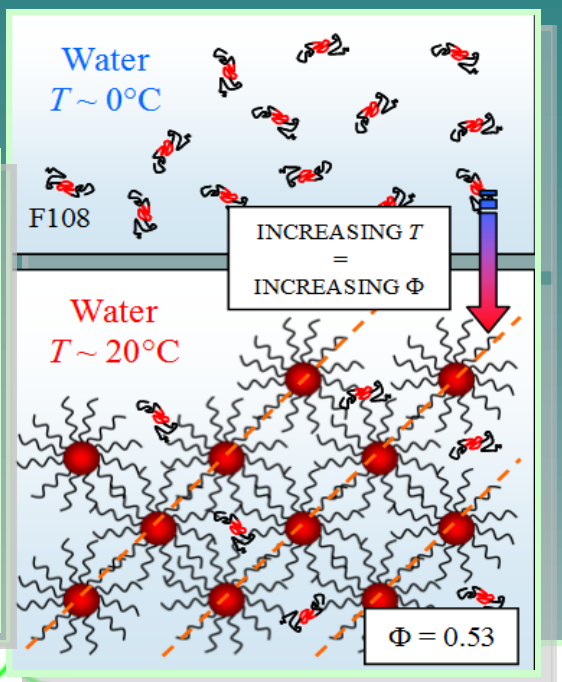
Water
T ~ 0°C
F108
INCREASING T
=
INCREASING Φ
Water
T ~ 20°C
Φ = 0.53

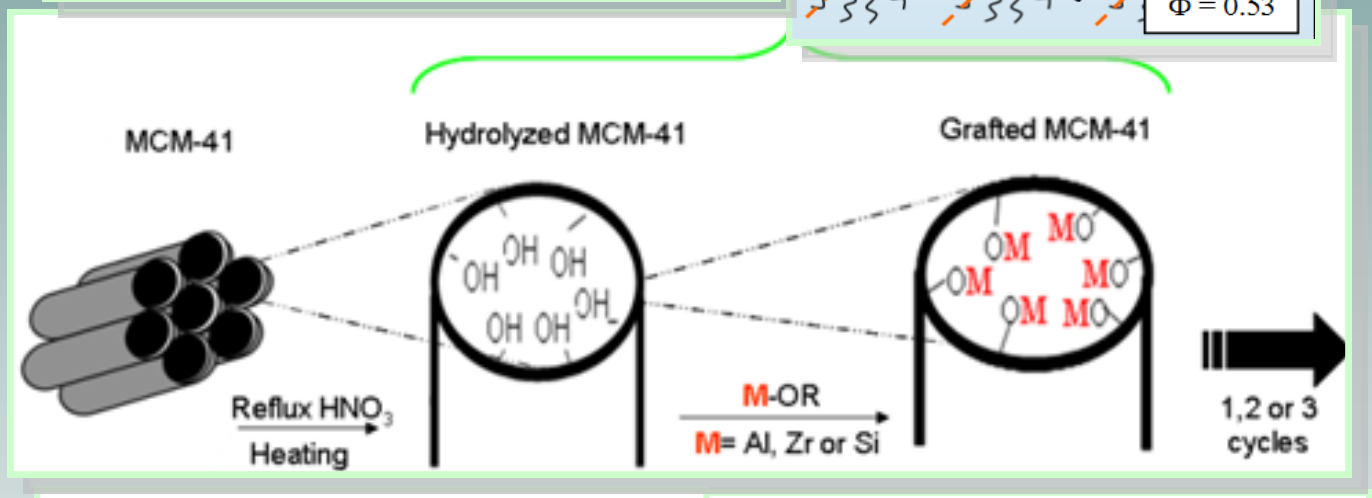
MCM-41
Hydrolyzed MCM-41
Grafted MCM-41
Reflux HNO3
Heating
M-OR
M= Al, Zr or Si
1,2 or 3
cycles

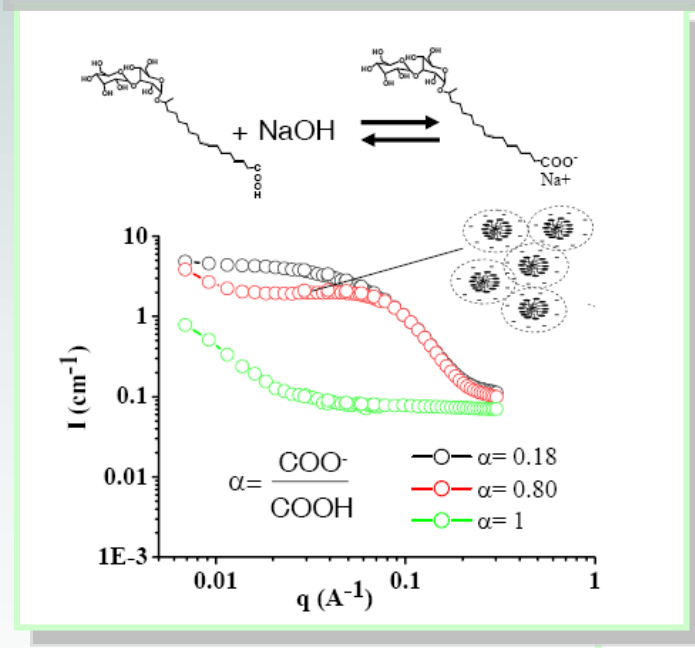
+ NaOH
COO-
Na+
I (cm-1)
q (A-1)
α= COO-/COOH
α= 0.18
α= 0.80
α= 1

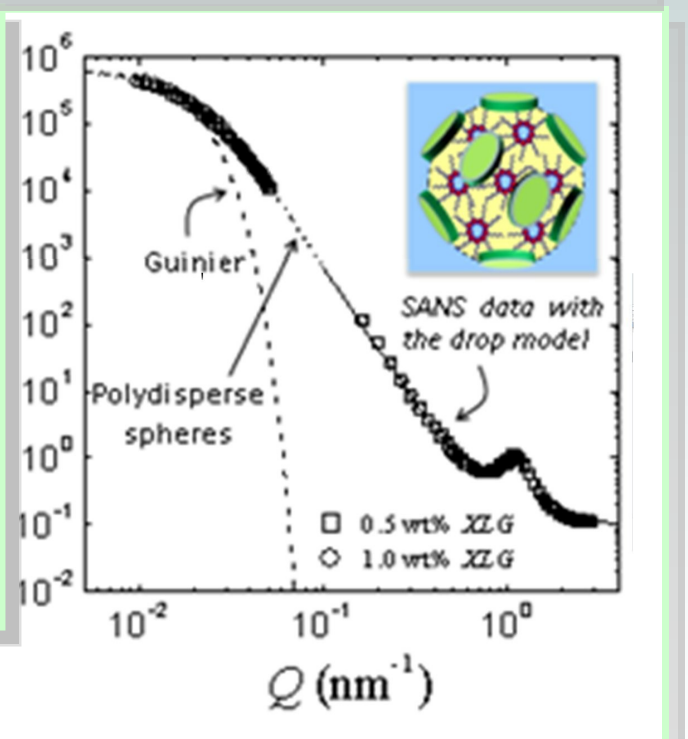
Guinier
Polydisperse
spheres
SANS data with
the drop model
0.5 wt% XLG
1.0 wt% XLG
Q (nm-1)

AXE 3:

Soft Matter and Biophysics.

The third scientific axis concerns soft matter and biophysics. Flourishing of many new systems, combining different components, many involving nanoscales (1-100 nm) has become a major current trend in soft mater. At LLB, researchers have developed in similar directions keeping some of the historical specificities of the lab.: involving polymers is one of the components illustrating the advantages of neutron scattering, *i.e.* labelling and contrast matching, while we often marry the reciprocal space (SANS but also SAXS) with other techniques, in real space or at macroscopic scales. The following topics are investigated: nanoparticles and hybrid systems; organic systems and self-organization; polymer dynamics; electrostatics complexes. The research at the interface of physics and biology is based on three main topics: 1) Proteins in complex media viewed as model systems for living environments. Experiments are concerned with macro- or supra-molecular scales and their analysis is strongly influenced by our background in polymer physics, statistical physics and phase transition physics; 2) Local dynamics of proteins and hydration water in relation with the dynamical transition of proteins and their enzymatic activity. Neutron scattering techniques, that are very sensitive to protons, are particularly suitable for these studies; 3) Water and its specific properties are fundamentally related to life and to the very peculiar properties of some biological molecules like proteins. Here, water properties are studied in relation with the dynamics of hydrogen bonds network, the notions of hydrophobicity and confinement.

- **Impact of pore size and pore surface composition on the dynamics of confined water in highly ordered porous silica**
  I. Matar Briman, D. Rébiscoul, O. Diat, J-M. Zanotti, P. Jollivet, P. Barboux and S. Gin

- **Colloidal metallurgy: investigating the structure of nanoparticles embedded in micellar polycrystals**
  E. Tamborini, N. Ghofraniha, J. Oberdisse, L. Cipelletti and L. Ramos

- **Study of the pH-dependency self-assembly of a glycolipid biosurfactant combining SANS and modelisation**
  N. Baccile, F. Babonneau, I.Van Bogaert and J.S. Pedersen

- **Crystallized droplets stabilized by solid particles: the combination of two principles for a well controlled distribution**
  F. Muller, J. Degrouard , J. Jestin, A. Brûlet and A. Salonen

- **Water management in fuel cells at sub-zero temperature: an in operando SANS-EIS coupled study**
  A. Morin, Z. Peng, J. Jestin, M. Detrez and G. Gebel

Impact of pore size and pore surface composition on the dynamics of confined water in highly ordered porous silica

I. MATAR BRIMAN[A], D. RÉBISCOUL[A], O. DIAT[B], J-M. ZANOTTI[C], P. JOLLIVET[A], P. BARBOUX[D], S. GIN[A]

a CEA, DEN, DTCD/ SECM/LCLT - Marcoule, F-30207 Bagnols-sur-Cèze, France

b CEA, Institut de Chimie Séparative de Marcoule, Marcoule, F-30207 Bagnols-sur-Cèze, France

c Laboratoire Léon Brillouin, CEA Saclay, France

d Laboratoire de Chimie de la Matière Condensée, Chimie ParisTech, 11 rue Pierre et Marie Curie 75231 Paris Cedex 05, France

diane.rebiscoul@cea.fr

The impact of pore size and pore surface composition on water dynamics confined in highly ordered porous silica material (MCM-41) was investigated using neutron scattering for correlation times in the picosecond range. Samples were synthesized by hydrothermal route and grafted via hydrolytic surface sol-gel method in order to obtain pore wall surfaces with Si-OH, Al-OH or Zr-OH terminations and pore sizes from 2 to 2.7 nm. While the water translational diffusion coefficients are close to the bulk value whatever the samples, the amounts of fixed protons depend on the pore size and the ability of the grafted layers to immobilize the water molecules. This last result highlights that pore surface composition could be the predominant parameter affecting the fixed protons content at this time scale.

Water dynamics at various timescales are strongly affected by the size and the surface chemistry of confinement at the nanoscale[1]. These motions modifications coming from the local organization of molecules can strongly modify the thermodynamic properties such as freezing temperatures or gas solubility[2]. Previous studies showed that water motions can be slowed down by a decrease of the confinement size, the chemical nature of the interfaces as well as the presence of ions in solution. These results show the important effect of size and pore surface composition of the confinement and also the ions presence on the water dynamics. Meanwhile, regarding these three system characteristics, a question remains still open: what is the predominant factor affecting the dynamics? To intend to bring elements to solve this question we have used model materials, *i.e.* porous silica-based material (MCM41), synthesized by hydrothermal route[3] and grafted via hydrolytic surface sol-gel method4 in order to obtain pore wall surfaces with Si-OH, Al-OH or Zr-OH terminations and pore sizes between 2.7 nm and 2.0 nm (Fig. 1 and Fig. 2).

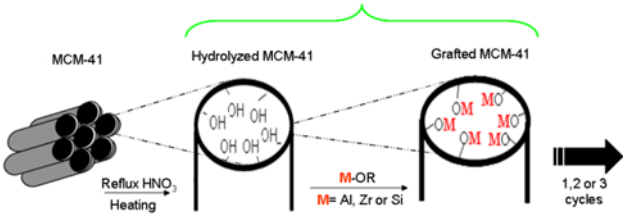

Figure 1. Schematic concept of Hydrolytic Sol Gel (HSS) grafting method.

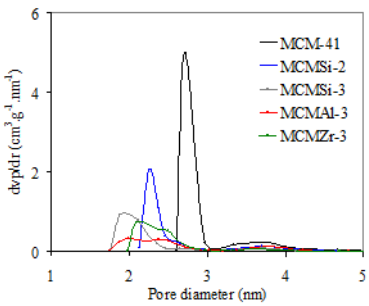

Figure 2. BJH Pore size distributions for samples

The materials were placed at a relative humidity (RH) of 86 % at 25°C allowing the complete filling of the porosity.

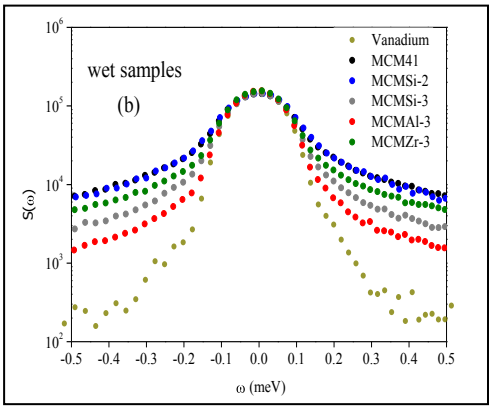

Figure 3. Sum of QENS spectra of hydrated samples and vanadium obtained at room temperature and λ=5.2 Å

To analyse the water dynamics and more especially the dynamics of mobile protons, quasi elastic neutron scattering experiments were carried out on the time of flight spectrometer Mibemol at the Laboratoire Léon Brillouin at Saclay (France). The incident wavelength of 5.2 Å determining an energy resolution of 40 µeV and a correlation time range of 4.5 picoseconds was used. The QENS experiments were performed at 300 K and the signal was analysed using QENSH program provided by LLB and dedicated for this kind of treatment.

Fig. 3 shows the sum over Q of the QENS spectra collected for the different model materials hydrated with pure water. All the samples show a much broader signal as compared with vanadium foil used as a reference to show the instrumental resolution. The QENS data $S(Q,\omega)$ were fitted with an equation using one Lorentzian function characterizing only one mode of diffusion.

The evolution of the half width at half maximum $\Gamma_t(Q)$ obtained from the fitting of QENS spectra are presented in Fig. 4 as a function of Q^2. The

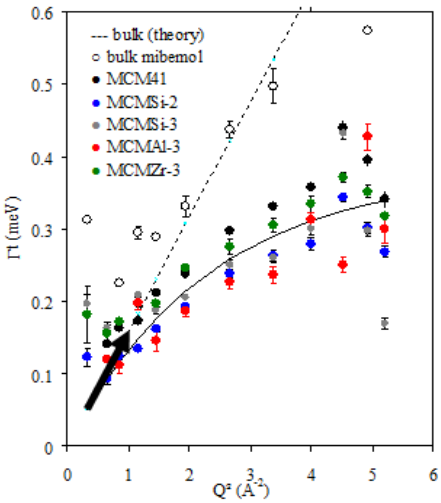

Figure 4. Half width at half maximum $\Gamma_t(Q)$ obtained from the fitting of QENS spectra.

behaviour of confined water in all samples is rather different from the bulk water characteristic of a Brownian diffusion. Γ_t asymptotically reaches a constant value which can be described by a jump diffusion model and related to the fact that the solvent can be considered as a discrete medium whereas at low Q, the asymptotic behaviour (in Q^2) is more like a diffusive dynamic. This is why Γ_t was fitted using the Singwi and Sjolander model[5] (SS) based on an exponential distribution of jump lengths (1):

$$\Gamma_t(Q) = \frac{\hbar D_t Q^2}{1 + D_t Q^2 \tau_t} \quad (1)$$

With $\hbar$ the reduced Planck constant, D_t translational diffusion coefficient, τ_t the average residence time between two consecutive jumps .

At a picosecond time window and taking into account the poor statistic of the QENS data at low Q-values, we can consider on one hand that diffusion coefficient D_t of water (protons) within pores of model materials, are close to that of bulk water measured in the same conditions $D_t = (2.9 \pm 0.5) \times 10^{-9}$ m²/s and $\tau_t = 2.6 \pm 0.2$. To determine the fraction of fixed protons in each sample, the elastic incoherent structure factor (EISF), *i.e.* the fractional intensity of the elastic part, was plotted.The EISF were determined from the elastic and quasi-elastic intensity obtained from the quasi-elastic spectra analysis and the results were fitted using the model $EISF_M$ of Volino and Dianoux [6] which considers the motion of the mobile hydrogen atoms as a restricted diffusion within a sphere of radius R. We have taken into account the contribution of the fraction of fixed protons f at the time scale of the experiment [7]:

$$EISF_M(Q) = (1 - f) + f\left[\frac{3 j_1(QR)}{QR}\right]^2$$

Where $j_1(QR)$ is the first order spherical Bessel function.

The experimental results for hydrated samples are presented in Fig. 5. Indeed, for the hydrated MCM41 and MCMSi-2 a ratio of 0.27 and 0.26 of fixed protons respectively is obtained while a ratio of 0.45 of protons is fixed in the MCMSi-3. However, the nature of the grafted layers also impacts on the mobile water content. The fraction of fixed proton is higher in the water filled pores of MCMAl-3 (f = 0.72) and of MCMZr-3 (f = 0.42) than in those pores of MCMSi-2 (f = 0.26). This confirms the ability of the Zr-OH and many more Al-OH terminated surface to immobilize water molecules. These results could be explained by the formation of coordination bonds of water molecules with Al-OH and Zr-OH groups which behave as Lewis acids with stronger H-bonds or by the fact that alumina or zirconia-base surfaces strongly interact with the water dipoles and texture the water layers more strongly because they are more ionic than silica.

Supposing that any water is trapped in the grafted layers, these results show that water dynamics mostly depends on the surface composition than the pore size for pore size lower than 2.3 nm.

These first results enhance the importance to study the water dynamics in such model systems to better understand its behaviour in more complex nanoconfined media such as glasses, clays or corrosion layers at the surface of altered glass, where the effect of pore size, surface composition and the presence of ions are difficult to dissociate.

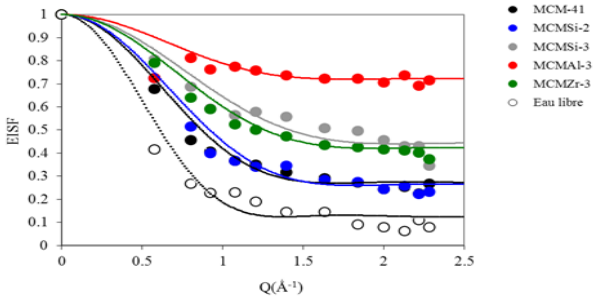

Figure 5. Experimental EISF and fitted $EISF_M$ curves as a function of Q for hydrated (filled dot) samples at T = 300K

References

1. J. Teixeira *et al*, *Physica B*, 234-236, 370.
2. X. Liu *et al.*, *J. of Phys. Chem.* B 114, 4145.
3. H. Chen *et al.*, *Ceramics International* 28, 541
4. I. Ichinose *et al.*, *Chem. Letters* 10, 831.
5. K.S. Singwi *et al.*, *Phys. Rev.* 1960; 119: 863.
6. F. Volino *et al.*, *Molercular Physics* 1980; 41: 271.
7. M.C. Bellissent *et al*, *J. de Phys.* I; 2: 995.

Colloidal metallurgy: investigating the structure of nanoparticles embedded in micellar polycrystals

E. TAMBORINI[A,B], N. GHOFRANIHA[A,B], J. OBERDISSE[A,B], L. CIPELLETTI[A,B], L. RAMOS[A,B]

a Université Montpellier 2, Laboratoire Charles Coulomb UMR 5221, F-34095, Montpellier, France

b CNRS, Laboratoire Charles Coulomb UMR 5221, F-34095, Montpellier, France

laurence.ramos@univ-montp2.fr

Confined colloids may be used to investigate or create new materials. Confinement of nanoparticles in the grain-boundaries (GBs) of polycrystalline soft materials allows the visualization of GBs by light or confocal microscopy. The structure of the nanoparticles concentrated in the GBs during the crystallization process has been studied by contrast variation small angle neutron scattering (SANS) at LLB. Two different solvent mixtures were used to investigate separately the dispersion of the nanoparticles and the structure of the micellar lattice of otherwise identical samples. In the silica- matched samples, the crystal lattice was found to be unaffected by the nanoparticles on a local scale. In the polymer-matched samples, a strong peak due to the interacting silica particles is interpreted as the signature of a crowding of nanoparticles in the GBs.

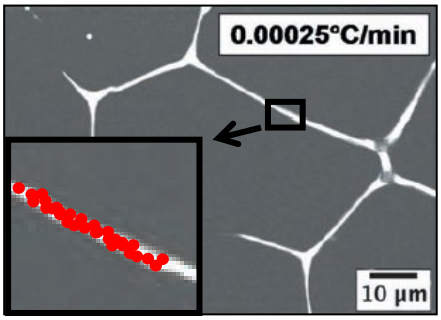

We have studied a polycrystalline matrix made of an aqueous solution of tribloc copolymer (Pluronics® F108). This molecule in water forms spherical micelles arranged on a crystal lattice upon heating samples to room temperature (Fig. 1).

The structure of the pure micellar matrix has been investigated by SANS and the result is shown in Fig. 2.

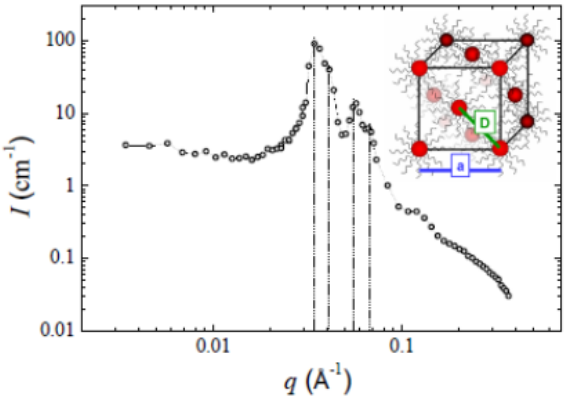

Figure 2 : Micellar crystal lattice as seen by SANS. The four vertical lines indicate the position of the main lattice diffraction peaks at 32%w/w of polymer in D_2O

Silica nanoparticles (D = 30 nm) have been added to the solution at low temperature, before micelle formation. During the heating phase, crystal grains are nucleated in the sample. These grains expel a part of the nanoparticles, and once the crystal formation is finished at high temperature, the nanoparticles are concentrated in the grain boundaries (*i.e.* between grains).

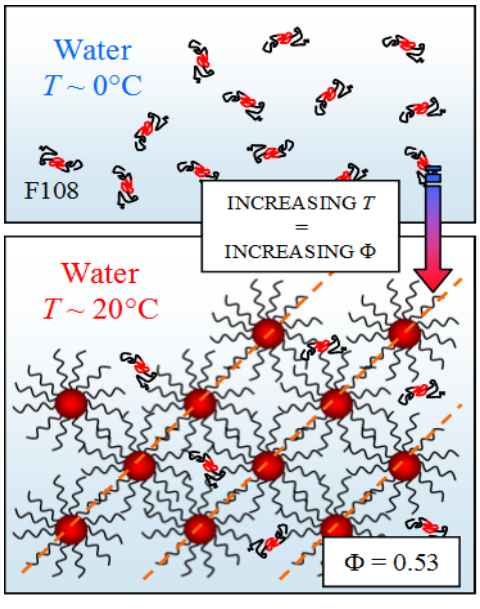

Figure 1 : Pluronics phase diagram.

In order to verify this scenario, the nanoparticle dispersion in the final sample has been characterized. We have prepared two contrast situations using H_2O/D_2O mixtures. In one case (silica-matched, 'SM'), the structural changes of the micellar lattice can be studied[1]. In Fig. 3, scattering of samples with various concentrations of (unvisible) silica are shown. The high-q range is found to be unaffected by the silica, underlining the robustness of the micellar grain structure which is not modified by the silica beads. At low q, a peak is found. This peak is also present in the polymer-matched ('PM') samples, *i.e.* it is a signature of the silica structure, and in particular of the strongly interacting silica nanoparticles. Its visibility in the silica-matched case indicates rearrangement of the lattice polymer in the grain boundaries, and possibly polymer adsorption. The concentration deduced from the peak posi-

tion corresponds to about 10%v, *i.e.* ten times more than the average concentration, and is thus identified with a measurement of the nanoparticle concentration within the grain boundaries.

The segregation of the nanoparticles in the grain boundaries can also be verified on a larger scale. We have visualized the local concentration of fluorescent (latex) nanoparticles using confocal microscopy[2], for samples with different thermal histories (heating rates), leading to different

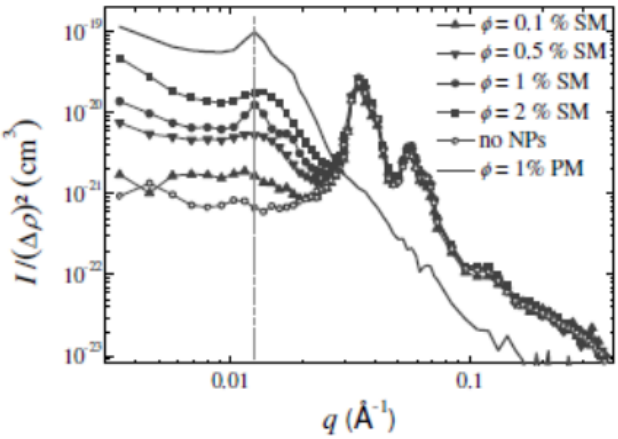

Figure 3: Microstructure of the micellar polycrystal for different silica nanoparticle volume fractions. SM samples are 'silica-matched', PM 'polymer-matched'.

average grain size. In Fig. 4, and also in the header of this article, the granular structure is visible, and the size of the grains can be measured. Note that similar pictures of samples with silica nanoparticules using microscopy have also been obtained.

To summarize, the use of contrast variation SANS allows for a determination of pair correlations in complex ternary mixtures containing both micelles and nanoparticles. Our findings confirm (and measure) the concentration of nanoparticles in grain boundaries of the soft colloidal polycrystal formed by the micelles.

Outlook

Our project on colloidal metallurgy aims at studying the plasticity of polycrystals. It takes advantage of the much larger characteristic length and time scales, much softer elasticity, and the optical transparency of a colloidal polycrystal as compared to atomic crystals to obtain unprecedented space- and time-resolved information on the deformation of a polycrystal under load. By using a unique colloidal analog of atomic polycrystals, we hope to be able to elucidate the different mechanisms at play, at a microscopic level, in the plasticity of polycrystals, these processes being still largely unknown.

Figure 4: Grain boundaries (obtained with different crystallization rates) visualized by confocal microscopy using fluorescence of the nanoparticles. The size of the grains varies from few microns to several tens of microns (Soft Matter cover, ref 2, reproduced with kind permission).

References

1. E. Tamborini,N. Ghofraniha, J. Oberdisse, L. Cipelletti and L. Ramos, *Langmuir* 28, 8562, (2012).
2. N. Ghofraniha, E. Tamborini, J. Oberdisse, L. Cipelletti and L. Ramos, *Soft Matter* 8, 6214 (2012). (cover article)

Study of the pH-dependency self-assembly of a glycolipid biosurfactant combining SANS and modelisation

N. BACCILE[A] F. BABONNEAU[A]; I. VAN BOGAERT[B]; J. S. PEDERSEN[C]

a UPMC-CNRS, UMR 7574, Chimie de la Matière Condensée de Paris, F-75005, Paris, France

b InBio, Department of Biochemical and Microbial Technology, Faculty of Bioscience Engineering, Ghent University, Coupure Links 653, 9000, Ghent, Belgium

c Department of Chemistry and iNANO Interdisciplinary Nanoscience Center, Aarhus University, DK -8000 Aarhus, Denmark

niki.baccile@upmc.fr

Acidic sophorolipids, SL-COOH, are pH-sensitive bio-derived glycolipids that form micelles whose electrostatic interactions can be tuned. Upon partial ionization of the COOH group, micelles become negatively charged and intermicellar interactions take place, as demonstrated by Small Angle Neutron Scattering. Numerical modeling and fitting of SANS spectra quantifies the effect of base addition in terms of effective surface charge.

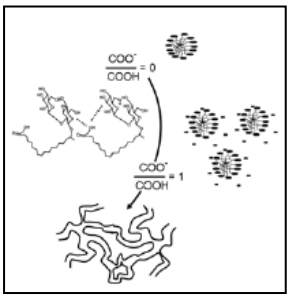

Sophorolipids (SL) are glucose-derived biosurfactants that have attracted a fair attention for applications in home and skin-care products because of their biological origin and low toxicity. Acidic sophorolipids, SL-COOH (Fig. 1), are particularly interesting as they are composed of a sophorose unit attached to an hydroxylated oleic acid moiety through a glycosidic bond on the C17 carbon atom of the fatty acid chain. This particular feature leaves the COOH group unaffected, making this compound sensitive to pH, knowing that stimuli-responsive properties (temperature, electric field, ionic strength and pH) in surfactants are extremely important for the development of a number of applications in many different fields: stabilization of emulsions, suspensions or foams, drug encapsulation and delivery, wettability control, enhancement of viscoelastic properties, recyclability, heat-transfer fluids, drag-reduction agents, dynamic templating for nanomaterials, smart hydrogels for wound healing, artificial muscle conception.

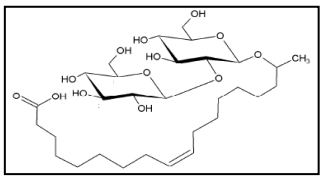

Figure 1 : Chemical formula of the acidic form of sophorolipids (SL-COOH).

Since the self-assembly and stimuli-responsive properties of sophorolipids have been scarcely studied in the past few years, we have carried out a specific SANS study to highlight and quantify them under pH variation.

SANS spectra recorded on the deionized form of sophorolipids (Fig. 2) show the strong effect of pH on the nature of the micellar assemblies. At low pH, micelles are isolated objects whose shape is mostly spherical/ellipsoidal. In mid-pH regions (and for the same SL-COOH concentration), the presence of a peak (red circles) identifies interaction forces between the micelles while at high pH (green circles), most micelles are disassembled in favor of large aggregates, difficult to detect under the current SANS configuration .

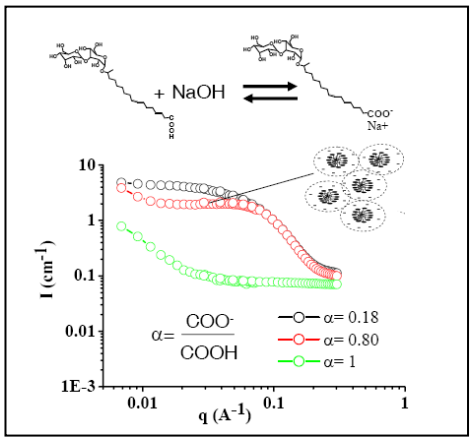

Figure 2 : SANS spectra of SL-COOH at various ionization degrees, a, controlled by adding sodium hydroxide.

To better understand the behaviour of SL-COOH in the mid-pH range, where intermicellar interactions become important, we run SANS experiments at small increasing amounts of NaOH, an experiment shown in Fig. 3a.

The spectral evolution from free micelles (black circles) towards interacting objects is put in evidence (blue circles). The I(q) function is known to be proportional to P(q) and S(q), the form and structure factors, as shown hereafter

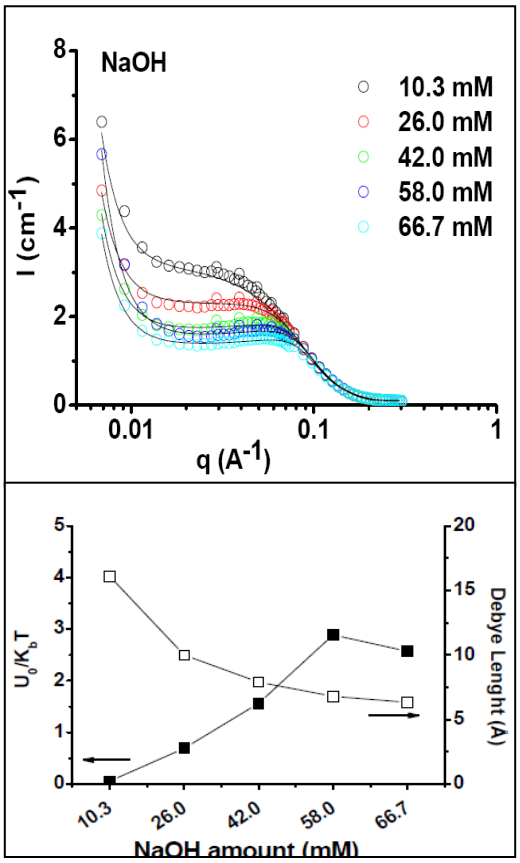

Figure 3 : a) Evolution of SANS spectra (lin-log scale) as a function of added base collected on an aqueous solution of SL-COOH; black continuous curves represent the numerical fits. b) Evolution of the interaction potential (U_0, in kbT scale) and Debye length. U_0 is obtained directly from the fits while the Debye Length is calculated using the GCDH theory.

$$I(q) \propto P(q)S(q)$$

To extract quantitative information from the I(q) curve shown in Fig. 3a, one must use specific models that are able to account for both components of the scattered intensity. In this specific system S(q) ≠ 1 because of the scattering peak. Here, micelles can be successfully modeled with an ellipsoidal of revolution form factor. As for S(q), considering that the surfactant concentration is constant for all experiments and that only the amount of charges (COOH à COO-) increases, it is reasonable to use a structure factor S(q) that combines hard-sphere and screened Coulomb (described by a repulsive Yukawa potential) potentials and whose analytical expression is obtained in the Mean Spherical Approximation (MSA).

For the Yukawa potential, we used the following expression.

$$U(r) = U_0 \frac{D_{HS}}{r} \exp(-\kappa(r - D_{HS})) \qquad r > D_{HS}$$

where r is the minimum distance between two micelles, D_{HS} is the hard-sphere interaction diameter, and U_0 the strength of the potential at r= D_{HS}. For $U_0 > 0$, the potential is repulsive while for < 0, the potential is attractive. κ stands for the range (inverse of the Debye length) of the potential. The potential strength can be related to the charge of the system according to the following.

$$|U_0| \propto \frac{Q^2}{D_{HS}(2+\kappa D_{HS})}$$

with Q being the particle charge (Q= Ze, the micellar valence and the electron charge). The expression for k in the case of a single ion of concentration c and charge q for an ideal solution, as predicted by the Gouy-Chapman Debye-Huckel Poisson-Boltzmann theory (GCDH), is $\kappa \propto c^{1/2} q$.

The fitted spectra are given by the black lines on Fig. 3a while the U_0 evolution as a function of the added base is given on Fig. 3b, which shows that the interaction potential becomes more and more positive. This trend proves the existence of repulsive interactions (according to the sign convention used to define U(r)) between micelles with increasing amounts of negative charges directly deriving from the COO^- groups. The calculated effective micellar charge, Z, ranges between 0.5 and 5.3 in the base concentrations typically explored here.

To conclude, acidic sophorolipids form micelles whose shape is an ellipsoid of revolution and come in strong repulsive interactions upon basification of the medium at constant SL-COOH concentration. Micelles being initially neutral, their effective surface charge increases upon addition of the base.

References

1. N. Baccile, F. Babonneau, J. Jestin, G. Pehau-Arnaudet, I. Van Bogaert, *ACS Nano*, 2012, 6, 4763 –4776

2. N. Baccile, G. Pehau-Arnaudet, J. S. Pedersen, I Van Bogaert, *Surface*, Submitted

Crystallized droplets stabilized by solid particles: the combination of two principles for a well controlled distribution

F. MULLER[A,B], J. DEGROUARD[C], J. JESTIN[A], A. BRÛLET[A], A. SALONEN[C]

a Laboratoire d'Analyse et Contrôle des Systèmes Complexes (LACSC), ECE Paris Ecole d'Ingénieurs, 37 Quai de Grenelle, F-75015 Paris, France

b Laboratoire Léon Brillouin, CEA Saclay, France

c Laboratoire de Physique des Solides, Université Paris Sud, CNRS UMR-8502, 91405 Orsay Cedex, France

francoi.muller@cea.fr

Stabilizing oil droplets in water is not so simple, these two liquids having a natural tendency to separate for minimizing the area of their contact interface. This is however essential in the vectorization of certain medications, or for making cosmetic creams. Conversely, we can also look to prevent the dissolution of particles that are active and soluble in a solvent. In this context, the controlled dispersion of droplets stabilized in water by nanostructuring methods, is one of possible approaches.

Researchers from CEA, ECE-Paris, CNRS and Paris-Sud University conducted an innovative work on this issue by neutron scattering techniques, exploring the distribution of nanostructured droplets stabilized in water by clay nanoparticles. The work opens new opportunities for applications of interest to pharmaceutical or cosmetics companies.

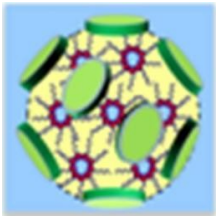

The principle of stabilizating oil droplets in water (forming an emulsion or "colloid") with solid particles, and not using the usual means of surfactant molecules is relatively old. This method is currently experiencing a growing success for the creation of functionalized nano-materials. According to the principle of Pickering, the particles surround the drops and thus isolate the hydrophobic molecules from the aqueous medium. By their nature or by functionalization, these stabilized emulsions form original nano-materials.

For their part, the aqueous dispersions of lipids in the form of crystallized particles of small size are of great interest for the cosmetic, food and pharmaceutical industries. They form simple vectors to transport hydrophobic AND hydrophilic molecules in an aqueous medium. Moreover their internal organization may be easily modified by simply changing the conditions of temperature, pH.

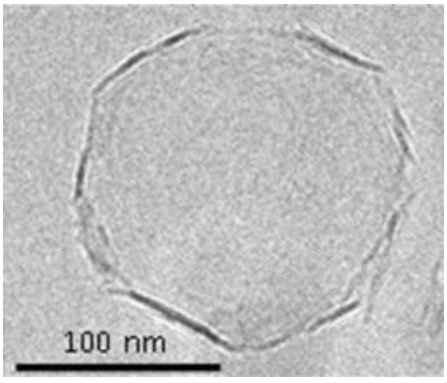

Figure 1:Electron microscope image of a drop stabilized in water.

It is only recently that these two principles (emulsion "Pickering" and dispersion of particles in crystallized form) were combined to obtain colloids combining the advantages of both approaches, and to create functional materials. In these new systems, the spatial distribution of the solid particles is a major parameter to control, because of its impact on the macroscopic and local properties of the materials.

With this objective, researchers from CEA, ECE-Paris, CNRS and Paris-Sud University were interested in this problem, that they approached by neutron studies. The system studied here consists of insoluble and nanostructured drops based on a lipid molecule called Phytantriol, widely used by the cosmetics industry as skin care. To stabilize drops in water, commercial nanometric clays (Laponite XLG) were added.

The samples were studied by neutron diffraction at the Laboratoire Léon Brillouin (LLB) in order to determine their molecular structure. By observing neutron scattering at small angles information on the organization of the material on a large scale is obtained, which gives access to the distribution of solid colloidal particles. Due to the high neutron scattering contrast between hydrogen and deuterium, using a mix-

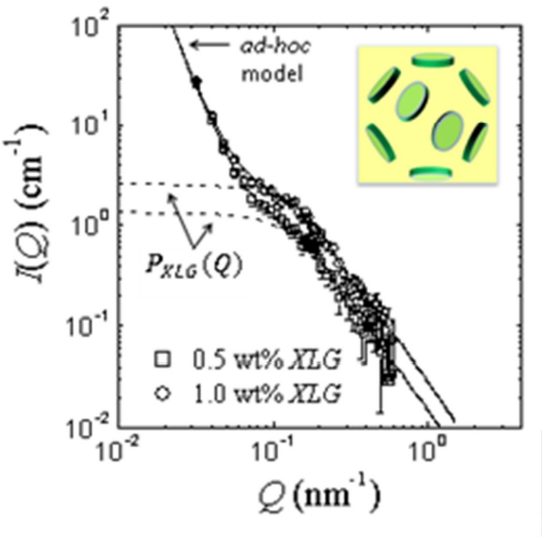

Figure 2; Signal of small angle scattering of two concentrations of Laponite XLG in a solvent hiding diffusion linked to the internal structure of the droplets. The rise to small Q values is characteristic of the formation of a Laponite XLG shell on the drops.

ture of light water and heavy water as solvent allows a complete information about this distribution. It was thus possible to determine accurately the invariance of the size and internal structure of the drops for different concentrations of Laponite XLG (charged particles disc shaped).

It was also shown that Laponite disks are located onto the surface of the drops, effectively forming a protective hard shell. This result is important because it shows that it is possible, by functionalization of the particles, to obtain nanoscale systems whose delivery may be controlled by external stimuli.

The shape of the drops was also studied by scattering at very small angles (TPA spectrometer newly available at the Laboratoire Léon Brillouin). The study shows that some particles deviate from spherical shape, exhibiting an angular shape. This transformation is a size effect that can be related to the ratio between their radius and that of the disks present on their surface. This trend is confirmed by additional experiments of electron microscopy.

The study by neutron scattering has thus proved to be a very efficient method to determine the global and local organization of such organized systems. A mathematical approach and simple models have been developed to explain the data. These results open new interesting applicative perspectives: it is indeed possible, in a stabilized and well characterized suspension, to add a function to the Laponite discs (post-stabilization) via soft chemistry methods to create systems that respond in a clearly defined manner to one or more external stimuli (magnetic, electrical, mechanical …).

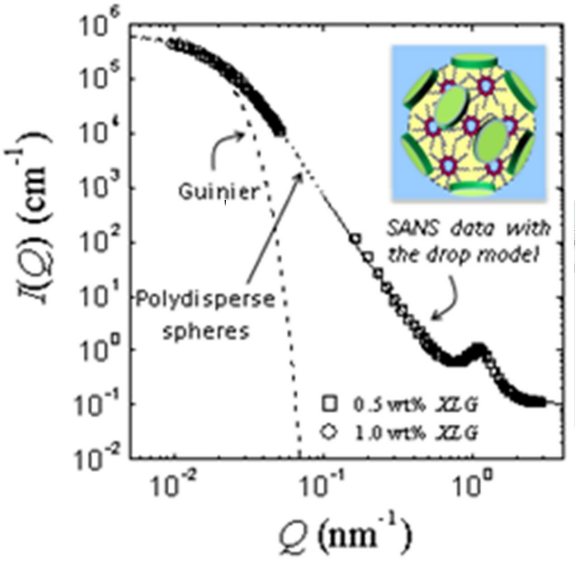

Figure 3: Signals diffused at very small angles and small angles for two Laponite XLG concentrations in a solvent, showing all available scales. The drops shape is generally spherical, however the details of adjustments indicate that some drops have an angular shape.

References

1. A. Salonen, F. Muller, O. Glatter, *Langmuir* **24** (2008) 5306.

2. F. Muller, A. Salonen, O. Glatter, *Journal of Colloid and Interface Science*, **342** (2010) 392.

3. C.M. Varma, F. Muller, J. Degrouard, J. Jestin, A. Brûlet, A. Salonen, *Soft Matter*, **8**(40) (2012) 10502.

Water management in fuel cells at sub-zero temperature: an *in operando* SANS-EIS coupled study

A. MORIN[A], Z. PENG[A], J. JESTIN[B], M. DETREZ[B], G. GEBEL[C]

a CEA-LITEN, Grenoble, France

b Laboratoire Léon Brillouin, CEA Saclay, France

c SPrAM, Grenoble, France

arnaud.morin@cea.fr

The water content in a proton exchange membrane was studied for the first time during fuel cell (PEMFC) operation at sub-zero temperature. The combined Small-Angle Neutron Scattering (SANS) and Electrochemical Impedance Spectroscopy (EIS) studies show that an increase of the current load at sub-zero temperature induces reversible membrane dehydration despite a higher production of water. This effect is revealed by the very good correlation between the increase of the membrane resistance measured by EIS and the decrease of water content in the membrane quantified from the SANS spectra. The predominance of the electro-osmosis on the back-diffusion, in addition to water crystallization in the channel and the gas diffusion layer, especially at the cathode side, explain the difficulty to operate a fuel cell at sub-zero temperature.

Proton exchange membrane fuel cells (PEMFCs) are considered as one of the most promising power sources for automotive, portable and stationary applications. The PEMFC performance and lifetime strongly depend on the water management. While several promising methods are currently developed such as the magnetic resonance imaging, the neutron radiography or the confocal raman microscopy, the Small-Angle Neutron Scattering (SANS) technique still appear as the most precise, less intrusive and more representative method for the study of the water distribution within the polymer membranes[1]. In previous studies, the SANS analysis was successfully applied to study the effect of many relevant operating parameters including gas hydration[2], gas flow configuration[3], the nature of the electrodes[4] or the behavior during ON/OFF cycling[5]. Most of these experiments were conducted with a fuel cell operating at 80°C. Nevertheless, it appears very interesting to study the fuel cell operation at sub-zero temperatures in order to elucidate the problems encountered with cold start during winter times.

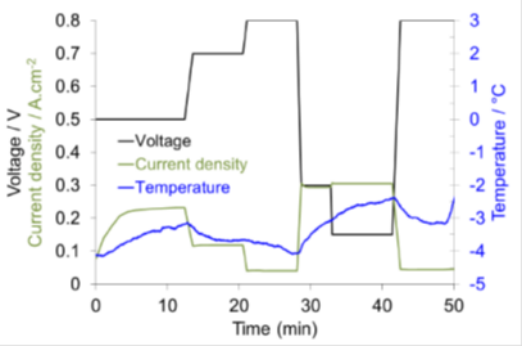

Figure 1 : Evolution of the voltage, the current density and the temperature during operation at subzero temperature

When starting a fuel cell at a sub-zero temperature, the water produced at the cathode freezes which limits the access of the gas to the catalytic sites and induces the choking of the fuel cell. However, we suspected an additional process based on the membrane dehydration. The water production at the cathode and the electro-osmosis process (water molecule transport due to proton migration from the anode to the cathode) generates a concentration gradient across the membrane and a back-diffusion in the opposite direction to proton transport. The temperature then appears as a first order parameter for the water repartition within the membrane. At high temperature, the diffusion coefficient is very large. It compensates the electro-osmosis drag and stationary conditions can be found. At low temperature, the diffusion coefficient significantly drops (typically by two orders of magnitude) while the electro-osmotic drag almost remain constant. It was then expected that the back-diffusion cannot compensate anymore the electro-osmosis process and that the membrane will dehydrate, especially at the anode side.

The main objective of this work is the study of the water management at sub-zero temperatures in order to validate the possibility to emphasize the electro-osmosis versus the back-diffusion.

A fuel cell transparent to neutron[1-5] was operated at subzero temperature and SANS spectra were regularly recorded (every 150 s). It can be noticed that the temperature within the cell slightly vary depending on the current load but remains nega-

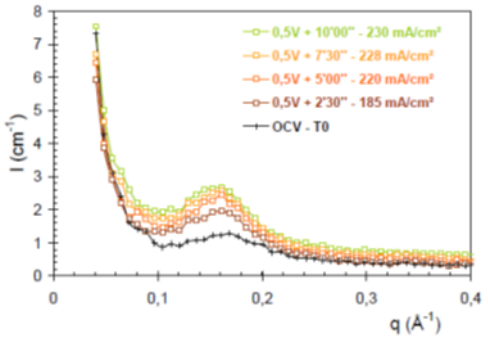

Figure 2 : SANS spectra recorded during fuel cell operation at around 200 mA/cm²

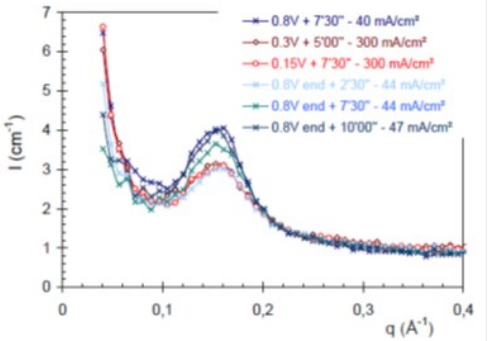

Figure 3 : Evolution of the SANS spectra after a step of current at 300 mA/cm² revealing a fast membrane dehydration and a slower recovery.

tive during the overall experiment. In addition, a series of SANS spectra were recorded at swelling equilibrium at 23°C in order to extract water concentration profiles across the membrane thickness during operation according to the previously published method[1-5].

Despite the sub-zero temperature, the water produced by the fuel cell is first used to swell the membrane as revealed by the increase of the ionomer peak intensity and its shift toward smaller q values. The membrane swelling is accompanied by a decrease of the membrane ohmic resistance measured simultaneously by electrochemical impedance spectroscopy (EIS). After stabilization of the membrane resistance, the current load was then decreased inducing a further increase of the membrane water content. We attributed this result to a decrease of the electro-osmosis effect. In order to verify this point, the current load was then significantly increased (300 mA/cm²) resulting in a very fast membrane dehydration observed simultaneously on the SANS and EIS data.

When decreasing again the current load, the membrane rehydrates with a slower kinetic. This result is a confirmation of our interpretation since the equilibration under diffusion appears significantly slower than the effect of electro-osmosis.

The results lead to a better understanding of the links between fundamental transport mechanisms of water and fuel cell operation.

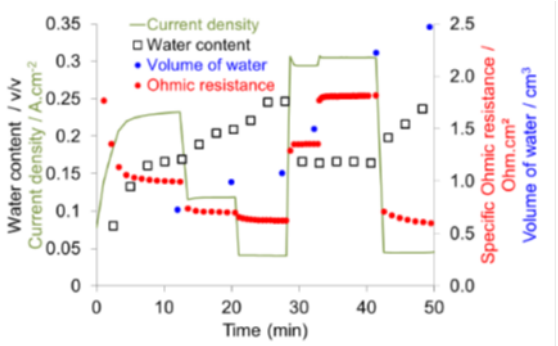

Figure 4 : Evolution of the ohmic resistance and the average water content in the membrane and the volume of water produced as a function of the current density.

References

1. S. Deabate, G. Gebel, P. Huguet, A. Morin, G. Pourcelly, *Energy Environ. Sci.*, (2012) 5, 8824
2. F. Xu, O. Diat, G. Gebel,A. Morin, A., *J. Electrochem.Soc.*, (2007) 154 B1389
3. A. Morin, F. Xu, G., Gebel, O., Diat, *Int. J. Hydrogen Energy*, (2011) 36 3096
4. G. Gebel, O. Diat, S. Escribano, R. Mosdale, *J. Power Sources*,(2008) 179, 132
5. Morin, A., Xu, F., Gebel, G., Diat, O. *Fuel Cells*, (2012) 12 156


reflets de la PHYSIQUE
n° 31
octobre 2012
www.refletsdelaphysique.fr
Revue de la Société Française de Physique
Dossier Supraconductivité
Les supraconducteurs à haute température critique
Avancées de la recherche
Découverte du boson de Higgs au LHC ?
Problèmes inverses en physique
Science et société
Une journée « Science et Médias »
www.sfpnet.fr

PUBLICATIONS
2012

1. P. A. Alekseev, J. M. Mignot, K. S. Nemkovski, A. V. Rybina, V. N. Lazukov, A. S. Ivanov, F. Iga and T. Takabatake, 'Interplay of low-energy phonons and magnetic excitations in the Kondo insulator YbB_{12}', *Journal of Physics -Condensed Matter*, 24 (2012).

2. P. A. Alekseev, K. S. Nemkovski, J. M. Mignot, E. A. Goremychkin, V. N. Lazukov, N. Y. Shitsevalova and A. V. Dukhnenko, 'Influence of an electron doping on spin dynamics of YbB_{12}', *Solid State Sciences*, 14 (2012), pp. 1584-1586.

3. P. A. Alekseev, K. S. Nemkovski, J. M. Mignot, V. N. Lazukov, A. A. Nikonov, A. P. Menushenkov, A. A. Yaroslavtsev, R. I. Bewley, J. R. Stewart and A. V. Gribanov, 'Magnetic excitations in $EuCu_2(Si_xGe_{1-x})_2$: from mixed valence towards magnetism', *Journal of Physics-Condensed Matter*, 24 (2012).

4. B. F. Alfonso, C. Pique, C. Trobajo, J. R. Garcia, E. Kampert, I. Mirebeau, N. Rey, J. Rodríguez Fernández, M. T. Fernandez-Díaz and J. A. Blanco, 'Neutron powder diffraction investigation in ammonium iron(III) bis (hydrogenphosphate)', *Journal of Physics: Conference Series*, 340 (2012), p. 012059.

5. M. Allix, S. Alahrache, F. Fayon, M. Suchomel, F. Porcher, T. Cardinal and G. Matzen, 'Highly Transparent $BaAl_4O_7$ Polycrystalline Ceramic Obtained by Full Crystallization from Glass', *Advanced Materials*, 24 (2012), pp. 5570-5575.

6. N. Baccile, F. Babonneau, J. Jestin, G. Pehau-Arnaudet and I. Van Bogaert, 'Unusual, pH-Induced, Self-Assembly Of Sophorolipid Biosurfactants', *Acs Nano*, 6 (2012), pp. 4763 -4776.

7. M. Baglioni, D. Berti, J. Teixeira, R. Giorgi and P. Baglioni, 'Nanostructured Surfactant-Based Systems for the Removal of Polymers from Wall Paintings: A Small-Angle Neutron Scattering Study', *Langmuir*, 28 (2012), pp. 15193-15202.

8. M. Baldini, L. Capogna, M. Capone, E. Arcangeletti, C. Petrillo, I. Goncharenko and P. Postorino, 'Pressure induced magnetic phase separation in $La_{0.75}Ca_{0.25}MnO_3$ manganite', *Journal of Physics-Condensed Matter*, 24 (2012).

9. L. F. Barquin, D. A. Venero, C. Echevarria-Bonet, R. G. Calderon, D. P. Rojas, J. Rodriguez-Carvajal and Q. A. Pankhurst, 'Scrutinising magnetic disorder through metastable 3d-and 4f-nanostructured alloys', *Journal of Alloys and Compounds*, 536 (2012), pp. S259-S264.

10. M. S. Barrow, P. R. Williams, H. H. Chan, J. C. Dore and M. C. Bellissent-Funel, 'Studies of cavitation and ice nucleation in 'doubly-metastable' water: time-lapse photography and neutron diffraction', *Physical Chemistry Chemical Physics*, 14 (2012), pp. 13255-13261.

11. D. Bazin, G. Andre, R. Weil, G. Matzen, V. Emmanuel, X. Carpentier and M. Daudon, 'Absence of Bacterial Imprints on Struvite-containing Kidney Stones: A Structural Investigation at the Mesoscopic and Atomic Scale', *Urology*, 79 (2012), pp. 786-790.

12. D. Bhowmik, N. Malikova, J. Teixeira, G. Meriguet, O. Bernard, P. Turq and W. Haussler, 'Study of tetrabutylammonium bromide in aqueous solution by neutron scattering', *European Physical Journal-Special Topics*, 213 (2012), pp. 303-312.

13. O. Borisova, L. Billon, M. Zaremski, B. Grassl, Z. Bakaeva, A. Lapp, P. Stepanek and O. Borisov, 'Synthesis and pH - and salinity-controlled self-assembly of novel amphiphilic block-gradient copolymers of styrene and acrylic acid', *Soft Matter*, 8 (2012), pp. 7649-7659.

14. F. Bouanani, D. Bendedouch, J. Teixeira, L. Marx and P. Hemery, 'Characterization of a miniemulsion by DLS and SANS', *Colloids and Surfaces a-Physicochemical and Engineering Aspects*, 404 (2012), pp. 47-51.

15. J. Bourgeois, G. Andre, S. Petit, J. Robert, M. Poienar, J. Rouquette, E. Elkaim, M. Hervieu, A. Maignan, C. Martin and F. Damay, 'Evidence of magnetic phase separation in $LuFe_2O_4$', *Physical Review B*, 86 (2012).

16. J. Bourgeois, M. Hervieu, M. Poienar, A. M. Abakumov, E. Elkaim, M. T. Sougrati, F. Porcher, F. Damay, J. Rouquette, G. Van Tendeloo, A. Maignan, J. Haines and C. Martin, 'Evidence of oxygen-dependent modulation in $LuFe_2O_4$', *Physical Review B*, 85 (2012).

17. I. M. Briman, D. Rebiscoul, O. Diat, J. M. Zanotti, P. Jollivet, P. Barboux and S. Gin, 'Impact of Pore Size and Pore Surface Composition on the Dynamics of Confined Water in Highly Ordered Porous Silica', *Journal of Physical Chemistry C*, 116 (2012), pp. 7021-7028.

18. F. Carn, F. Boue, M. Djabourov, N. Steunou, T. Coradin, J. Livage, S. Floquet, E. Cadot and E. Buhler, 'Biopolymer folding driven nanoparticle reorganization in bio-nanocomposites', *Soft Matter*, 8 (2012), pp. 2930-2944.

19. C. V. Cerclier, M. Ndao, R. Busselez, R. Lefort, E. Grelet, P. Huber, A. V. Kityk, L. Noirez, A. Schonhals and D. Morineau, 'Structure and Phase Behavior of a Discotic Columnar Liquid Crystal Confined in Nanochannels', *Journal of Physical Chemistry C*, 116 (2012), pp. 18990-18998.

20. M. Ceretti, A. Piovano, A. Cousson, T. Berthier, M. Meven, G. Agostini, J. Schefer, O. Hernandez, C. Lamberti and W. Paulus, 'Growth and characterization of large high quality brownmillerite $CaFeO_{2.5}$ single crystals', *Crystengcomm*, 14 (2012), pp. 5771-5776.

21. G. Chaboussant, S. Desert and A. Brulet, 'Recent developments and projects in SANS instrumentation at LLB-Orphee', *European Physical Journal-Special Topics*, 213 (2012), pp. 313-325.

22. G. Chaboussant, S. Desert, P. Lavie, A. Brulet and Iop, 'PA20: A new SANS and GISANS project for soft matter, materials and magnetism', in *5th European Conference on Neutron Scattering* (2012).

23. C. V. Colin, A. G. Perez, P. Bordet, C. Goujon and C. Darie, 'Symmetry adapted analysis of the magnetic and structural phase diagram of $Bi_{1-x}Y_xCrO_3$', *Physical Review B*, 85 (2012).

24. S. Combet and J. M. Zanotti, 'Further evidence that interfacial water is the main "driving force" of protein dynamics: a neutron scattering study on perdeuterated C-phycocyanin', *Physical Chemistry Chemical Physics*, 14 (2012), pp. 4927-4934.

25. C. Cornu, J. L. Bonardet, S. Casale, A. Davidson, S. Abramson, G. Andre, F. Porcher, I. Grcic, V. Tomasic, D. Vujevic and N. Koprivanac, 'Identification and Location of Iron Species in Fe/SBA-15 Catalysts: Interest for Catalytic Fenton Reactions', *Journal of Physical Chemistry C*, 116 (2012), pp. 3437-3448.

26. Y. Corvis, L. Barre, J. Jestin, J. Gummel and F. Cousin, 'Asphaltene adsorption mechanism under shear flow probed by in situ neutron reflectivity measurements', *European Physical Journal-Special Topics*, 213 (2012), pp. 295-302.

27. S. D'Ambrosio, V. Pashchenko, J. M. Mignot, O. Ignatchik, R. O. Kuzian, A. Savoyant, Z. Golacki, K. Grasza and A. Stepanov, 'Competing exchange interactions in Co-doped ZnO: Departure from the superexchange picture', *Physical Review B*, 86 (2012).

28. D. Damiron, J. Mazzolini, F. Cousin, C. Boisson, F. D'Agosto and E. Drockenmuller, 'Poly(ethylene) brushes grafted to silicon substrates', *Polymer Chemistry*, 3 (2012), pp. 1838-1845.

29. S. De Almeida-Didry, Y. Sidis, V. Baledent, F. Giovannelli, I. Monot-Laffez and P. Bourges, 'Evidence for intra-unit-cell magnetic order in $Bi_2Sr_2CaCu_2O_{8+\delta}$', *Physical Review B*, 86 (2012).

30. C. de la Calle, M. J. Martinez-Lope, V. Pomjakushin, F. Porcher and J. A. Alonso, 'Structure and magnetic properties of In_2RuMnO_6 and In_2RuFeO_6: Heavily transition-metal doped In_2O_3-type bixbyites', *Solid State Communications*, 152 (2012), pp. 95-99.

31. J. P. de Silva, F. Cousin, A. R. Wildes, M. Geoghegan and M. Sferrazza, 'Symmetric and asymmetric instability of buried polymer interfaces', *Physical Review E*, 86 (2012).

32. F. Dehouche, P. Archirel, H. Remita, N. Brodie-Linder and A. Traverse, 'Alcohol to water catalyzed by Pt nanoparticles: an experimental and computational approach', *Rsc Advances*, 2 (2012), pp. 6686-6694.

33. D. Delagnes, F. Pettinari-Sturmel, M. H. Mathon, R. Danoix, F. Danoix, C. Bellot, P. Lamesle and A. Grellier, 'Cementite-free martensitic steels: A new route to develop high strength/high toughness grades by modifying the conventional precipitation sequence during tempering', *Acta Materialia*, 60 (2012), pp. 5877-5888.

34. W. Deng, A. Brulet, P. A. Albouy, P. Keller, X. G. Wang and M. H. Li, 'Morphology study of a series of azobenzene-containing side-on liquid crystalline triblock copolymers', *Chinese Journal of Polymer Science*, 30 (2012), pp. 258-268.

35. L. Desgranges, Y. Pontillon, P. Matheron, M. Marcet, P. Simon, G. Guimbretiere and F. Porcher, 'Miscibility Gap in the U-Nd-O Phase Diagram: a New Approach of Nuclear Oxides in the Environment?', *Inorganic Chemistry*, 51 (2012), pp. 9147-9149.

36. M. Deutsch, N. Claiser, S. Pillet, Y. Chumakov, P. Becker, J. M. Gillet, B. Gillon, C. Lecomte and M. Souhassou, 'Experimental determination of spin-dependent electron density by joint refinement of X-ray and polarized neutron diffraction data', *Acta Crystallographica Section A*, 68 (2012), pp. 675-686.

37. A. J. Dos Santos-Garcia, E. Climent-Pascual, J. M. Gallardo-Amores, M. G. Rabie, Y. Doi, J. R. de Paz, B. Beuneu and R. Saez-Puche, 'Synthesis and magnetic properties of the high-pressure scheelite-type $GdCrO_4$ polymorph', *Journal of Solid State Chemistry*, 194 (2012), pp. 119-126.

38. C. Doubrovsky, G. Andre, F. Bouquet, E. Elkaim, M. Li, M. Greenblatt and P. Foury-Leylekian, 'Magnetic structure and physical properties of the multiferroic compound $PrMn_2O_5$', *Physica B-Condensed Matter*, 407 (2012), pp. 1718-1721.

39. C. Doubrovsky, G. Andre, A. Gukasov, P. Auban-Senzier, C. R. Pasquier, E. Elkaim, M. Li, M. Greenblatt, F. Damay and P. Foury-Leylekian, 'Magnetic phase transitions in $PrMn_2O_5$: Importance of ion-size threshold size effects in RMn_2O_5 compounds (R = rare earth)', *Physical Review B*, 86 (2012).

40. S. Dourdain, I. Hofmeister, O. Pecheur, J. F. Dufreche, R. Turgis, A. Leydier, J. Jestin, F. Testard, S. Pellet-Rostaing and T. Zemb, 'Synergism by Coassembly at the Origin of Ion Selectivity in Liquid-Liquid Extraction', *Langmuir*, 28 (2012), pp. 11319-11328.

41. W. Essafi, A. Abdelli, G. Bouajila and F. Boue, 'Behavior of Hydrophobic Polyelectrolyte Solution in Mixed Aqueous/Organic Solvents Revealed by Neutron Scattering and Viscosimetry', *Journal of Physical Chemistry B*, 116 (2012), pp. 13525-13537.

42. H. Euchner, S. Pailhes, L. T. K. Nguyen, W. Assmus, F. Ritter, A. Haghighirad, Y. Grin, S. Paschen and M. de Boissieu, 'Phononic filter effect of rattling phonons in the thermoelectric clathrate $Ba_8Ge_{40+x}Ni_{6-x}$', *Physical Review B*, 86 (2012).

43. A. L. Fameau, F. Cousin, F. Boue, F. Nallet, L. Navailles, F. Ott, B. Novales and J. P. Douliez, 'Multi-scale structural characterizations of fatty acid tubes with temperature tuneable diameter in bulk and at the air/water interface', *Neutron News*, 23 (2012), pp. 25-28.

44. A. L. Fameau, J. Ventureira, B. Novales and J. P. Douliez, 'Foaming and emulsifying properties of fatty acids neutralized by tetrabutylammonium hydroxide', *Colloids and Surfaces a-Physicochemical and Engineering Aspects*, 403 (2012), pp. 87-95.

45. F. Fillaux and A. Cousson, 'Neutron scattering studies of $K_3H(SO_4)_2$ and $K_3D(SO_4)_2$: The particle-in-a-box model for the quantum phase transition', *Journal of Chemical Physics*, 137 (2012).

46. F. Gal, H. Perez, V. Noel and G. Carrot, 'Water-Soluble Polymer-Grafted Platinum Nanoparticles for the Subsequent Binding of Enzymes. Synthesis and SANS', *Journal of Polymer Science Part a-Polymer Chemistry*, 50 (2012), pp. 289-296.

47. C. G. Gamys, E. Beyou, E. Bourgeat-Lami, L. David and J. Oberdisse, 'SAXS and SANS characterization of gelable polystyrene-b-poly(acryloxy propyl triethoxysilane) (PS-b-PAPTES) diblock copolymer micelles before and after hydrolysis-condensation', *Soft Matter*, 8 (2012), pp. 6564-6572.

48. A. C. Genix, M. Tatou, A. Imaz, J. Forcada, R.

Schweins, I. Grillo and J. Oberdisse, 'Modeling of Intermediate Structures and Chain Conformation in Silica-Latex Nanocomposites Observed by SANS During Annealing', *Macromolecules*, 45 (2012), pp. 1663-1675.

49. G. Gibrat, L. Assairi, C. T. Craescu, G. H. B. Hoa, D. Loew, B. Lombard, L. Blouquit and M. C. Bellissent-Funel, 'Use of SANS and biophysical techniques to reveal subtle conformational differences between native apocalmodulin and its unfolded states', *Biochimica Et Biophysica Acta-Proteins and Proteomics*, 1824 (2012), pp. 1097-1106.

50. R. Greget, G. L. Nealon, B. Vileno, P. Turek, C. Meny, F. Ott, A. Derory, E. Voirin, E. Riviere, A. Rogalev, F. Wilhelm, L. Joly, W. Knafo, G. Ballon, E. Terazzi, J. P. Kappler, B. Donnio and J. L. Gallani, 'Magnetic Properties of Gold Nanoparticles: A Room-Temperature Quantum Effect', *Chemphyschem*, 13 (2012), pp. 3092-3097.

51. R. Guantes, B. Cayrol, F. Busi and V. Arluison, 'Positive regulatory dynamics by a small noncoding RNA: speeding up responses under temperature stress', *Molecular Biosystems*, 8 (2012), pp. 1707-1715.

52. A. Guyomard-Lack, C. Cerclier, N. Beury, B. Jean, F. Cousin, C. Moreau and B. Cathala, 'Nano-structured cellulose nanocrystals-xyloglucan multilayered films for the detection of cellulase activity', *European Physical Journal-Special Topics*, 213 (2012), pp. 291-294.

53. I. Harsanyi and L. Pusztai, 'Hydration structure in concentrated aqueous lithium chloride solutions: A reverse Monte Carlo based combination of molecular dynamics simulations and diffraction data', *Journal of Chemical Physics*, 137 (2012).

54. I. Harsanyi, L. Temleitner, B. Beuneu and L. Pusztai, 'Neutron and X-ray diffraction measurements on highly concentrated aqueous LiCl solutions', *Journal of Molecular Liquids*, 165 (2012), pp. 94-100.

55. M. Hatnean, J. Robert, M. T. F. Diaz, E. Ressouche, A. Cousson, L. Pinsard-Gaudart and S. Petit, 'Neutron scattering study of the magnetoelectric compound $GaFeO_3$', *European Physical Journal-Special Topics*, 213 (2012), pp. 69-76.

56. C. Herriot, S. Khatun, E. T. Fox, P. Judeinstein, M. Armand, W. A. Henderson and S. Greenbaum, 'Diffusion Coefficients from C-13 PGSE NMR Measurements-Fluorine-Free Ionic Liquids with the $DCTA^-$ Anion', *Journal of Physical Chemistry Letters*, 3 (2012), pp. 441-444.

57. V. Hutanu, A. Sazonov, M. Meven, H. Murakawa, Y. Tokura, S. Bordacs, I. Kezsmarki and B. Nafradi, 'Determination of the magnetic order and the crystal symmetry in the multiferroic ground state of $Ba_2CoGe_2O_7$', *Physical Review B*, 86 (2012).

58. M. Iorgulescu, P. Roussel, N. Tancret, N. Renault, F. Porcher, G. Andre, H. Kabbour and O. Mentre, 'Mixed Metallic $Ba(Co,Fe)X_{0.2}O_{3.\delta}$ (X = F, Cl) Hexagonal Perovskites: Drastic Effect of Fe-Incorporation on Structural and Electronic Features', *Inorganic Chemistry*, 51 (2012), pp. 7598-7608.

59. B. Isare, G. Pembouong, F. Boue and L. Bouteiller, 'Conformational Control of Hydrogen-Bonded Aromatic Bis-Ureas', *Langmuir*, 28 (2012), pp. 7535-7541.

60. M. Ivanov, J. Banys, C. Bogicevic and J. M. Kiat, 'Size Effects on Dielectric Properties of Nanograin PSN Ceramics', *Ferroelectrics*, 429 (2012), pp. 43-47.

61. S. A. Ivanov, R. Tellgren, F. Porcher, T. Ericsson, A. Mosunov, P. Beran, S. K. Korchagina, P. A. Kumar, R. Mathieu and P. Nordblad, 'Preparation, structural, dielectric and magnetic properties of $LaFeO_3$-$PbTiO_3$ solid solutions', *Materials Research Bulletin*, 47 (2012), pp. 3253-3268.

62. S. A. Ivanov, R. Tellgren, C. Ritter, P. Nordblad, R. Mathieu, G. Andre, N. V. Golubko, E. D. Politova and M. Weil, 'Temperature-dependent multi-k magnetic structure in multiferroic Co_3TeO_6', *Materials Research Bulletin*, 47 (2012), pp. 63-72.

63. K. Iwasa, L. J. Hao, M. Kohgi, K. Kuwahara, J. M. Mignot, H. Sugawara, Y. Aoki, T. D. Matsuda and H. Sato, 'Magnetic Excitation in Totally Symmetric Staggered Ordered Phase of $PrFe_4P_{12}$', *Journal of the Physical Society of Japan*, 81 (2012).

64. E. Janod, F. Leclercq-Hugeux, H. Mutka and J. Teixeira, 'Neutrons, sciences and perspectives', *European Physical Journal-Special Topics*, 213 (2012), pp. 1-3.

65. M. Josse, M. El-Ghozzi, D. Avignant, G. Andre, F. Bouree and O. Isnard, 'Magnetic behaviour of the $MTbF_6$ fluoroterbates (M=Cd, Ca, Sr, (α/β)-Ba)', *Journal of Solid State Chemistry*, 185 (2012), pp. 229-237.

66. N. Jouault, F. Dalmas, F. Boue and J. Jestin, 'Multiscale characterization of filler dispersion and origins of mechanical reinforcement in model nanocomposites', *Polymer*, 53 (2012), pp. 761-775.

67. H. Kabbour, R. David, A. Pautrat, H. J. Koo, M. H. Whangbo, G. Andre and O. Mentre, 'A Genuine Two-Dimensional Ising Ferromagnet with Magnetically Driven Re-entrant Transition', *Angewandte Chemie-International Edition*, 51 (2012), pp. 11745-11749.

68. A. U. Khan, C. A. Nunes, G. C. Coelho, P. A. Suzuki, A. Grytsiv, F. Bourree, G. Giester and P. F. Rogl, 'Boron site preference in ternary Ta and Nb boron suicides', *Journal of Solid State Chemistry*, 190 (2012), pp. 1-7.

69. A. Koutsioubas, D. Lairez, S. Combet, G. C. Fadda, S. Longeville and G. Zalczer, 'Crowding effect on helix-coil transition: Beyond entropic stabilization', *Journal of Chemical Physics*, 136 (2012).

70. A. Koutsioubas, D. Lairez, G. Zalczer and F. Cousin, 'Slow and remanent electric polarization of adsorbed BSA layer evidenced by neutron reflection', *Soft Matter*, 8 (2012), pp. 2638-2643.

71. S. Kozhevnikov, F. Ott and F. Radu, 'Data representations of Zeeman spatial beam splitting in polarized neutron reflectometry', *Journal of Applied Crystallography*, 45 (2012), pp. 814-825.

72. Y. V. Kul'velis, V. T. Lebedev, V. A. Trunov, S. S. Ivanchev, O. N. Primanchenko and S. Y. Khaikin, 'Investigation of polymer hydrogels with memory effect for cefazolin immobilization by small-angle neutron scattering', *Journal of Surface Investigation-X-Ray Synchrotron and Neutron Techniques*,

6 (2012), pp. 825-832.

73. Y. V. Kul'velis, V. T. Lebedev, V. A. Trunov, O. N. Primachenko, S. Y. Khaikin, D. Torok and S. S. Ivanchev, 'Effect of preparation conditions on nanostructural features of the NAFION (R) type perfluorinated proton conducting membranes', *Petroleum Chemistry*, 52 (2012), pp. 565-570.
74. G. M. Kuz'micheva, I. A. Kaurova, V. B. Rybakov, S. S. Khasanov, A. Cousson, O. Zaharko, E. N. Domoroschina and A. B. Dubovsky, 'The color of langatate crystals and its relationship with composition and optical properties', *Crystal Research and Technology*, 47 (2012), pp. 131-138.
75. M. Laurent-Brocq, F. Legendre, M. H. Mathon, A. Mascaro, S. Poissonnet, B. Radiguet, P. Pareige, M. Loyer and O. Leseigneur, 'Influence of ball-milling and annealing conditions on nanocluster characteristics in oxide dispersion strengthened steels', *Acta Materialia*, 60 (2012), pp. 7150-7159.
76. M. L. P. Le, L. Cointeaux, P. Strobel, J. C. Lepretre, P. Judeinstein and F. Alloin, 'Influence of Solvent Addition on the Properties of Ionic Liquids', *Journal of Physical Chemistry C*, 116 (2012), pp. 7712-7718.
77. A. Lehoux, L. Ramos, P. Beaunier, D. B. Uribe, P. Dieudonne, F. Audonnet, A. Etcheberry, M. Jose-Yacaman and H. Remita, 'Tuning the Porosity of Bimetallic Nanostructures by a Soft Templating Approach', *Advanced Functional Materials*, 22 (2012), pp. 4900-4908.
78. M. Lenertz, J. Alaria, D. Stoeffler, S. Colis, A. Dinia, O. Mentre, G. Andre, F. Porcher and E. Suard, 'Magnetic structure of ground and field-induced ordered states of low -dimensional α-CoV2O6: Experiment and theory', *Physical Review B*, 86 (2012).
79. A. Lerbret, F. Affouard, A. Hedoux, S. Krenzlin, J. Siepmann, M. C. Bellissent-Funel and M. Descamps, 'How Strongly Does Trehalose Interact with Lysozyme in the Solid State? Insights from Molecular Dynamics Simulation and Inelastic Neutron Scattering', *Journal of Physical Chemistry B*, 116 (2012), pp. 11103-11116.
80. Y. Li, G. Yu, M. K. Chan, V. Baledent, N. Barisic, X. Zhao, K. Hradil, R. A. Mole, Y. Sidis, P. Steffens, P. Bourges and M. Greven, 'Two Ising-like magnetic excitations in a single-layer cuprate superconductor', *Nature Physics*, 8 (2012), pp. 404-410.
81. S. Longeville and W. Doster, 'Protein Dynamics and Function', in V. Garcia Sakail, C. Alba-Simionesco and S. H. Chen (eds.) *Dynamics of Soft Matter* (Springer US, 2012), pp. 205-246.
82. W. Maalej, S. Vilminot, G. Andre, Z. Elaoud, T. Mhiri and M. Kurmoo, 'Crystal and Magnetic Structures and Magnetic Properties of Selenate Containing Natrochalcite, $A^{I}M_2^{II}(H_3O_2)(SeO_4)_2$ Where A = Na or K and M = Mn, Co, or Ni', *Inorganic Chemistry*, 51 (2012), pp. 1953-1962.
83. O. L. Makarova, A. V. Tsvyashchenko, G. Andre, F. Porcher, L. N. Fomicheva, N. Rey and I. Mirebeau, 'Neutron diffraction study of the chiral magnet MnGe', *Physical Review B*, 85 (2012).
84. B. Malard, B. Remy, C. Scott, A. Deschamps, J. Chene, T. Dieudonne and M. H. Mathon, 'Hydrogen trapping by VC precipitates and structural defects in a high strength Fe-Mn-C steel studied by small-angle neutron scattering', *Materials Science and Engineering a-Structural Materials Properties Microstructure and Processing*, 536 (2012), pp. 110-116.
85. N. Malikova, S. Cebasek, V. Glenisson, D. Bhowmik, G. Carrot and V. Vlachy, 'Aqueous solutions of ionenes: interactions and counterion specific effects as seen by neutron scattering', *Physical Chemistry Chemical Physics*, 14 (2012), pp. 12898-12904.
86. N. Martin, L.-P. Regnault and S. Klimko, 'Neutron Larmor Diffraction study of the $BaM_2(XO_4)_2$ (M = Co, Ni; X = As, P) compounds', *Journal of Physics: Conference Series*, 340 (2012), p. 012012.
87. M. J. Martinez-Lope, M. Retuerto, C. de la Calle, F. Porcher and J. A. Alonso, 'Why $MnIn_2O_4$ spinel is not a transparent conducting oxide?', *Journal of Solid State Chemistry*, 187 (2012), pp. 172-176.
88. M. H. Mathon, M. Perrut, S. Y. Zhong and Y. de Carlan, 'Small angle neutron scattering study of martensitic/ferritic ODS alloys', *Journal of Nuclear Materials*, 428 (2012), pp. 147-153.
89. V. Maurice, C. Slostowski, N. Herlin-Boime and G. Carrot, 'Polymer-Grafted Silicon Nanoparticles Obtained Either via Peptide Bonding or Click Chemistry', *Macromolecular Chemistry and Physics*, 213 (2012), pp. 2498-2503.
90. C. Mayer, E. Gaudin, S. Gorsse, F. Porcher, G. Andre and B. Chevalier, 'Magnetic structure of the ferromagnetic new ternary silicide Nd_5CoSi_2', *Journal of Physics-Condensed Matter*, 24 (2012).
91. F. Michaux, J. L. Blin, J. Teixeira and M. J. Stebe, 'Structural Investigation of Nonionic Fluorinated Micelles by SANS in Relation to Mesoporous Silica Materials', *Journal of Physical Chemistry B*, 116 (2012), pp. 261-268.
92. I. Mirebeau and S. Petit, 'Recent results and perspectives in neutron studies of geometrically frustrated magnets', *European Physical Journal-Special Topics*, 213 (2012), pp. 37-51.
93. T. Mongstad, C. Platzer-Bjorkman, J. P. Maehlen, B. C. Hauback, S. Z. Karazhanov and F. Cousin, 'Surface oxide on thin films of yttrium hydride studied by neutron reflectometry', *Applied Physics Letters*, 100 (2012).
94. F. Muller, J. Degrouard, J. Jestin, A. Brulet and A. Salonen, 'How clay colloids surround internally self-assembled phytantriol drops', *Soft Matter*, 8 (2012), pp. 10502-10510.
95. A. Munoz, J. A. Alonso, M. J. Martinez-Lope, V. Pomjakushin and G. Andre, 'On the magnetic structure of $PrMn_2O_5$: a neutron diffraction study', *Journal of Physics-Condensed Matter*, 24 (2012).
96. L. Noirez and P. Baroni, 'Identification of a low-frequency elastic behaviour in liquid water', *Journal of Physics-Condensed Matter*, 24 (2012).
97. L. Noirez, P. Baroni and H. J. Cao, 'Identification of Shear Elasticity at Low Frequency in Liquid n-Heptadecane, Liquid Water and RT-Ionic Liquids emim

Tf2N', *Journal of Molecular Liquids*, 176 (2012), pp. 71-75.

98. L. Noirez, H. Mendil-Jakani, P. Baroni and J. H. Wendorff, 'Richness of Side-Chain Liquid-Crystal Polymers: From Isotropic Phase towards the Identification of Neglected Solid-Like Properties in Liquids', *Polymers*, 4 (2012), pp. 1109-1124.

99. P. Ondrejkovic, M. Kempa, Y. Vysochanskii, P. Saint-Gregoire, P. Bourges, K. Z. Rushchanskii and J. Hlinka, 'Neutron scattering study of ferroelectric $Sn_2P_2S_6$ under pressure', *Physical Review B*, 86 (2012).

100. F. Onufrieva and P. Pfeuty, 'Low-Doping Anomalies in High-T-c Cuprate Superconductors as Evidence of a Spin-Fluctuation-Mediated Superconducting State', *Physical Review Letters*, 109 (2012).

101. G. Pabst, C. Lonez, M. Vandenbranden, J. Jestin, A. Radulescu, J. M. Ruysschaert and T. Gutberlet, 'Stalk-free membrane fusion of cationic lipids via an interdigitated phase', *Soft Matter*, 8 (2012), pp. 7243-7249.

102. E. Pachoud, K. Singh, Y. Breard, C. Martin, G. Andre, V. Hardy, C. Simon and A. Maignan, 'Magnetic dilution and steric effects in the multiferroic delafossite $CuCrO_2$', *Physical Review B*, 86 (2012).

103. J. Panarin, S. Raymond, G. Lapertot and J.-M. Mignot, 'Effects of impurities in $CeCoIn_5$ using inelastic neutron scattering', *Journal of Physics: Conference Series*, 340 (2012), p. 012073.

104. D. Parshall, G. Chen, L. Pintschovius, D. Lamago, T. Wolf, L. Radzihovsky and D. Reznik, 'Competition between commensurate and incommensurate magnetic ordering in $Fe_{1+y}Te$', *Physical Review B*, 85 (2012).

105. A. Pautrat, A. Brulet, C. Simon and P. Mathieu, 'Flux-lines lattice order and critical current studied by time-of-flight small-angle neutron scattering', *Physical Review B*, 85 (2012).

106. M. Perrut, M. H. Mathon and D. Delagnes, 'Small-angle neutron scattering of multiphase secondary hardening steels', *Journal of Materials Science*, 47 (2012), pp. 1920-1929.

107. S. Petit, P. Bonville, I. Mirebeau, H. Mutka and J. Robert, 'Spin dynamics in the ordered spin ice $Tb_2Sn_2O_7$', *Physical Review B*, 85 (2012).

108. S. Petit, P. Bonville, J. Robert, C. Decorse and I. Mirebeau, 'Spin liquid correlations, anisotropic exchange, and symmetry breaking in $Tb_2Ti_2O_7$', *Physical Review B*, 86 (2012).

109. M. Poienar, V. Hardy, B. Kundys, K. Singh, A. Maignan, F. Damay and C. Martin, 'Revisiting the properties of delafossite $CuCrO_2$: A single crystal study', *Journal of Solid State Chemistry*, 185 (2012), pp. 56-61.

110. P. Pullmannova, M. Bastos, G. Y. Bai, S. S. Funari, I. Lacko, F. Devinsky, J. Teixeira and D. Uhrikova, 'The ionic strength effect on the DNA complexation by DOPC - gemini surfactants liposomes', *Biophysical Chemistry*, 160 (2012), pp. 35-45.

111. N. Qureshi, P. Steffens, Y. Drees, A. C. Komarek, D. Lamago, Y. Sidis, L. Harnagea, H. J. Grafe, S. Wurmehl, B. Buchner and M. Braden, 'Inelastic Neutron-Scattering Measurements of Incommensurate Magnetic Excitations on Superconducting LiFeAs Single Crystals', *Physical Review Letters*, 108 (2012).

112. D. Renard, C. Garnier, A. Lapp, C. Schmitt and C. Sanchez, 'Structure of arabinogalactan-protein from Acacia gum: From porous ellipsoids to supramolecular architectures', *Carbohydrate Polymers*, 90 (2012), pp. 322-332.

113. M. Retuerto, C. de la Calle, M. J. Martinez-Lope, F. Porcher, K. Krezhov, N. Menendez and J. A. Alonso, 'Double perovskite $Sr_2FeMoO_{6-x}N_x$ (x=0.3, 1.0) oxynitrides with anionic ordering', *Journal of Solid State Chemistry*, 185 (2012), pp. 18-24.

114. A. S. Robbes, F. Cousin, F. Meneau, C. Chevigny, D. Gigmes, J. Fresnais, R. Schweins and J. Jestin, 'Controlled grafted brushes of polystyrene on magnetic γ-Fe2O3 nanoparticles via nitroxide-mediated polymerizatio$_n$', *Soft Matter*, 8 (2012), pp. 3407-3418.

115. A. S. Robbes, F. Cousin, F. Meneau, F. Dalmas, R. Schweins, D. Gigmes and J. Jestina, 'Polymer-Grafted Magnetic Nanoparticles in Nanocomposites: Curvature Effects, Conformation of Grafted Chain, and Bimodal Nanotriggering of Filler Organization by Combination of Chain Grafting and Magnetic Field', *Macromolecules*, 45 (2012), pp. 9220-9231.

116. J. Robert, J. M. Mignot, S. Petit, P. Steffens, T. Nishioka, R. Kobayashi, M. Matsumura, H. Tanida, D. Tanaka and M. Sera, 'Anisotropic Spin Dynamics in the Kondo Semiconductor $CeRu_2Al_{10}$', *Physical Review Letters*, 109 (2012).

117. V. Ryukhtin, B. Saruhan, R. Ochrombel, L. Noirez and A. Wiedenmann, 'Studying of PYSZ and FYSZ turbine blade coatings by small-angle neutron scattering', *Journal of Physics: Conference Series*, 340 (2012), p. 012097.

118. C. Said-Mohamed, J. Niskanen, D. Lairez, H. Tenhu, P. Maioli, N. Del Fatti, F. Vallee and L. T. Lee, 'Polymer-Modulated Optical Properties of Gold Sols', *Journal of Physical Chemistry C*, 116 (2012), pp. 12660-12669.

119. A. P. Sazonov, A. Gukasov, I. Mirebeau and P. Bonville, 'Double-layered monopolar order in the $Tb_2Ti_2O_7$ spin liquid', *Physical Review B*, 85 (2012).

120. M. Schoeffel, N. Brodie-Linder, F. Audonnet and C. Alba -Simionesco, 'Wall thickness determination of hydrophobically functionalized MCM-41 materials', *Journal of Materials Chemistry*, 22 (2012), pp. 557-567.

121. L. Shi, F. Carn, F. Boue, G. Mosser and E. Buhler, 'Nanorods of Well-Defined Length and Monodisperse Cross -Section Obtained from Electrostatic Complexation of Nanoparticles with a Semiflexible Biopolymer', *Acs Macro Letters*, 1 (2012), pp. 857-861.

122. Y. Shor, E. Yahel and G. Makov, 'Short range order in anomalous liquid metals', *Journal of Non-Crystalline Solids*, 358 (2012), pp. 2687-2694.

123. A. Slodczyk, P. Colomban, D. Lamago, G. Andre, O. Zaafrani, O. Lacroix, A. Sirat, F. Grasset and B. Sala, 'Optimum temperature range for the proton dynamics in H -doped $BaZrO_3$:Yb dense ceramics-a neutron scattering study', *Journal of Materials Research*, 27 (2012), pp. 1939-

1949.

124. A. Slodczyk, P. Colomban, G. Andre, O. Zaafrani, F. Grasset, O. Lacroix and B. Sala, 'Structural modifications induced by free protons in proton conducting perovskite zirconate membrane', *Solid State Ionics 18 Proceedings of the 18th International Conference on Solid State Ionics Warsaw, Poland, July 3 -8, 2011*, 225 (2012), pp. 214-218.

125. A. Solignac, R. Guerrero, P. Gogol, T. Maroutian, F. Ott, L. Largeau, P. Lecoeur and M. Pannetier-Lecoeur, 'Dual Antiferromagnetic Coupling at $La_{0.67}Sr_{0.33}MnO_3$/ $SrRuO_3$ Interfaces', *Physical Review Letters*, 109 (2012).

126. A. Solignac, R. Guerrero, P. Gogol, T. Maroutian, F. Ott, P. Lecoeur, C. Fermon and M. Pannetier-Lecoeur, 'Temperature Study of the Antiferromagnetic Coupling at the Interface of $La_{0.7}Sr_{0.3}MnO_3$ and $SrRuO_3$ Bilayers', *Ieee Transactions on Magnetics*, 48 (2012), pp. 4363-4366.

127. R. Sood, C. Iojoiu, E. Espuche, F. Gouanve, G. Gebel, H. Mendil-Jakani, S. Lyonnard and J. Jestin, 'Proton Conducting Ionic Liquid Doped Nation Membranes: Nano-Structuration, Transport Properties and Water Sorption', *Journal of Physical Chemistry C*, 116 (2012), pp. 24413-24423.

128. G. Sudre, D. Hourdet, F. Cousin, C. Creton and Y. Tran, 'Structure of Surfaces and Interfaces of Poly(N,N-dimethylacrylamide) Hydrogels', *Langmuir*, 28 (2012), pp. 12282-12287.

129. G. Sudre, E. Siband, D. Hourdet, C. Creton, F. Cousin and Y. Tran, 'Synthesis and Characterization of Poly(acrylic acid) Brushes: "Grafting-Onto" Route', *Macromolecular Chemistry and Physics*, 213 (2012), pp. 293-300.

130. E. Tamborini, N. Ghofraniha, J. Oberdisse, L. Cipelletti and L. Ramos, 'Structure of Nanoparticles Embedded in Micellar Polycrystals', *Langmuir*, 28 (2012), pp. 8562-8570.

131. J. Teixeira, 'Recent experimental aspects of the structure and dynamics of liquid and supercooled water', *Molecular Physics*, 110 (2012), pp. 249-258.

132. M. Tharcis, T. Breiner, J. Belleney, F. Boue and L. Bouteiller, 'Hydrogen bonded supramolecular polymers in protic solvents: role of multitopicity', *Polymer Chemistry*, 3 (2012), pp. 3093-3099.

133. L. Toualbi, C. Cayron, P. Olier, J. Malaplate, M. Praud, M. H. Mathon, D. Bossu, E. Rouesne, A. Montani, R. Loge and Y. de Carlan, 'Assessment of a new fabrication route for Fe-9Cr-1W ODS cladding tubes', *Journal of Nuclear Materials*, 428 (2012), pp. 47-53.

134. R. Troc, M. Pasturel, O. Tougait, A. P. Sazonov, A. Gukasov, C. Sulkowski and H. Noel, 'Single-crystal study of the kagome antiferromagnet $U_3Ru_4Al_{12}$', *Physical Review B*, 85 (2012).

135. D. Uhrikova, N. Kucerka, A. Lengyel, P. Pullmannova, J. Teixeira, T. Murugova, S. S. Funari and P. Balgavy, 'Lipid bilayer - DNA interaction mediated by divalent metal cations: SANS and SAXD study', *Journal of Physics: Conference Series*, 351 (2012), p. 12011.

136. H. Ulbrich, P. Steffens, D. Lamago, Y. Sidis and M. Braden, 'Hourglass Dispersion in Overdoped Single-Layered Manganites', *Physical Review Letters*, 108 (2012).

137. M. Viret, D. Rubi, D. Colson, D. Lebeugle, A. Forget, P. Bonville, G. Dhalenne, R. Saint-Martin, G. Andre and F. Ott, 'β-$NaFeO_2$, a new room-temperature multiferroic material', *Materials Research Bulletin*, 47 (2012), pp. 2294-2298.

138. I. Voleska, J. Akola, P. Jovari, J. Gutwirth, T. Wagner, T. Vasileiadis, S. N. Yannopoulos and R. O. Jones, 'Structure, electronic, and vibrational properties of glassy $Ga_{11}Ge_{11}Te_{78}$: Experimentally constrained density functional study', *Physical Review B*, 86 (2012).

139. F. Weber, L. Pintschovius, K. Hradil and D. Petitgrand, 'Phonon line shapes in the vortex state of the phonon-mediated superconductor YNi_2B_2C', *Physical Review B*, 85 (2012).

140. P. Wisniewski, P. Swatek, A. Gukasov and D. Kaczorowski, 'Ferromagnetism in UMn_2Al_{20} studied with polarized neutron diffraction and bulk magnetic measurements', *Physical Review B*, 86 (2012).

141. K. Yoshida, K. Vogtt, Z. Izaola, M. Russina, T. Yamaguchi and M. C. Bellissent-Funel, 'Alcohol induced structural and dynamic changes in β-lactoglobulin in aqueous solution: A neutron scattering study', *Biochimica Et Biophysica Acta-Proteins and Proteomics*, 1824 (2012), pp. 502-510.

142. K. Yoshida, T. Yamaguchi, S. Kittaka, M. C. Bellissent-Funel and P. Fouquet, 'Neutron spin echo measurements of monolayer and capillary condensed water in MCM-41 at low temperatures', *Journal of Physics-Condensed Matter*, 24 (2012).

143. J. M. Zanotti, K. Lagrene, N. Malikova, P. Judeinstein, K. Panesar, J. Ollivier, S. Rols, M. Mayne-L'Hermite, M. Pinault and P. Boulanger, 'Nanometric confinement: Toward new physical properties and technological developments Relevance and potential contributions of neutron scattering', *European Physical Journal-Special Topics*, 213 (2012), pp. 129-148.

144. J.-M. Zanotti and D. Morineau, 'Surface and Confinement Effects in Nano/Mesoporous Materials', in V. Garcia SakaiI, C. Alba-Simionesco and S. H. Chen (eds.) *Dynamics of Soft Matter* (Springer US, 2012), pp. 367-409.

145. X. W. Zhang, S. Boisse, C. Bui, P. A. Albouy, A. Brulet, M. H. Li, J. Rieger and B. Charleux, 'Amphiphilic liquid-crystal block copolymer nanofibers via RAFT-mediated dispersion polymerization', *Soft Matter*, 8 (2012), pp. 1130-1141.

146. S. Y. Zhong, J. Ribis, V. Klosek, Y. de Carlan, N. Lochet, V. Ji and M. H. Mathon, 'Study of the thermal stability of nanoparticle distributions in an oxide dispersion strengthened (ODS) ferritic alloys', *Journal of Nuclear Materials*, 428 (2012), pp. 154-159.

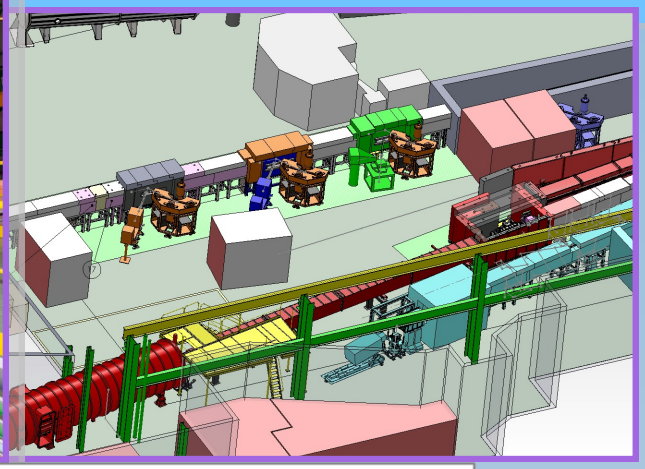

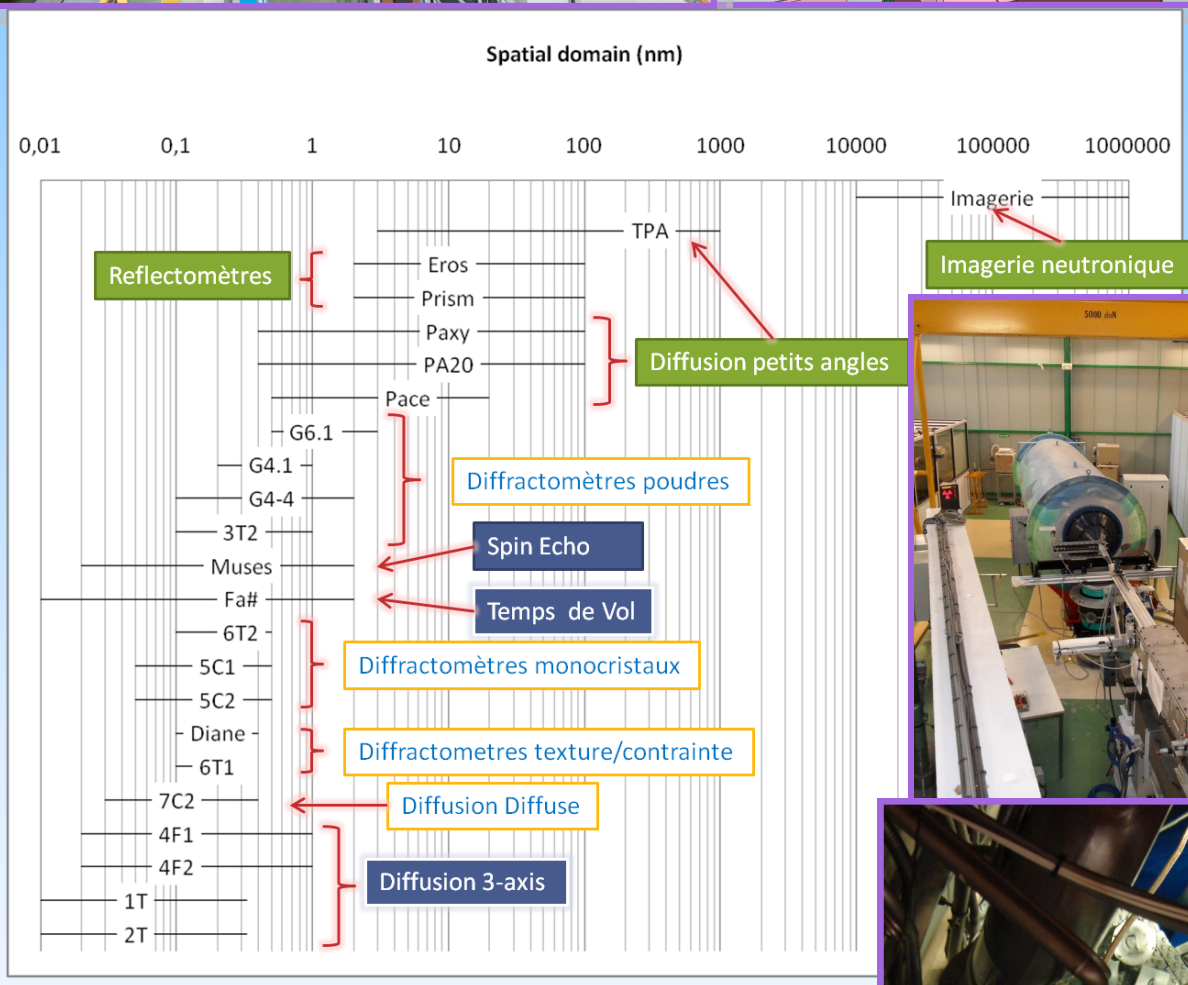
Spatial domain (nm)
0,01
0,1
1
10
100
1000
10000
100000
1000000
Imagerie
TPA
Reflectomètres
Eros
Prism
Paxy
PA20
Pace
Diffusion petits angles
Imagerie neutronique
G6.1
G4.1
G4-4
3T2
Muses
Fa#
Diffractomètres poudres
Spin Echo
Temps de Vol
6T2
5C1
5C2
Diane
6T1
Diffractomètres monocristaux
Diffractometres texture/contrainte
7C2
4F1
4F2
1T
2T
Diffusion Diffuse
Diffusion 3-axis

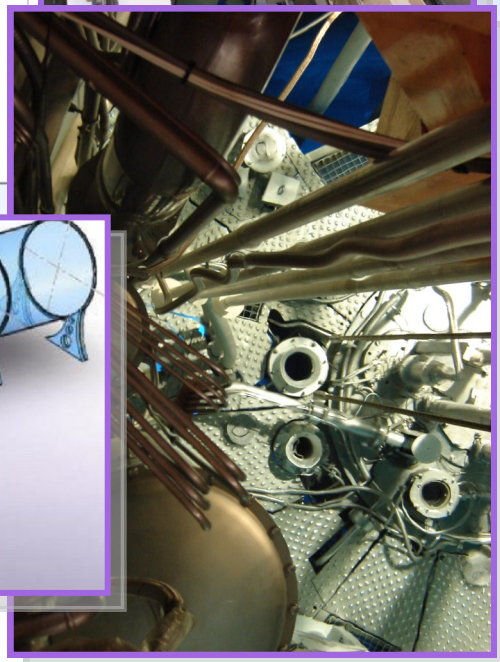

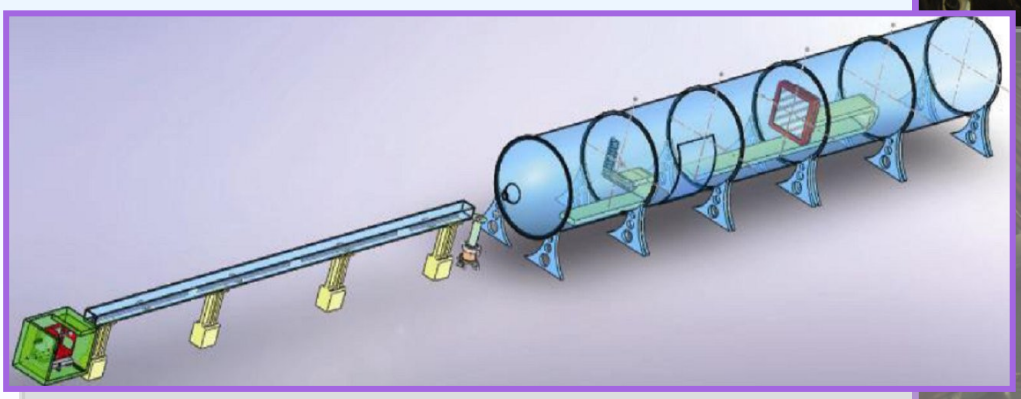

REACTOR AND SPECTROMETERS

REPLACEMENT OF COLD SOURCES SF1 AND SF2

After 15 years of use, cold sources SF1 and SF2 were replaced during the summer break of 2012. This working, in charge of Orphée Reactor operators, required a complete strain and drying of the reactor pool and concluded a two-years period of conception and preparation work.

The new cold source and its thimble

A tidy operation : inserting SF2 inside its thimble !

Preparing the assembling in Reactor Hall

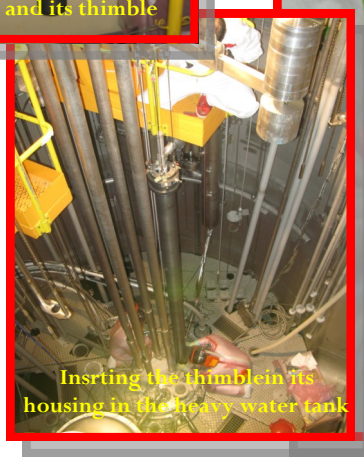

Insrting the thimblein its housing in the heavy water tank

Finishing the installation in the reactor pool

REPLACEMENT OF 9F COLD-BEAM THIMBLE

The 9F thimble, feeding guides G5 and G6 with cold neutrons, was also changed during the same period. For that heavy operation, 2/3 of the reactor Hall instruments were dismounted and parked away in order to make room for the extraction/mounting machine.

The reactor Hall before...

... and during ...

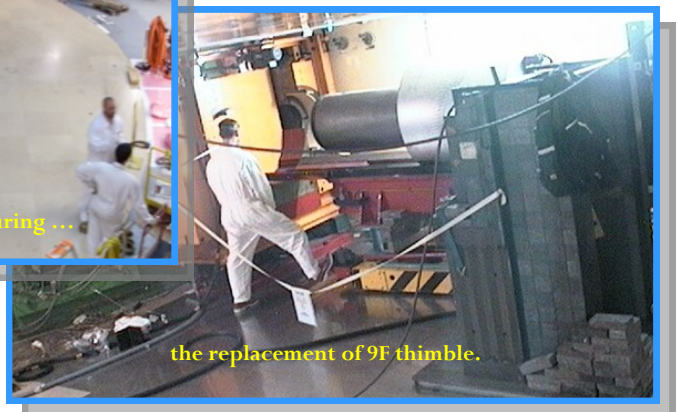

the replacement of 9F thimble.

PREPARING THE ARRIVAL OF PA20 SMALL-ANGLE SPECTROMETER

In the same time the LLB technical team prepared the arrival of new small-angle spectrometer PA20 . The installation of PA20 upset the SW part of the Hall of Guides, where Back-Scattering spectrometer MIBEMOL and small-angle machine PAXE were decommissioned in 2012.

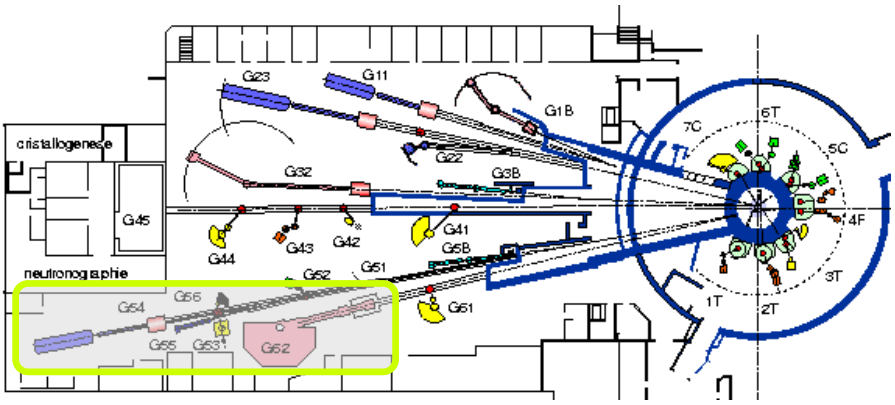


Guide G5 before dismounting (former experimental areas of material diffractometer DIANE, relocated of G4, and test diffractometer G5.6)


1 month after : guides G5 and G6 are gone….

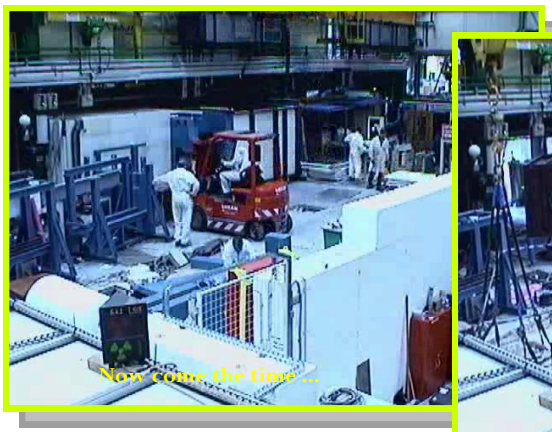
Now come the time …

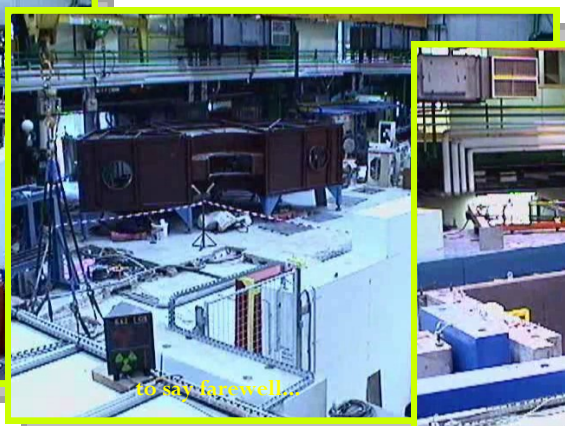
to say farewell…


to MIBEMOL !

2012: 1st common call for thesis organized by LLB and SOLEIL

Neutron schools

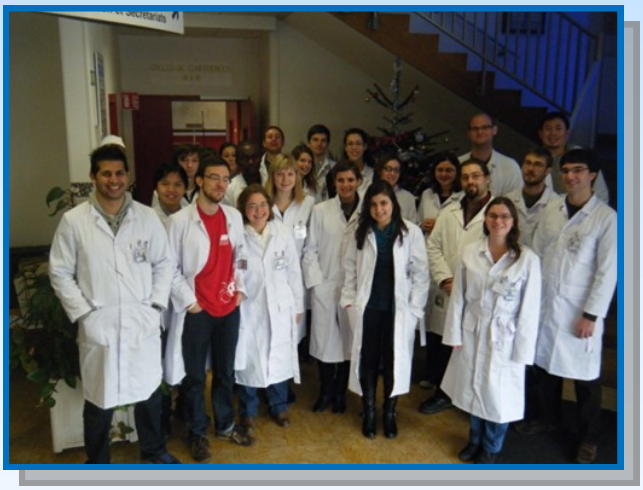

Masters:

lectures, practical work, students visits in connection with universities (Paris, Bordeaux, Rennes…)

TEACHING AND EDUCATION

FAN DU LLB (NOVEMBER 26-29 2012)

FAN du LLB is an annual school delivered in French and offering young French-speaking researchers a first contact with real experimental neutron scattering. The school is aimed at students and post-docs working in all scientific areas where neutrons can provide valuable insights, although *priority is given to those having never had any contact with neutrons scattering*. After an introduction to neutron sources and neutron scattering, ten different thematic subjects based on different scientific problems that can be addressed by neutron scattering, are proposed to the students. In groups of four to five, the students are then introduced to two different neutrons scattering technique, during three days devoted to experiments and data analysis. One of the distinguishing features of our school is that the students often come with their own samples, which are tested during the training together with our demonstration samples. This ensures a good and efficient participation of the students. In 2012, the number of participants was 31.

Website: http://www-llb.cea.fr/fan

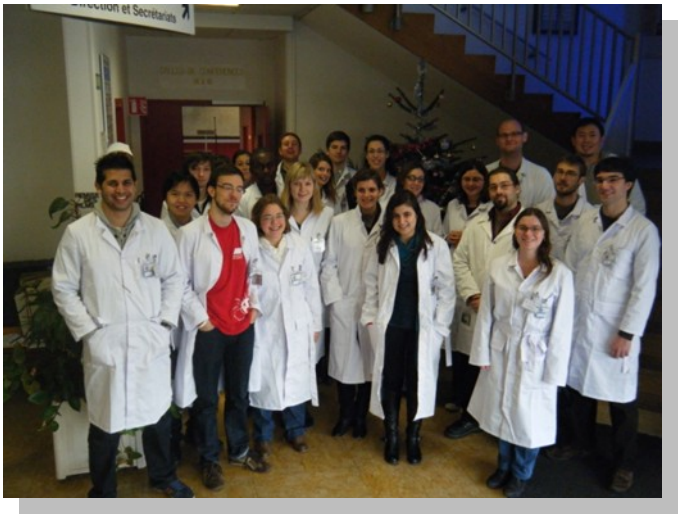

JDN 20 (MAY 18-24 2012)

Every year, the French Neutron Society (SFN), with the help of LLB and ILL centers and Grenoble UJF University, organizes the "Journées de la Neutronique", that gathers the national neutrons community. Exceptionnaly, there were no thematic school in the 19th edition, but the duration of Rossat-Mignod meeting was lengthened in order to present the state of the art and the new scientific and technological perspectives of Neutron scattering.

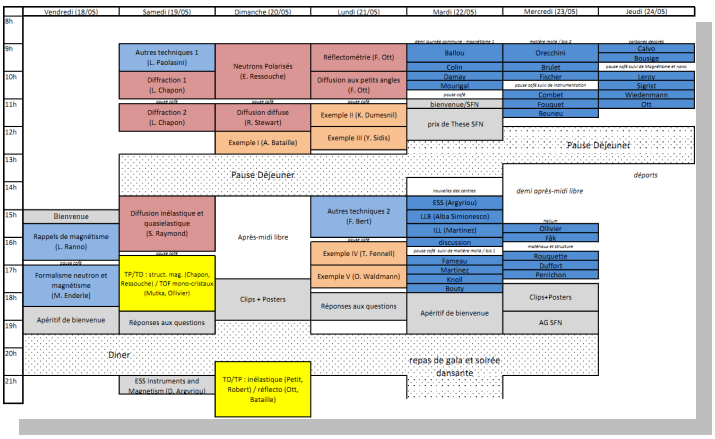

NEW PHD STUDENTS IN 2012

MANGIN-THRO Lucile-CNRS/CEA-2012-2015

"Phase de "Boucles de courants circulants" dans les supraconducteurs à haute température critique"

Supervisor : P. Bourges
(*Strongly Correlated Quantum Materials and Magnetism*)

GUITTENY Solène-CEA-2012-2015

"Structure et dynamique de spin dans les pyrochlores géométriquement frustrés"

Supervisor : S. Petit
(*Strongly Correlated Quantum Materials and Magnetism*)

FERDEGHINI Filippo-CNRS/CEA-2012-2015

« Liquide ionique sous confinement nanométrique 1D »

Supervisor : J.M. Zanotti (*Soft matter and Biophysics*)

FOUCHER Damien – Grant UVSQ-2012-2015

(**Call LLB/SOLEIL 2012**)

«Impact de l'eau dans la flexibilité des MOF, Méthodologie conjointe de mesure par XRD Synchrotron, RMN et diffraction/diffusion des neutrons »

Supervisors : F. Taulelle (Versailles) / F. Porcher - (LLB)
(*Materials and Nanosciences: Fundamental Studies and Applications*)

BLOUZON Camille– CEA-2012-2015

(**Call LLB/SOLEIL 2012**)

«Manipulation d'une aimantation par l'action d'un champ électrique en utilisant un matériau 'multiferroïque' »

Supervisors : M. Viret (CEA Saclay) / F. Ott - (LLB)
(*Materials and Nanosciences: Fundamental Studies and Applications*)

KAHL Philipp – CEA/Région Pays de Loire-2012-2015

« Identification de nouvelles propriétés dynamiques dans les liquides : corrélations solides à longue portée & rôle de l'interaction fluide/substrat »

Supervisor : L. Noirez
(*Materials and Nanosciences: Fundamental Studies and Applications*)

THESES DEFENDED IN 2012

BOURGEOIS Julie– March 27 2012

«Les ferrites du type RFe_2O_4 à valence mixte »

Supervisors : C. Martin (Caen) / F. Damay
(*Strongly Correlated Quantum Materials and Magnetism*)

HATNEAN Monica – December 17 2012

«Etude magnétique et structurale des composés magnétoélectriques $GaFeO_3$ »

Supervisors : L. Pinsard (Orsay) / S. Petit
(*Strongly Correlated Quantum Materials and Magnetism*)

ZHONG Shengyi – July 12 2012

«Étude des évolutions microstructurales à haute température en fonction des teneurs initiales en Y, Ti et O et, de leur incidence sur les hétérogénéités de déformation dans les aciers ODS Fe-14Cr1W »

Supervisor : M.-H. Mathon
(*Materials and Nanosciences: Fundamental Studies and Applications*)

HABILITATIONS TO SUPERVIZE PHD STUDENTS (HDR)

"Apport de la Cristallographie à l'étude de systèmes hybrides (molécule@microporeux) "

Florence PORCHER (September 27 2012)

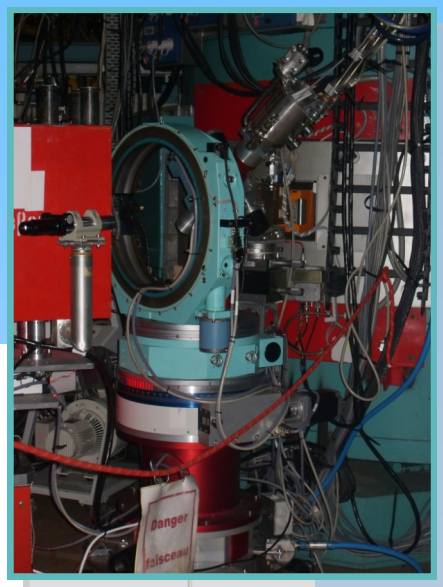
Danger
faisceau

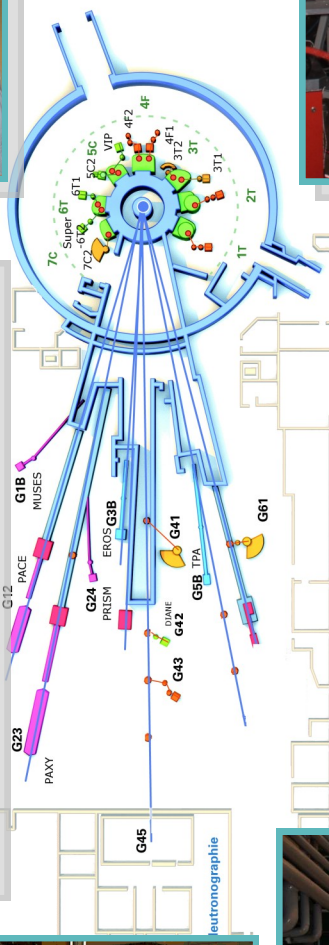
4F
4F2
VIP
5C2
5C
6T1
6T
Super
6C
7C2
7C
4F1
3T2
3T
3T1
2T
1T
G1B
MUSES
G3B
EROS
G41
TPA
G61
G12
PACE
G24
PRISM
G5B
DIANE
G42
G43
G23
PAXY
G45
Neutronographie

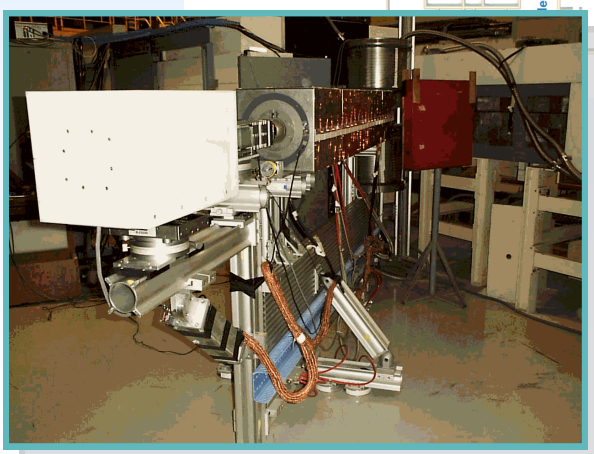

BEAMTIME ACCESS

GENERAL LAYOUT OF THE SPECTROMETERS

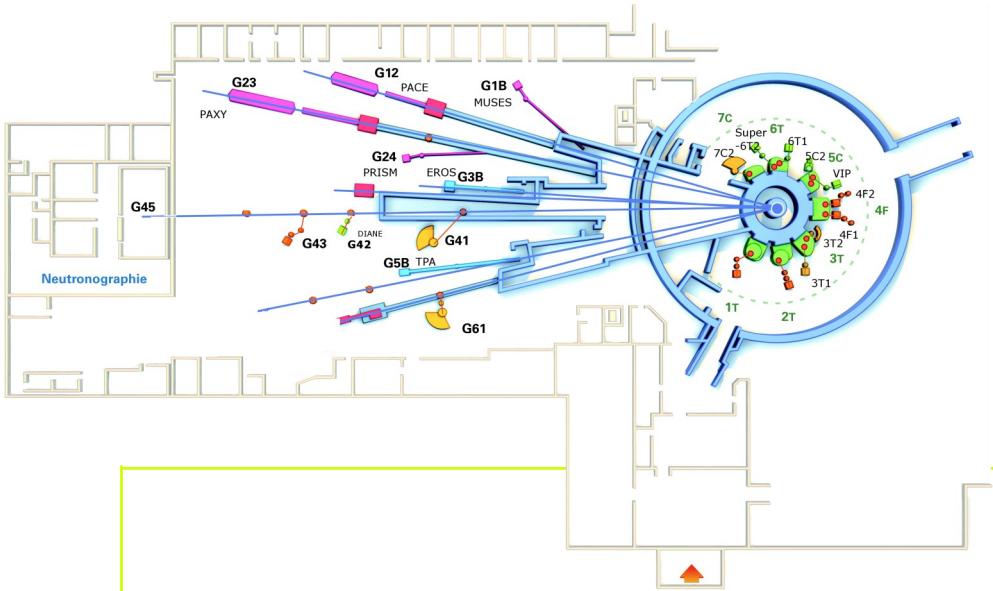

	SPECTROMETERS OPEN TO USERS	CONTACTS
	Powder diffractometers	
3T2	Florence Porcher	florence.porcher@cea.fr
G4.1	Gilles André	gilles.andre@cea.fr
G6.1	Isabelle Mirebeau	isabelle.mirebeau@cea.fr
	Single crystal diffractometers	
5C1 - VIP	Béatrice Gillon	beatrice.gillon@cea.fr
5C1	Alain Cousson	alain-f.cousson@cea.fr
Super 6T2	Alexandre Bataille	alexandre.bataille@cea.fr
	Diffuse scattering instrument	
7C2	Brigitte Beuneu	brigitte.beuneu@cea.fr
	Small-angle scattering instruments	
G1.2 - PACE	Didier Lairez	didier.lairez@cea.fr
G2.3 - PAXY	Alain Lapp	alain.lapp@cea.fr
G5bis - TPA	Annie Brûlet	annie.brulet@cea.fr
	Diffractometers for material science studies	
6T1	Marie-Hélène Mathon	marie-helene.mathon@cea.fr
G4.2 - DIANE	Vincent Klosek	vincent.klosek@cea.fr
	Reflectometers	
G3bis - EROS	Fabrice Cousin	fabrice.cousin@cea.fr
G2.4 - PRISM	Frédéric Ott	frederic.ott@cea.fr
	Triple-axis instruments	
1T	John Paul Castellan / Yvan Sidis (CRG Instrument Karlsruhe/LLB)	john-paul.castellan@cea.fr / yvan.sidis@cea.fr
2T	Philippe Bourges	philippe.bourges@cea.fr
4F1	Sylvain Petit	sylvain.petit@cea.fr
4F2	Daniel Petitgrand	daniel.petitgrand@cea.cr
	Quasi-elastic instruments	
G1bis - MUSES	Stéphane Longeville	stephane.longeville@cea.fr
	Neutron radiography	
G4.5	Guy Bayon	guy.bayon@cea.fr

The LLB-Orphée neutron scattering and imaging instruments

Powder diffractometers

3T2 "Thermal neutrons" 2-axis (50 detectors) high resolution, mainly for nuclear structure determination.

G4.1 "Cold neutrons" 2-axis (multidetector 800 cells) high flux, mainly for magnetic structure determination

G6.1 "Cold neutrons" 2-axis (multidetector 400 cells) with long wavelength (~5Å) and high flux, for the study of very small powder samples (<1mm^3). Very high pressure cell available (40 GPa).

Single crystal diffractometers

5C1 "Hot neutrons" 2-axis with lifting arm, polarized neutrons, magnetic field (8 Tesla) for spin-density maps determination

5C2 "Hot neutrons" 4-circle for nuclear structure determination.

6T2 "Thermal neutrons" 2-axis, lifting arm and 4-circle, mainly for magnetic structure determination. 12 Tesla magnetic field available, 2D detector.

Diffuse scattering instruments

7C2 "Hot neutrons" 2-axis (multidetector 640 cells) for local order studies in liquid or amorphous systems. Cryostat and furnace available (1.2K to 1300°C).

Small-angle scattering instruments

G1.2 "Cold neutrons" (annular detector, 30 rings) for study of large scale structures in isotropic systems (mainly polymers and colloids).

G2.3 "Cold neutrons" (X-Y detector, 128x128 cells) for study of large scale structures (10 to 500 Å) in anisotropic systems (polymers under stress, metallurgical samples, vortex in superconductors).

G5bis Very Small Angle Neutrons Scattering spectrometer

Diffractometers for material science studies

6T1 "Thermal neutrons" 4-circle for texture determination.

G4.2 "Cold neutrons" 2-axis for internal strain determination in bulk samples with spatial resolution ~ 1mm^3.

Reflectometers

G3bis "Cold neutrons" reflectometer operating in time-of-flight mode for multipurpose surface studies.

G2.4 "Cold neutrons" reflectometer with polarized neutrons and polarization analysis for the study of magnetic layers.

Triple-axis instruments

1T "Thermal neutrons" high-flux 3-axis instrument with focussing monochromator and analyser, mainly devoted to phonon dispersion curves measurements. Very high pressure cell (100 Kbar) available.
CRG Instrument operated in collaboration between the INFP Karlsruhe and the L.L.B

2T "Thermal neutrons" high-flux spectrometer with focussing monochromator and analyser, mainly devoted to spin-waves and magnetic excitations studies (1.5 to 80 meV).

4F1
4F2 "Cold neutrons" high flux 3-axis instruments with double monochromator and analyzer, mainly devoted to the study of low-energy (15µeV to 4meV) magnetic excitations. Polarized neutrons and polarization analysis option available.

Quasi-elastic instruments

G1bis "Cold neutrons", high resolution and high flux spin-echo instrument. It can study, in a large Q range, slow dynamics of large molecules in biology or long relaxation times like in glassy transition (Fourier times ~ 20ns)

Neutron Radiography

G4.5 Imaging technique : white beam facility for non-destructive control or dynamics imaging.

AUXILLIARY SERVICES AVAILABLE

Laboratories for sample preparation:

- Chemistry laboratory
- Biological laboratory

Technical help for:

- Vacuum/Cryogenics
- Cryostat, Furnace (0.1 – 2000 K)
- High pressures (up to 10 GPa)
- High magnetic fields (up to 10 T)
- Mechanics

http://www-llb.cea.fr/fr-en/spectros_p.php

Access to beamtime

LLB has been selected in the frame of the European Community – Access activities of the Neutron scattering and Muon spectroscopy Integrated Infrastructure Initiative (NMI3-II) which supports access to neutron beams for the selected user teams, travel and subsistence fees of visiting scientists. The program is opened to E.C. users and to scientists of the associated states.

http://nmi3.eu

Beamtime access is free of charge for any experimentalist from the French Scientific community. LLB takes in charge the expenses (travel and stay) of 2 people during the experiment.

Beamtime on the 20 open-access spectrometers can be requested by submission of:

- *An experimental application to a Selection Committee (Normal Procedure)*
  This procedure is open to any public/industrial researcher that is interested in using neutron scattering for his research. Results should be free to be totally or partially published in a Scientific Review.
  DEADLINE FOR APPLICATION: April 1st and October 1st
  http://www-llb.cea.fr/en/fr-en/proposal.php

- *An experimental application to the Directors (Exceptional)*
  This special procedure should only be used exceptionally for hot topics, confidentiality reasons or if an anomaly in the review procedure is suspected. The delay between the acceptation decision and the realization of the experiment is shortened to the minimum.
  No deadline applies for such propositions (Application all along the year).
  http://www-llb.cea.fr/en/fr-en/proposal.php

- *A fast access application*
  This procedure allows a rapid access (1 to 2 months delay) to the spectrometers in order to perform a short experiment (1 day max.). It can be used for feasibility tests, sample characterization, obtaining complementary results…
  No deadline applies for such propositions (Application all along the year).
  http://www-llb.cea.fr/en/fr-en/prop-rap.php

CONTACT AT LABORATOIRE LEON BRILLOUIN

Laboratoire Léon Brillouin

Scientific Office

CEA SACLAY

Bâtiment 563 *F - 91191 Gif-sur-Yvette Cedex*

Tel. : 33(0) 1 69 08 60 38 *Fax : 33 (0) 1 69 08 82 61*

Selection committees

Proposals are examined by 5 Selection Committees. Each is composed of 8 to 10 senior scientists that are nominated by the management of LLB for 3 years. At least half of them do not belong to the LLB and 2 or 3 are coming from foreign institutes.

For each spectrometer, LLB gives a beam-time available which is shared out by the committee; each proposal gets a grade A or B or C.

A : The experiment must be done and the committee allocates a beam-time

B : The experiment might be done if there is some extra beam-time,

C : The experiment is refused on scientific arguments.

Selection Committees are asked to take care of the educational duty of the LLB when proposal comes from new young searcher.

SELECTION COMMITEES: SCIENTIFIC FOCUS AND SUB-FOCUS

Theme I Chemical physics, biological systems

- I.01 Polymers and Supramolecular Structures
- I.02 Water, aqueous solutions, polyelectrolytes, surfactants
- I.03 System of biological interest, Biophysics
- I.04 Colloids, nanostructures
- I.05 Gels, composite materials
- I.06 Other…

Theme II Crystallographic and magnetic structures

- II.01 Crystalline structures
- II.02 Phases transitions
- II.03 Magnetic Structures
- II.04 High pressures (on powders
- II.05 Other…

Theme III Magnetism: Single-crystal systems and thin layers

- III.01 Magnetic thin layers
- III.02 Spin density
- III.03 Systems with strong quantum correlations
- III.04 Extreme conditions (strong fields, high pressures)
- III.05 Magnetic nanosystems
- III.06 Other…

Theme IV Disordered Systems, nanostructured materials and materials

- IV.01 Liquid and amorphous structures
- IV.02 Dynamics of disordered systems
- IV.03 Thin film materials
- IV.04 Nanostructured materials, precipitation, cavities,…
- IV.05 Crystallographic textures
- IV.06 Strains and residual stresses
- IV.07 Other…

Theme V Excitations

- V.01 Magnons
- V.02 Supraconductivity
- V.03 Coupling spin-network
- V.04 Dynamics in frustrated systems
- V.05 Polarized neutrons with polarization analysis
- V.06 Phonons
- V.07 Other…

LLB 2012 Reviewing committees

LLB members	French users		European users	

COLLEGE 1: Chemical physics, biological systems

Organisers: J. Jestin, G. Fadda

F. Cousin	S. Lyonnard	CEA, Grenoble	F. Gabel‡	IBS, Grenoble
	F. Nallet	CRPP, Bordeaux	M. Sferrazza [pdt]	Université de Bruxelles
	R Schweins	ILL, Grenoble		
	Y. Tran	ESPCI, Paris		

COLLEGE 2: Crystallographic and magnetic structures

Organisers: F. Porcher, S. Petit

F. Damay	M. Josse [pdt]	Université Bordeaux 1	J. A. Blanco‡	Université Oviedo, ES
I. Mirebeau‡	S. Ravy	Soleil, St Aubin	A. Daoud-Aladine	ISIS, UK
	P. Roussel	UCC, Villeneuve d'Ascq		

COLLEGE 3: Magnetism: Single-crystal systems and thin layers

Organisers: A. Bataille, F. Ott

G André	T. Hauet	Université Nancy I	F. Palacio	Université Zaragoza, ES
	E. Ressouche	ILL, Grenoble	K. Temst [pdt]	Université Louvain, B

COLLEGE 4: Disordered Systems, nanostructured materials and materials

Organisers: V. Klosek, P. Judenstein, M.H. Mathon‡*

F. Audonnet	J. Henry [Pdt]	CEA, Saclay	M. Fitzpatrick	Milton Keynes, UK
	L. Cormier	Universités Paris 6 et 7	M. Gonzalez	ILL, Grenoble

COLLEGE 5: Excitations

Organisers: Y. Sidis, D. Petitgrand‡, J. Robert*

D. Lamago	M. Boehm [pdt]	ILL, Grenoble	J. Hlinka	ASCR, Prague
	P. Foury	LPS, Orsay	A. Huxley	Université Edinburg, UK
	L.-P. Regnault	CEA, Grenoble	B. Roessli‡	PSI, Villingen, CH
			L. Paolasini*	ESRF

‡ Only for spring session - * Only for automn session

Laboratoire Léon Brillouin
CEA-Saclay
Bât 563
F-91191 GIF-SUR-YVETTE Cedex
FRANCE

+33 (0)1 69 08 52 41
+33 (0)1 69 08 82 61
www-llb.cea.fr